NOVEL SOLID-STATE MILLIMETRE-WAVE SOURCES

Malcolm R. Robertson

A Thesis Submitted for the Degree of PhD
at the
University of St Andrews

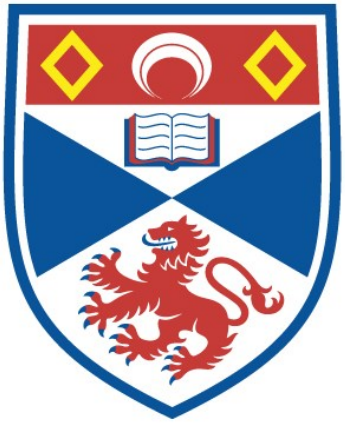

1993

Novel Solid-State Millimetre-Wave Sources

A thesis presented by
Malcolm R. Robertson, BSc.

to the

University of St.Andrews
in application for the degree of
Doctor of Philosophy

July 1992

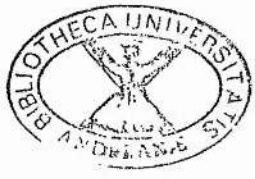

Acknowledgements

I wish to thank Jim Lesurf for his support and guidance as head of the Millimetre Wave Group. Thanks must also go to the members of the group, Darrel Smith, Mike Leeson, Michael Webb, Duncan (my brother), and especially Graham Smith and Andy Harvey. The mechanical workshop deserves my gratitude, with a special mention for George Radley. Finally I wish to thank my parents for their constant love and support.

Declarations

I hereby certify that this thesis has been composed by myself, that it is a record of my own work, and that it has not been presented for partial or complete fulfilment of any other higher degree.

This research was carried out in the Department of Physics and Astronomy at the University of St.Andrews under the supervision of Dr J.C.G.Lesurf.

M.R.ROBERTSON
JULY 1992

I hereby certify that Malcolm Robert Robertson has fulfilled the conditions of the Resolution and Regulations appropriate to the degree of Doctor of Philosophy.

J.C.G.LESURF
JULY 1992

Abstract

A study of some principal solid-state millimetre-wave sources was carried out, using mainly quasi-optical techniques developed at St.Andrews. A review of the theory of operation of Gunn oscillators was undertaken, and a number of wideband tunable Gunn oscillators were built, incorporating Gunn diodes from several different manufacturers. Characterisation of their frequency range, power output, bias tuning, and frequency stability were measured. Effects such as bias oscillations and frequency jumps were also noted, and the iterative techniques required to build an oscillator to a certain specification were presented.

Frequency multipliers are widely used to extend the frequency range of solid-state oscillators, and the techniques used to design frequency multipliers were studied. The use of non-linear capacitors (varactor diodes), and non-linear resistors (varistors and resonant-tunneling diodes) was considered in some detail. An experimental doubler block was designed and built, and doubling using both varactors and varistors was measured and evaluated.

A number of resonant-tunneling double-barrier diodes, or quantum-well devices, was made available through collaboration with Nottingham University. The tunneling process in these devices is inherently fast, making these devices suitable for high-frequency operation as detectors, oscillators, multipliers and mixers. The theory of operation of double-barrier diodes was studied, and methods of evaluating their maximum oscillation frequency were compared. Several different devices were mounted in a whisker-contacted waveguide circuit, and oscillations at W-band were measured. A whisker-contacted multiplier block was designed and built, and zero-bias tripling to 254GHz was observed. Resonant-tunneling diodes were also shown to be capable of acting as self-oscillating mixers at W-band. Effects such as injection locking and chaotic oscillations were measured.

A new class of noise source, the chaotic or semi-chaotic noise source, was considered as a future device. Its potential applications, and its advantages over conventional noise sources, was discussed.

Contents

Glossary

BWO	Backward Wave Oscillator
CW	Continuous Wave
DBD	Double Barrier Diode
DFTS	Dispersive Fourier Transform Spectroscopy
ECA	Electron Cyclotron Absorption
ECE	Electron Cyclotron Emission
ECRH	Electron Cyclotron Resonance Heating
FEL	Free Electron Laser
FIR	Far Infra Red
FM	Frequency Modulation
FWHM	Full Width Half Maximum
IF	Intermediate Frequency
IHS	Integral Heat Sink
IMPATT	Impact Avalanche Transit Time
JCMT	James Clerk Maxwell Telescope
LDS	Low Dimensional Structure
MBE	Molecular Beam Epitaxy
MOCVD	Metal-Organic Chemical Vapour Deposition
MPI	Martin-Puplett Interferometer
NDC	Negative Differential Conductance
NDR	Negative Differential Resistance
NPL	National Physical Laboratory
PSD	Phase Sensitive Detection
QW	Quantum Well
QWITT	Quantum Well Injection Transit Time
RF	Radio Frequency
SIS	Semiconductor-Insulator-Semiconductor
TED	Tranferred Electron Device
VSWR	Voltage Standing Wave Ratio
WKB	Wentzel Kramers Brillouin

1. Millimetre Wave Applications.

1.1. Introduction.

The millimetre and submillimetre wave parts of the electromagnetic spectrum lie between the microwave region and the far infra-red. Millimetre waves cover the range from 30GHz to 300GHz while submillimetre waves extend upwards to frequencies approaching 1THz. In some respects the millimetre wave region is a transitional one where techniques are borrowed both from microwave technology - for example, the use of waveguide structures - and from optics, which has contributed to areas such as quasi-optics and resonator design. Yet millimetre wave techniques are not totally similar to either the microwave or the FIR regions: they have their own unique characteristics. The full exploitation of the millimetre and submillimetre band has lagged behind neighbouring frequency bands mainly because of a lack of sources. The purpose of this introductory section is to outline major areas of interest within this frequency band, and to describe briefly the type, frequency coverage and relative merits of millimetre and submillimetre wave sources.

1.2. Some Principal Millimetre Wave Applications.

1.2.1. Radar.

Millimetre wave radar has its origins in the microwave radars developed during World War II which operated up to X-band (10GHz). The trend towards ever higher operating frequencies was stimulated largely by the military who recognised the particular advantages which millimetre wave radar can offer; namely small size, high bandwidth, low beamwidth, better resolution, increased immunity from interference or interception, and penetration of adverse atmospheric conditions, especially smoke and dust. The choice of radar operating frequency is influenced by the atmospheric attenuation characteristics in the millimetre wave region. Absorption by atmospheric gases such as water (H_2O), carbon dioxide (CO_2), oxygen (O_2) and ozone (O_3) produce frequency ranges where the attenuation is very high. At other frequencies the

gaseous absorption is at a minimum, and these are known as atmospheric windows. The main atmospheric windows in the millimetre wave band are at 35, 94, 140 and 220GHz, and most research and development effort has been concentrated at these frequencies as a result [1,2].

While military applications for millimetre wave radar technology such as missile guidance systems continue to expand, there are also some important applications in the civilian sector. One specific area which could attract much commercial interest is that of anti-collision radar for automobiles which has already been demonstrated at 50-60GHz in Japan [3].

1.2.2. Remote Sensing.

Examples of remote sensing in the millimetre wave region include measurements of the propagation characteristics of the atmosphere in the presence of water vapour at 96GHz [4] and at frequencies up to 246GHz [5]. Measurements have also been carried out to determine the backscatter characteristics of snow surfaces at 215GHz [6] and to measure raindrop sizes [7]. Other forms of environmental monitoring in the millimetre and submillimetre wave regions include sea surface temperature distributions, land surface temperature, crop and soil distribution, measurement of the ozone distribution in the atmosphere, and of the 'greenhouse gases' responsible for the deterioration of the ozone layer [8].

1.2.3. Communications.

The very large bandwidths offered by moving to higher carrier frequencies makes the use of millimetre waves for communications an attractive prospect, bearing in mind the limitations imposed by atmospheric attenuation [9]. Long distance communication links at millimetre wave frequencies perform better in the upper atmosphere where the effects of attenuation are less, which together with the small component size makes such a link between two satellites feasible.

The absorption bands, where attenuation is very high, may also be exploited to provide secure short range communications. The strong O_2 resonance at 60GHz is a commonly used 'secure' frequency. These communications links are especially useful

to the military since the narrow beamwidths and short ranges mean that the signals are very difficult to intercept. Military applications include tank-to-tank and aircraft-to-aircraft communications, artillery battery communications and local area information distribution [10].

Civilian applications of millimetre wave communication systems have been examined in the context of local area television distribution. British Telecom has investigated both street-level distribution and small town community coverage at frequencies of 30 and 60GHz [11].

1.2.4. Plasma Diagnostics.

For typical tokamak plasmas the electron cyclotron frequency and its harmonics lie in the millimetre and submillimetre region. Measurement of the electron cyclotron emission (ECE) is a valuable diagnostic technique which yields the electron temperature from the intensity of the detected radiation, and the magnetic field strength from the frequency of the radiation [12]. Given a knowledge of the topology of the plasma, it is possible to determine the electron temperature and pressure as a function of position in the plasma.

Another important measurement commonly made is of the electron density in the plasma. High density plasmas are transparent if the plasma frequency ω_p is less than the frequency ω of the probing wave [13]. The plasma frequency is proportional to the square root of the plasma density; hence the probing radiation will propagate through areas of low density and will reflect off areas of high density [14]. Using interferometric techniques to determine the time of flight of the incident radiation enables a density 'map' of the plasma to be built up. Alternatively, the same technique may be used to observe density fluctuations at a particular point.

Two other techniques operating in the millimeter wave region which may be mentioned are ECRH - Electron Cyclotron Resonance Heating, in which high power radiation is used to heat the plasma, and ECA, Electron Cyclotron Absorption, where the absorption characteristics of the plasma are used to determine the electron pressure [15].

1.2.5. Materials Measurement.

The optical constants of materials at millimetre and submillimetre wavelengths may be measured accurately in a number of different ways, the most important of which is Dispersive Fourier Transform Spectrometry [16,17]. This technique, in which the sample is placed in one arm of a two-beam interferometer, yields both phase and amplitude information, and is applicable to gases, liquids and solids. The sample may be measured either in transmission or reflection. Quantities measured by DFTS include the refractive indices of gases and liquids and the complex permittivities of solids.

1.2.6. Radio Astronomy.

Typically, astronomical observations in the millimetre and submillimetre wavelength region are of gas and dust clouds, and the rotational spectra of molecules therein. Telescopes operating in this region, such as the James Clerk Maxwell Telescope (JCMT) on Mauna Kea, normally have a range of receivers to cover the frequency bands of interest. Between September 1990 and February 1991, for example, the JCMT had receivers available to cover the 220-280GHz, 320-370GHz and 460-490GHz bands; the 690GHz and 800GHz windows; and a bolometer system for continuum observations over a range of wavelengths from 2mm to 0.35mm [18]. Heterodyne receiver systems require a stable, low-noise local oscillator source at the frequency of interest, and extremely sensitive mixers/detectors such as Schottky-barrier or SIS devices operating at liquid helium temperatures [eg.19,20].

1.3. Sources of Radiation.

Millimetric and far infra-red sources of radiation may be grouped into three main classes: lasers, vacuum tubes, and solid state devices. Broadly speaking, lasers offer high frequency, high power radiation at some specific frequencies; vacuum tube devices can offer wide tuneability with moderate power, or narrower bandwidths with high power; and solid state devices presently offer lower frequency, lower power and low noise.

1.3.1. Far Infra-Red Lasers.

Lasers operating in the far infra-red tend to fall into two main categories: optically pumped molecular lasers, and free electron lasers. Optically pumped molecular lasers use a pump source such as a CO_2 laser to achieve inversion to the excited level. The laser lines themselves correspond to a changes between rotational states of the molecules in the lasing medium which can result, in some cases, in the production of many discrete spectral lines. Optically pumped FIR lasers range in frequency from about 4.5THz (D_2O) to 250GHz ($C^{13}H_3F$), (although they are normally in use above about 600GHz) and can produce very high powers, especially in pulsed operation where power output can be 1MW or more [21]. In CW operation, the output powers are considerably less.

Free electron lasers are lasers in which the active medium is a stream of electrons. Radiation is produced from the stimulated backscattering of a low frequency pump (eg. a spatially periodic magnetic field, or a propagating electromagnetic field) from a relativistic electron beam [22]. The output frequency can be tuned by varying either the energy of the electron beam or the frequency of the pump. Power output from free electron lasers can be in the region of megawatts - for example, Columbia University achieved 8MW peak power at 200GHz. FEL's are normally operated at much higher frequencies however, and it is theoretically possible to construct a visible light free electron laser.

1.3.2. Vacuum Tube Devices.

Vacuum tube microwave and millimetre wave devices vary widely in frequency and power output. Klystrons are available up to about 200GHz at tens or hundreds of milliwatts of power, and magnetrons operate at lower frequencies up to about 100GHz at powers up to 1kW. Gyrotrons operate throughout the millimetre wave region at very high peak powers around a megawatt, and are used in high power applications such as plasma heating [23].

In certain applications where there is a requirement for a few milliwatts of power over a wide frequency range, backward-wave oscillators, also known as BWO's or carcinotrons, are often the obvious choice. BWO's rely on the interaction of the electron beam with a slow wave structure along which a wave is propagating. The

longitudinal component of the slow wave modulates the electron velocity and density, resulting in energy exchange between the beam kinetic energy and the wave electromagnetic energy [24]. The BWO is tuned in frequency by varying the beam voltage. Very large tuning ranges are common for BWO's, sometimes as much as a whole waveguide band. In addition, BWO's operate over the whole of the millimetre and submillimetre band at power levels of a few milliwatts to a few hundred milliwatts. However, BWO's require power supplies of a few kV, tend to have large amounts of FM noise, and have a limited lifetime.

1.3.3. Solid State Devices.

The two principal types of solid state device used as millimetre wave sources are IMPATT diodes and Gunn diodes. IMPATT is an acronym which stands for IMPact Avalanche Transit Time. IMPATT devices act as oscillators and amplifiers because of a frequency dependent negative resistance arising from the phase delay between the current and voltage waveforms, due to the avalanche breakdown and transit time effect [25]. IMPATT's can operate up to about 200GHz at powers of a few milliwatts. At lower frequencies, their power output can be much higher, especially when operated in pulsed mode.

Gunn diodes take their name from J.B.Gunn, who first reported current oscillations in a slice of GaAs in 1963 [26]. A more descriptive but less common name is the Transferred Electron Device or TED. Its operation depends on the transfer of conduction band electrons from a low-energy, high-mobility state to a high-energy, low-mobility state, resulting in a bulk negative resistance and the conversion of DC to RF energy. Gunn oscillators are available up to about 150GHz at power levels of a few milliwatts. A typical 94GHz diode will give a few tens of milliwatts of power, and can have very low FM noise [27].

A third type of two-terminal solid state device which may prove to be an alternative to Gunn diodes, especially at slightly higher frequencies, is the Quantum Well Device or Resonant Tunnelling Diode. This type of device also displays a region of negative resistance in its current-voltage characteristic and has been shown to oscillate at frequencies up to 712GHz [28]. The tunneling effect, in which electrons in

the conduction band tunnel through two thin barriers separating a central quantum well, is inherently very fast, and theoretically should allow oscillations up to 1THz.

Solid state devices offer certain advantages over FIR lasers and vacuum tube devices, the most obvious being size, cost, robustness, power consumption and longevity. Their disadvantages are mainly that power levels are generally much lower than those available from tube devices, and as yet the maximum oscillation frequencies are lower. Gunn oscillators have proved themselves to be reliable, low noise, widely tunable devices capable of producing adequate amounts of power for a range of applications. Their frequency range is very often extended by a factor of two or three with solid state multipliers based on varactor or varistor diodes. IMPATT diodes are capable of higher power output but are prone to suffer from noise originating from the avalanche process itself, and tend to be unreliable. Quantum well devices are still in their infancy, but the tunneling process has been demonstrated to be very fast, with future applications as high frequency oscillators, detectors, mixers and multipliers.

Subsequent chapters of this work concentrate on Gunn diodes and Gunn oscillators, frequency multipliers based on varactors and varistors, and quantum well devices as oscillators, detectors, mixers and multipliers.

Chapter 1 References.

[1] S.L.Johnston, ed., *Millimetre Wave Radar*. Dedham, MA: Artech House, Inc, 1980.

[2] R.W.McMillan, C.W.Trussell,Jr., R.A.Bohlander, J.C.Butterworth, and R.E.Forsythe, "An Experimental 225GHz Pulsed Coherent Radar", *IEEE Trans. Microwave Theory Tech.*, vol. 39, no.3, pp. 555-562, 1991.

[3] S.Kitazume and H.Kondo, "Advances in Millimeter-Wave Subsystems in Japan", *IEEE Trans. Microwave Theory Tech.*, vol.39, no.5, pp. 775-781, 1991.

[4] T.Manabe, R.O.Debolt, and H.J.Liebe, "Moist-Air Attenuation at 96GHz Over a 21-km Line-of-Sight Path", *IEEE Trans. Antenna Propagat.*, vol. 37, no.2, pp. 262-266, 1989.

[5] H.J.Liebe, T.Manabe, and G.A.Hufford, "Millimeter-Wave Attenuation and Delay rates Due to Fog/Cloud Conditions", *IEEE Trans. Antenna Propagat.*, vol. 37, no. 12, pp. 1617-1623, 1989.

[6] R.M.Narayanan and R.E.McIntosh, "Millimeter-Wave Characteristics of Multilayered Snow Surfaces", *IEEE Trans. Antenna Propagat.*, vol. 38, no. 5, pp. 693-703, 1990.

[7] J.Y.Huang, C.Wang, and Y.P.Wang, "Measurements of Raindrop Sizes and Canting Angles", *Int. J. Infrared and Millimeter Waves*, vol. 10, no.9, pp.1121-1130, 1989.

[8] N.Keen, "Infrared and Millimeter-Wave Measurements of the Environment: Status and Prospects", *Int. J. Infrared and Millimeter Waves*, vol. 11, no. 3, pp. 323-353, 1990.

[9] K.D.Anderson, "94-GHz Propagation in the Evaporation Duct", *IEEE Trans. Antenna Propagat.*, vol. 38, no. 5, p. 746-753, 1990.

[10] G.S.Sundarm, "Millimeter Waves - The Much Awaited Technological Breakthrough?", *International Defense Review*, vol.11, no.2, pp.271-277, 1979.

[11] R.G.Blake, "The Use of Millimetre-Waves for Broadband Local Distribution", *17th European Microwave Conference*, Rome, Italy, 1987.

[12] N.C.Luhmann,Jr., "Instrumentation and Techniques for Plasma Diagnostics: An Overview", *Infrared and Millimeter Waves*, vol.2, K.Button, ed., New York: Academic Press, 1979.

[13] D.Véron, "Submillimeter Interferometry of High-Density Plasmas", *Infrared and Millimeter Waves*, vol.2, K.Button, ed., New York: Academic Press, 1979.

[14] A.E.Costley, "Electron Density and Temperature Measurements on Large Tokamaks", 5th National Topical Meeting on High Temperature Plasma Diagnostics, Minsk, 1990.

[15] A.R.Harvey, Private Communication.

[16] J.R.Birch and T.J.Parker, "Dispersive Fourier Transform Spectrometry", *Infrared and Millimeter Waves*, vol.2, K.Button, ed., New York: Academic Press, 1979.

[17] F.I.Shimabukuro, S.Lazar, M.R.Cherninck, and H.B.Dyson, "A Quasi-Optical Method for Measuring the Complex Permittivity of Materials", *IEEE Trans. Microwave Theory Tech.*, vol. MTT-32, no.7, pp.659-665, 1984.

[18] "Protostar", Newsletter of the James Clerk Maxwell Telescope, No.9, 1990.

[19] J.W.Archer, "Multiple mixer, cryogenic receiver for 200-350 GHz", *Rev. Sci. Instrum.*, vol.54, no.10, pp.1371-1376, 1983.

[20] W.J.Wilson, "Submillimeter-Wave Receivers - A Status Report", *IEEE Trans. Microwave Theory Tech.*, vol. MTT-31, no.11, pp.873-878, 1983.

[21] T.A.DeTemple, "Pulsed Optically Pumped Far Infrared Lasers", *Infrared and Millimeter Waves*, vol.1, K.Button, ed., New York: Academic Press, 1979.

[22] P.Sprangle, R.A.Smith, and V.L.Granatstein, "Free Electron Lasers and Stimulated Scattering from Relativistic Electron Beams", *Infrared and Millimeter Waves*, vol.1, K.Button, ed., New York: Academic Press, 1979.

[23] W.M.Manheimer, "Electron Cyclotron Heating of Tokamaks", *Infrared and Millimeter Waves*, vol.2, K.Button, ed., New York: Academic Press, 1979.

[24] G.Kantorowicz and P.Palluel, "Backward Wave Oscillators", *Infrared and Millimeter Waves*, vol.1, K.Button, ed., New York: Academic Press, 1979.

[25] H.J.Kuno, "IMPATT Devices for Generation of Millimeter Waves", *Infrared and Millimeter Waves*, vol.1, K.Button, ed., New York: Academic Press, 1979.

[26] J.B.Gunn, "Microwave Oscillations of Current in III-V Semiconductors", *Solid State Communications*, vol.1, no.4, pp.88-91, 1963.

[27] G.M.Smith, "Transferred Electron Oscillators at MM Wave Frequencies And Their Characterisation Using Quasi-Optical Techniques", PhD Thesis, St.Andrews University, 1990.

[28] E.R.Brown, J.R.Söderström, C.D.Parker, L.J.Mahoney, K.M.Molvar, and T.C.McGill, "Oscillations up to 712GHz in InAs/AlSb resonant-tunneling diodes", *Appl. Phys. Lett.*, vol. 58, pp. 2291-2293, 1991.

2. Gunn Oscillators

2.1. The Gunn diode.

2.1.1. The Gunn Effect.

The Gunn effect relies on the bulk transport properties of a semiconductor. In theory a Gunn diode could be constructed from a uniform length of an appropriate semiconductor between two ohmic contacts, and would show the same properties regardless of the direction of current flow. The name *diode*, therefore, can be misleading. An alternative name is the Transferred Electron Device, or TED, which more accurately describes the way in which these devices operate.

A number of semiconductors exhibit transferred electron effects, but commercial Gunn diodes are grown from n-type GaAs or InP. The two materials differ in a number of respects [1], but the basic principle of operation remains the same. In both materials there is a transfer of conduction band electrons from the central Γ valley which is a high mobility, low energy state, into the satellite *L* valley, a low mobility, high energy state. The current density J arising from an applied field E can be expressed as a sum of the contributions from the two conduction bands

$$J = \sigma E = (n_l e\mu_l + n_h e\mu_h)E \qquad (2.1)$$

where n_l and μ_l are the electron density and mobility of the lower valley, and n_h and μ_h are the electron density and mobility of the upper valley. At low applied fields, most of the electrons are in the lower valley, and $n_l >> n_h$. As the applied field reaches a certain critical value known as the threshold field, the electrons gain sufficient energy to scatter into the upper valley in which their mobility is lower (and their effective mass is greater), and their drift velocity is lower. Thus the current density will tend to *fall* as the higher field enables a greater number of electrons to transfer to the satellite valley. The energy gap between the Γ and the *L* valleys is around 0.35eV in GaAs and 0.53eV in InP (Figure 2.1), hence the threshold field in InP is higher than that in GaAs - about $10kVcm^{-1}$ compared with $3.2kVcm^{-1}$ (Figure 2.2).

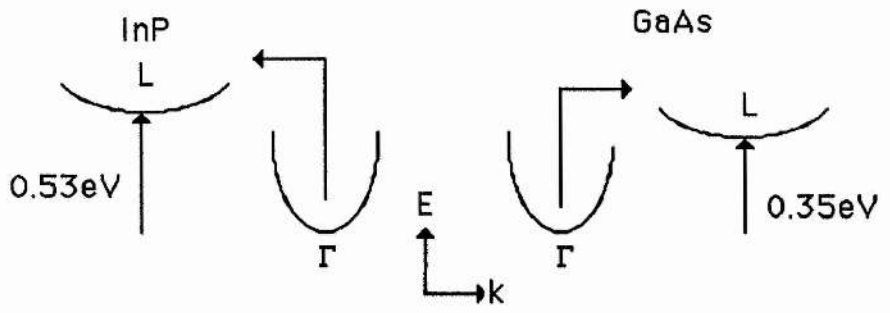

Figure 2.1. Schematic of band structure in GaAs and InP.

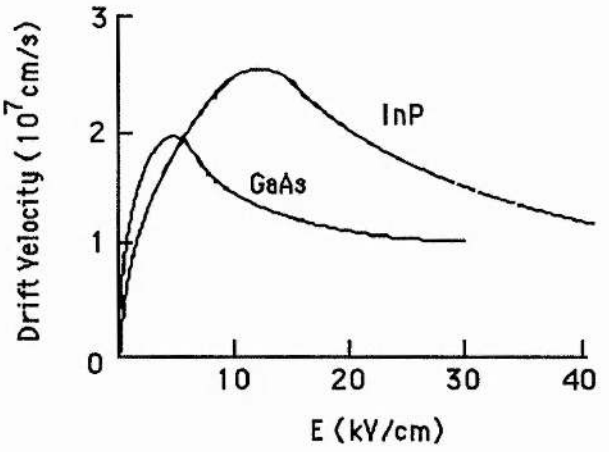

Figure 2.2. Electron drift velocity versus electric field.

The negative differential resistance (NDR) observed in the current-voltage characteristic of Gunn diodes is therefore a direct consequence of the velocity-field behaviour shown above. Generally speaking, any such two terminal device which shows a net negative resistance at a certain frequency should, in theory, oscillate at that frequency when placed in a suitable circuit and biased into the NDR region.

2.1.2. Modes of Operation.

As the electric field is increased beyond threshold, accumulations of charge tend to form within the active layer of the Gunn diode. The dynamics of these space charge regions are governed by two principal modes of operation: the classical domain mode, and the accumulation mode [2].

The classical domain mode is normally associated with low frequency Gunn diodes with long active layer lengths. Under a sufficiently high applied field (i.e. above threshold) electrons will leave the cathode and accelerate in the direction of the anode. These electrons will start to slow down as they are increasingly scattered into the low mobility satellite valley, and electrons arriving from behind catch up with the slower electrons, creating an accumulation zone. Electrons in front of the accumulation zone tend to move away towards the anode, creating a depletion region. In this way a high field dipole domain forms, which lowers the field below threshold in the rest of the sample thus preventing further domains from forming. The domain travels towards the anode at roughly the saturated satellite drift velocity (about $10^7 cms^{-1}$) until the domain runs into the anode, giving a pulse of current. The fields now are no longer high enough for the domain to exist, the domain disappears, the field rises once more toward threshold, and the process repeats.

Most Gunn diodes working at high frequencies (>20GHz) are believed to operate in some form of accumulation mode. The active layer length of these diodes is small, only a few microns or so long. The accumulation layer is formed at the cathode as before, but, mainly as a consequence of the short length of the device, the high field now persists as far as the anode - there is no depletion region. Thus a much greater proportion of electrons in the sample are in the satellite valley, resulting in greater efficiency compared with the domain mode. In addition, the effective transit velocity of small accumulation instabilities have been found to be up to three times greater than domain velocities [3].

2.1.3. Cathode Structures.

At high frequencies, as the device active layer length becomes smaller, the problem of 'dead space' at the cathode becomes significant. Assuming that the device

has an n^+ ohmic cathode, electrons are injected into the active layer with low energy and high mobility, and have to gain energy before being scattered into the satellite valley. This process takes both space and time, and has an adverse effect on the device efficiency since not all the active layer exhibits negative resistance, just the latter part nearest the anode. The rest of the active layer thus acts as a series positive resistance (Figure 2.3).

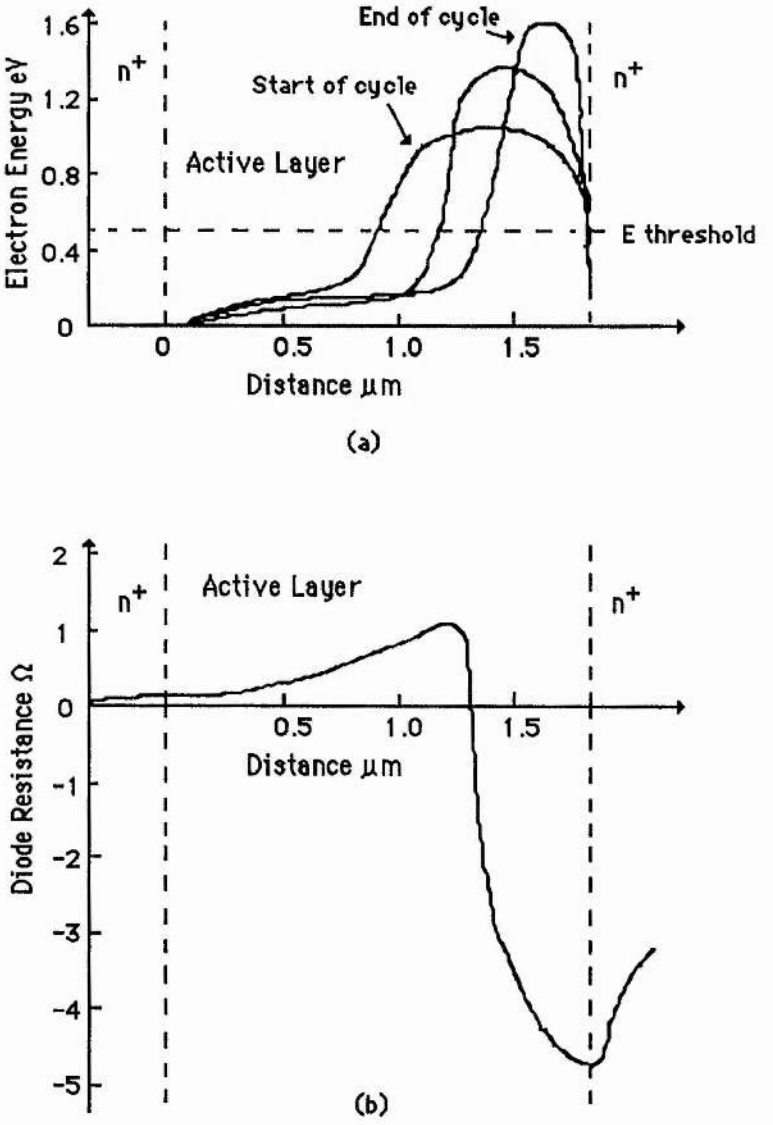

Figure 2.3 (a). Evolution of electron energy over the rf cycle and (b) diode resistance as a function of active layer length.

In order to reduce the dead space region and maximise the proportion of the active layer available for rf generation, alternative cathode structures are required. The principal aim is to inject hot electrons directly into the active layer with an energy close to the satellite valley energy, and this is usually achieved by creating a high field current-limiting cathode. This may be realised in a number of ways, for example using a metal contact (similar to a Schottky barrier), a highly-doped spike of varying geometries, graded active layer doping, or a combination of these techniques.

2.1.4. Harmonic Operation.

While the use of current-limiting cathodes leads to improvements in power, efficiency and operating frequency, it is generally accepted that GaAs diodes have an upper fundamental frequency limit of around 75GHz, and InP diodes have a limit of about 140GHz. This frequency limit is determined largely by the rate at which electrons gain or lose energy in the central Γ valley, as opposed to the inter-valley scattering rate which is much faster. GaAs diodes oscillating at frequencies above 75GHz, therefore, are usually operating in a second harmonic mode, with the diode's non-linear effects responsible for harmonic generation.

2.1.5. Device Design and Thermal Considerations.

Since the dc-rf conversion efficiency of Gunn diodes is low - about 2% for InP, less than 1% for GaAs - most of the device input power has to be removed as waste heat. Keeping the device length short reduces problems of heat sinking, since long devices must remove heat by thermal conduction through the length of the device. By constructing the device as an integral heat sink (IHS) structure, the active layer may be placed only a few microns from the heat sink (Figure 2.4).

The type of structure shown in Figure 2.4 is normally enclosed by a ceramic or quartz annulus topped by a gold lid (Figure 2.5). Bias is brought to the device via a metal tape or tapes, the inductance of which is an important design parameter. The resulting package is the usual format in which manufacturers will supply Gunn diodes, for example the 'N34' package for W-band (75-110GHz) diodes.

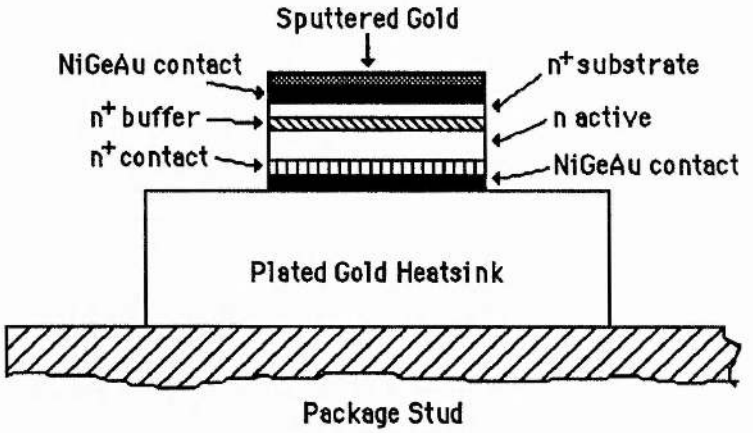

Figure 2.4. Schematic diagram of integral heat sink structure.

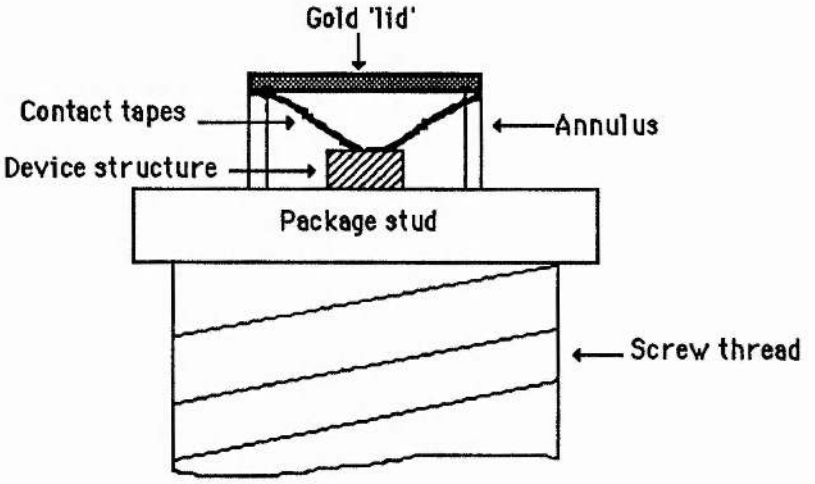

Figure 2.5. Commercial Gunn diode package.

The diode package must in turn be properly heat sunk to ensure that the active layer temperature does not exceed the maximum rating. Varian, for example, quote active layer temperatures of 260°C for GaAs diodes and 175°C for InP. If the diode is allowed to operate at temperatures in excess of the maximum ratings, then degradation will occur and the diode will almost certainly fail.

The device diameter is another critical parameter in the design of Gunn diodes. It is not possible to choose a large diameter of device in an attempt to lower the power

dissipation density because the shunt capacitance of the device will become significant, especially when the active length is short. Parasitic losses such as contact resistance, resistive losses in the semiconductor itself, and skin effect losses all become increasingly significant as the device dimensions become smaller. In general, for a given material (GaAs or InP) the bias voltage and power ouput will fall as the operating frequency rises. This is illustrated in Table 2.1. The values given are for Varian Gunn diodes, both GaAs and InP [4].

	Frequency (GHz)	Power (mW)	Bias (Max) (V)	Current (mA)
InP	35	250-350	12.0	300
	56	150-250	10.0	250
	94	30-60	7.5-11.0	350
GaAs	26-40	50-350	7.0	600-1100
	58-60	50-100	6.0	1000
	92-95	20-35	5.0	800-1000

Table 2.1. Comparison of Electrical Characteristics of Varian Gunn diodes.

The high frequency diodes listed above, i.e. those which oscillate at 94GHz, are operating in the second harmonic mode. Fundamental InP diodes for W-band are also available, both from Varian and other manufacturers. However, 94GHz GaAs diodes are only available as second harmonic devices.

2.2. Gunn Oscillators.

2.2.1. Impedance Matching.

The principal design criterion for any oscillator is that the impedances at the fundamental frequency and its harmonics are properly controlled. This becomes increasingly difficult at high frequencies as circuit resistive losses increase, and parasitics associated with the diode package become more significant. In the context

of millimetre wave oscillators the problem to be overcome is one of matching the device to a transmission line whose characteristic impedance differs considerably from the device impedance. Gunn diodes typically have a negative resistance of just a few ohms which needs to be matched to a waveguide which has a characteristic impedance of a few hundred ohms. To achieve this impedance transformation, the diode is embedded in a resonant circuit of some sort. The simplest example of a resonant circuit may be illustrated by the circuit shown in Figure 2.6.

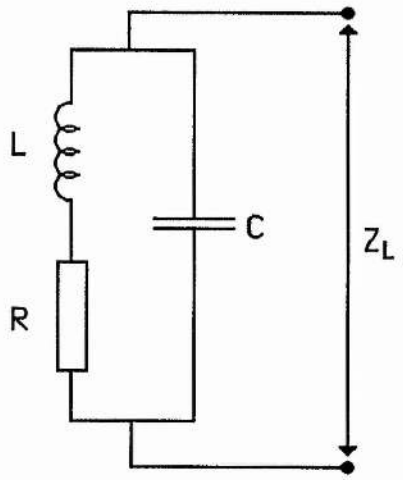

Figure 2.6. A simple resonant transformer.

From the working of Smith [2], it can be shown that at resonance (i.e. when Z_L is real),

$$R_L = \frac{L}{C}\cdot\frac{1}{R} = (Q^2 + 1)R \qquad (2.2)$$

which indicates the order of Q required to bring about the necessary impedance transformation.

We can extend this lumped element analysis to include the case of an arbitrary load of impedance $Z_T=R_T+jX_T$ across a transmission line of characteristic impedance Z_0.

Here, the line will be matched to the load only if $R_T = Z_0$ and $X_T = 0$. Clearly, this is rarely the case. If a backshort is now placed across the transmission line at a distance l behind the load (Figure 2.7) the condition for matching becomes:

$$R_T = Z_0 \sin^2(\beta L) \qquad X_T = (Z_0/2) \sin(2\beta L) \qquad (2.3)$$

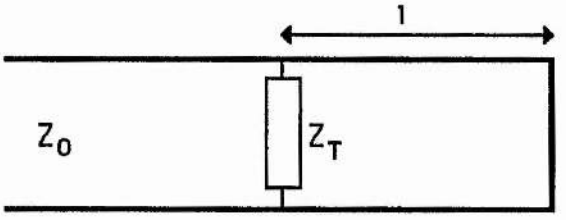

Figure 2.7. Matching of a load to a transmission line with a backshort.

From equation 2.3 we can see that, provided $R_T < Z_0$, the load can be critically coupled to the transmission line if X_T is the appropriate value. In general, it is normally possible to match the reactive part of the impedance across the transmission line with a backshort: however, matching the resistive part can prove to be less straightforward.

2.2.2. Oscillator Circuits.

Practical oscillator circuits which have been developed over the last few years tend to fall into one or other of two popular topologies - inductive post, and resonant cap. The inductive post coupling using either full-height or reduced-height waveguide tends to be used at lower frequencies, with the Gunn diode operating in the fundamental mode. The frequency tuning is acheived by means of the adjustable backshort behind the diode (Figure 2.8).

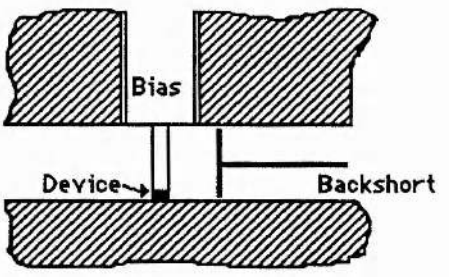

Figure 2.8. Schematic of inductive post circuit.

The resonant cap circuit is the circuit most commonly found in high frequency Gunn oscillators where the diode and disc form a resonator and impedance transformer. If, in addition, the length of the post above the cap can be altered through the incorporation of a coaxial cavity, the resulting circuit provides the basis for wideband tuneable Gunn oscillators (Figure 2.9).

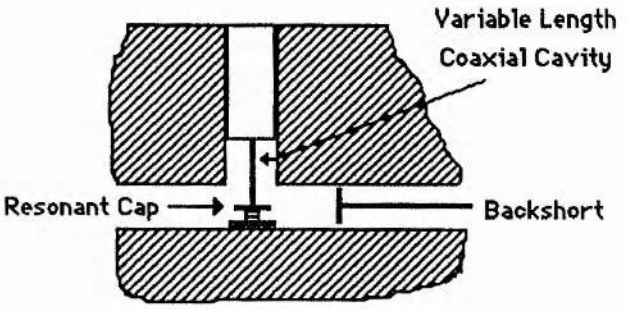

Figure 2.9. Schematic of resonant cap circuit with coaxial cavity.

This type of circuit has been extensively studied both for the fundamental and the harmonic operation of Gunn diodes [e.g. 5,6], and the basic design has been adopted by us for all the Gunn oscillators in use at St.Andrews. If the waveguide cut-off frequency is lower than the fundamental frequency of the diode then the oscillator will operate as a fundamental oscillator in which both the length of the coaxial cavity and the position of the backshort will affect the resonant circuit presented to the diode. Fundamental oscillators often operate with no cap at all, in which case the cavity acts as a simple coaxial resonator, with the frequency determined by the half wavelength resonance in the cavity.

If the waveguide cut-off frequency is arranged to be above the fundamental frequency of the diode, then the fundamental is entirely contained within the coaxial cavity and only harmonics can propagate down the waveguide - usually the second harmonic, although the third harmonic can sometimes be detected. Since the fundamental is fully contained within the cavity, very high Q's (at the fundamental) may be achieved, with the loading principally due to resistive losses in the cavity. The presence of the resonant cap, the dimensions of which have a critical effect on the second harmonic in terms of both power and frequency, will of course mean that the simple coaxial resonance mentioned above is now perturbed by the discontinuity of the cap. The backshort provides a reactive termination for the second harmonic and affects the output frequency to a much lesser extent than in a fundamental oscillator, since the output frequency is determined by the fundamental.

It is important to point out that the second harmonic also operates in a quasi-coaxial mode, so that both the fundamental and the second harmonic are coupled into modes in the coaxial cavity, although the second harmonic is coupled more weakly. Furthermore, since the condition for resonance at the second harmonic is likely to differ from that of the fundamental at a given frequency, with the result that neither of the two modes are truly coaxial. The situation is further complicated by the presence of the cap and its associated capacitance. The impedance transformation at any particular frequency, therefore, is a function of the impedance seen by the quasi-coaxial mode at the second harmonic, as well as a function of the impedance transforming effects of the radial disc [2]. Changing disc parameters such as radius, thickness and height, all affect the impedance transformation in a complex manner. Carlstrom et al [6] performed a comprehensive series of measurements in which the effects of varying the disc parameters on frequency and power were investigated. For a given cavity height and diameter, their results may be summarised as follows. Increasing the disc diameter increases the capacitive loading of the cavity (at the fundamental) and therefore lowers the oscillation frequency; increasing the disc diameter also has the effect of increasing the length of the radial line transformer (at the second harmonic) and thus optimises the power output at the lower end of the frequency range. Increasing the disc's height above the diode (by means of a short length of post between the cap and the diode) moves the cap into a region of stronger electric field, which increases the capacitive loading of the cavity and so lowers the oscillation frequency. Increasing the disc's height can also adversely affect the impedance transformation ratio at the second harmonic and thus lower the output

power. Lastly, increasing the thickness of the disc mimics both the effects of increased diameter due to increased fringing capacitance, and of increased height.

The next section details some of the Gunn oscillators which have been built at St.Andrews University, based on (but not identical to) the design by Carlstrom et al.

Chapter 2 References.

[1] I.G.Eddison, "Indium Phosphide and Gallium Arsenide Transferred-Electron Devices", *Infrared and Millimeter Waves*, vol.11, K.Button, ed., New York: Academic Press 1984.

[2] G.M.Smith, "Transferred Electron Oscillators at MM Wave Frequencies And Their Characterisation Using Quasi-Optical Techniques", PhD Thesis, St.Andrews University, 1990.

[3] D.Jones and H.D.Rees, "Accumulation Transit Mode in Transferred-Electron Oscillators", *Electron. Lett*, vol.8, no.23, pp.566-567, 1972.

[4] Varian, Solid State Microwave Division, 3251 Olcott Street, Santa Clara, CA 95054.

[5] W.M.Haydl, "Fundamental and Harmonic Operation of Millimeter-Wave Gunn Diodes", *IEEE Trans. Microwave Theory Tech.*, vol.MTT-31, no.11, pp.879-889, 1983.

[6] J.E.Carlstrom, R.L.Plambeck, and D.D.Thornton, "A Continuously Tunable 65-115 GHz Gunn Oscillator", *IEEE Trans. Microwave Theory Tech.*, vol.MTT-33, no.7, pp.610-619, 1985.

3. Gunn Diode Characterisation

3.1. The Oscillator Block.

3.1.1. General Description.

As mentioned in the previous section, the Gunn oscillator circuits which have been developed at St.Andrews are based on a second harmonic resonant cap design with a variable height coaxial cavity [1-3]. A vertical section through a typical oscillator block is shown schematically in Figure 3.1.

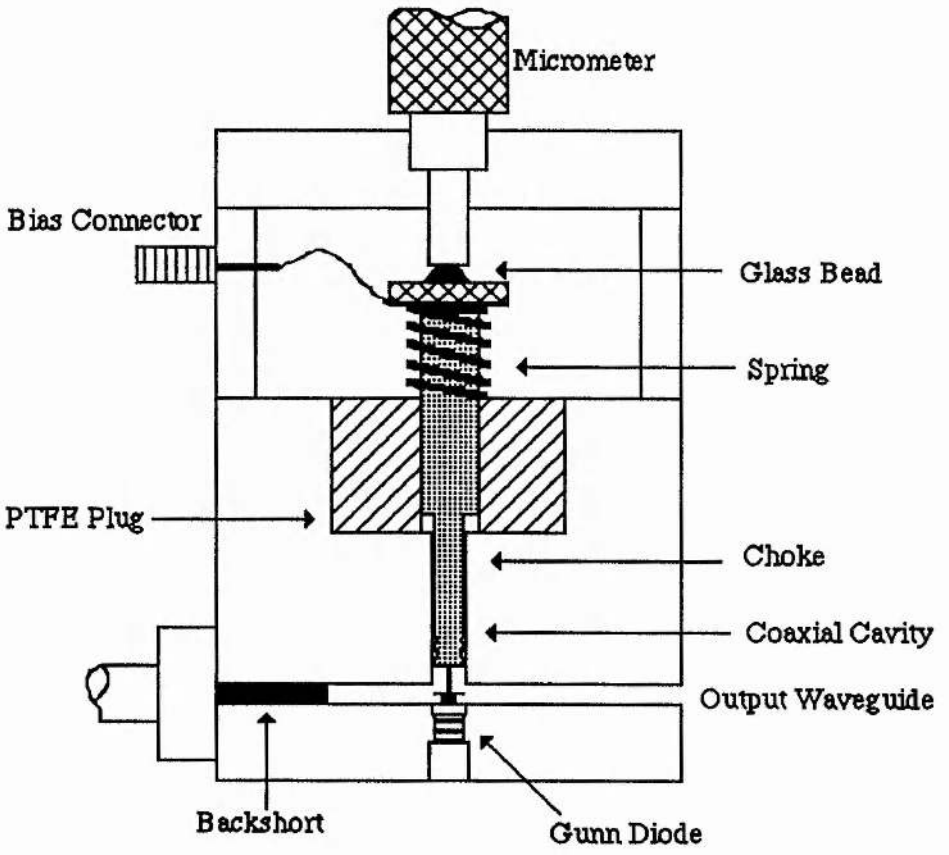

Figure 3.1. Schematic of Gunn Oscillator.

The oscillator blocks are machined from aluminium, and are made in four main sections. The top section is simply a 'lid' in which the top micrometer is mounted,

and the next section provides space for the SMA bias connector, over-voltage Zener diode and anti-spike RC network. The centre section contains the coaxial cavity and the output waveguide, and the bottom section houses the diode. A spring-loaded, sliding, contacting backshort is situated behind the diode in the waveguide. The four sections of the block are assembled accurately using precision machined dowels and are held together by stainless steel bolts.

3.1.2. The Choke Structure.

Essentially, the choke structure performs two functions: it slides up and down in the coaxial cavity to tune the frequency of the oscillator, and it carries the bias current to the diode. In order to maintain electrical contact to the diode whatever the position of the choke, the cap and post is spring-loaded as shown in Figure 3.2.

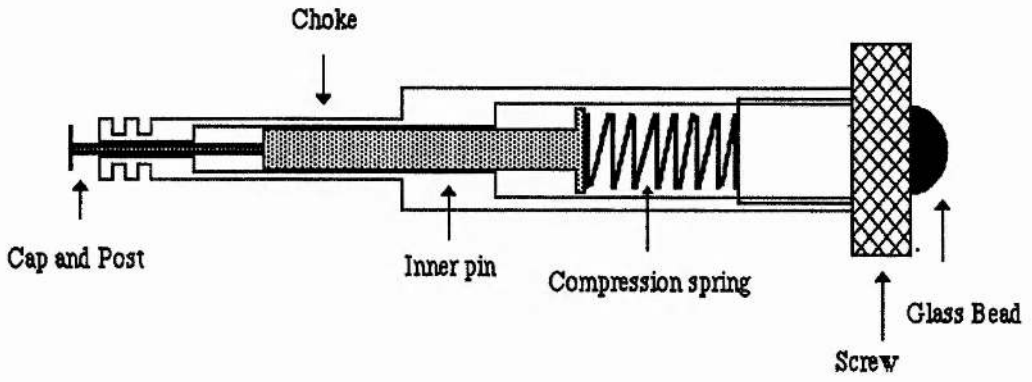

Figure 3.2. Detail of spring-loaded cap and post within the choke.

The spring itself is chosen carefully. It should be strong enough to give a good contact to the diode at all times, yet not so strong as to risk crushing the diode package, especially at low cavity heights where the spring is near maximum compression. Since the aluminium choke must also be isolated electrically from the wall of the coaxial cavity, it is anodised to provide a thin insulating layer. The anodised finish can be scratched quite easily, however, and care must be taken in machining the coaxial cavity to as smooth a finish as possible. A tiny amount of very light oil has been found to be effective in prolonging the life of the anodised finish.

The filter structure at the lower (diode) end of the choke is a low-pass, five section low/high impedance design which has been used successfully by Smith [1]. The cut-off frequency is 15GHz, well below the passband edge. The lengths of the various sections had been calculated both for a maximally flat Butterworth filter and a 1dB ripple Chebyshev filter. In practice, it was found that the exact dimensions were not critical, provided that the section lengths were made between $\lambda/8$ and $3\lambda/8$ and avoided half-wave resonance. Similarly, the difference in radius between the low and high impedance sections should be large so that the reflection coefficient is also large, but should again avoid half-wave resonance. The dimensions of the choke filter are shown in Figure 3.3.

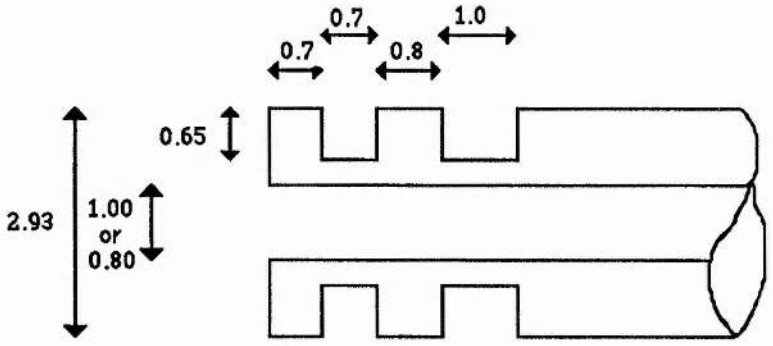

Figure 3.3. Choke filter dimensions.

The cap and post are machined as a single unit from brass or aluminium. The diameter of the post is either 0.8mm or 1.0mm (depending on the particular choke) to give a good sliding fit in the centre hole of the choke, and a range of cap diameters can be machined. The caps are usually machined as thin as possible without sacrificing too much mechanical strength - a thickness of about 0.2mm is normal. The overall length of each cap and post is around 10mm. The optimum diameter of the cap depends on the particular diode one is using and on the desired output characteristics, and is determined empirically.

3.2. Measurement of GEC Prototype Gunn Diodes.

3.2.1. Device Description.

This section details the results obtained from measurements performed on prototype Gunn diodes supplied by GEC in late 1987. The devices originated from three wafers labelled DB420, DB429 and DB421, all with transit lengths of 1.5μm. Wafers DB420 and DB429 should be nominally identical since DB429 was a regrowth of DB420. Wafer DB421 has the same injector and transit region as DB420, but the substrate is on the opposite side. This was done as there was a question as to whether the efficiency could be improved by heat sinking the anode. Diodes from DB421 therefore required a negative dc bias supply (Figure 3.4).

Measurements were made on six samples each of DB429 and DB421, and on one sample of DB420. Unfortunately, six of these diodes failed within a few minutes of switch-on - two open-circuit (DB429) and four short-circuit (one DB429, three DB421). This high failure rate was probably due solely to the prototype nature of the diodes.

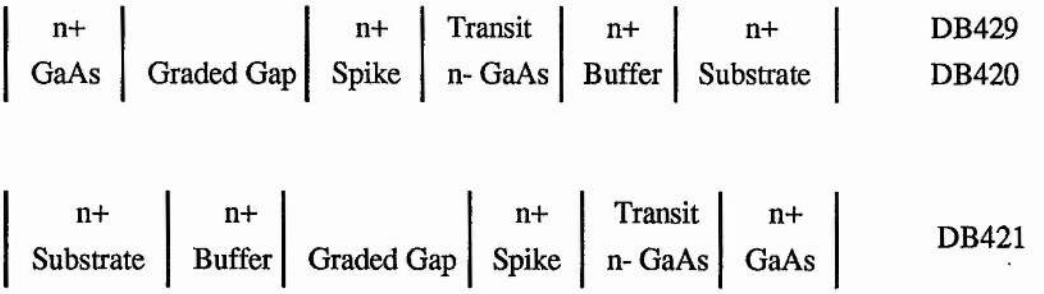

Figure 3.4. Gunn diode layer profile.

3.2.2. Frequency and Power Measurement.

Two oscillator blocks were used in the characterisation of the diodes. Designated EEV5 and EEV8, the waveguide sizes were WG27 (2.54 x 1.27mm) and WG28 (2.00 x 1.00mm) respectively, and the coaxial cavities were 'standard' 3.00mm diameter

cavities. The cap and post dimensions used in all the measurements were a 2.00mm diameter cap, 0.2mm thick, on a 0.8mm post.

Frequencies were measured with a Martin-Puplett polarising interferometer [4] and Golay detector. Power was measured using an Anritsu power meter with a WG27 detector head and WG27/WG28 taper where appropriate. The position of the backshort and the bias voltage were optimised for maximum power at each frequency. In addition, the diodes were raised slightly in the cavity in order to optimise power by improving the impedance matching between the diode and the waveguide. Power-frequency curves are shown in Figures 3.5 to 3.13.

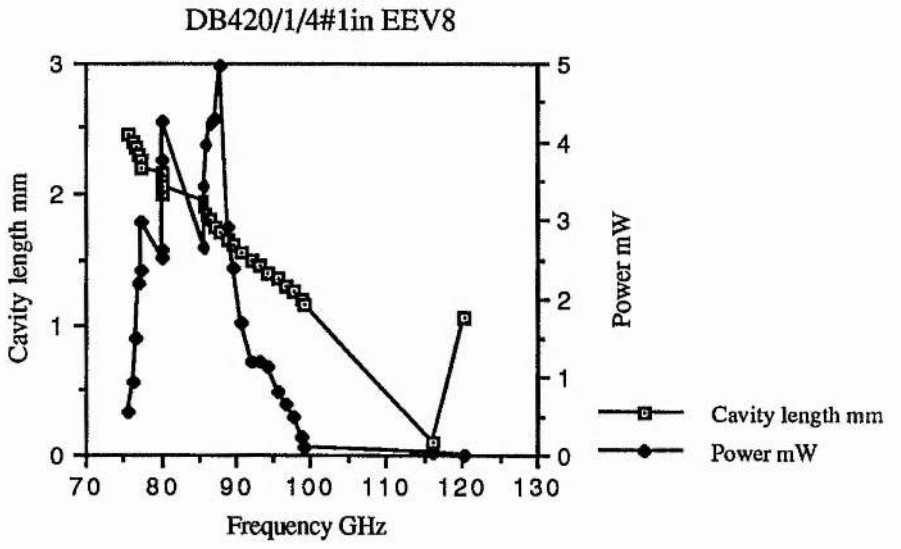

Figure 3.5.

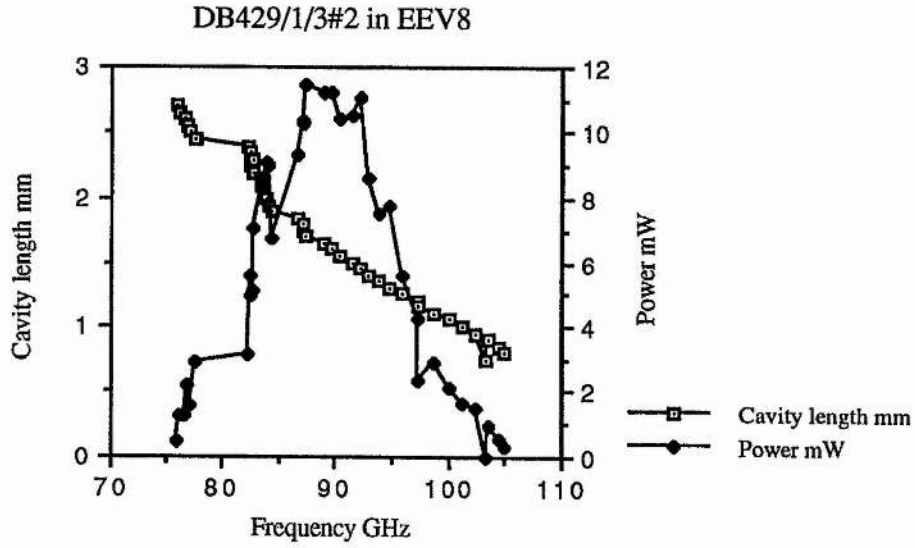

Figure 3.6.

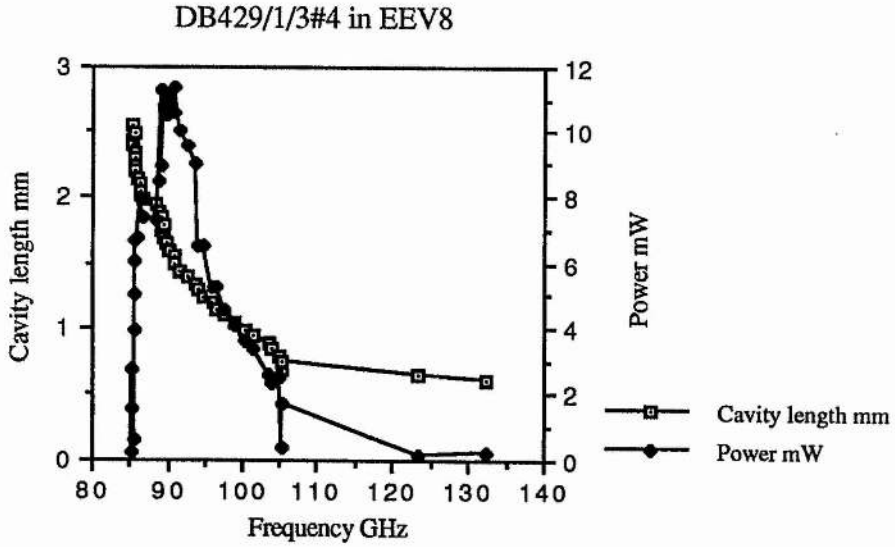

Figure 3.7.

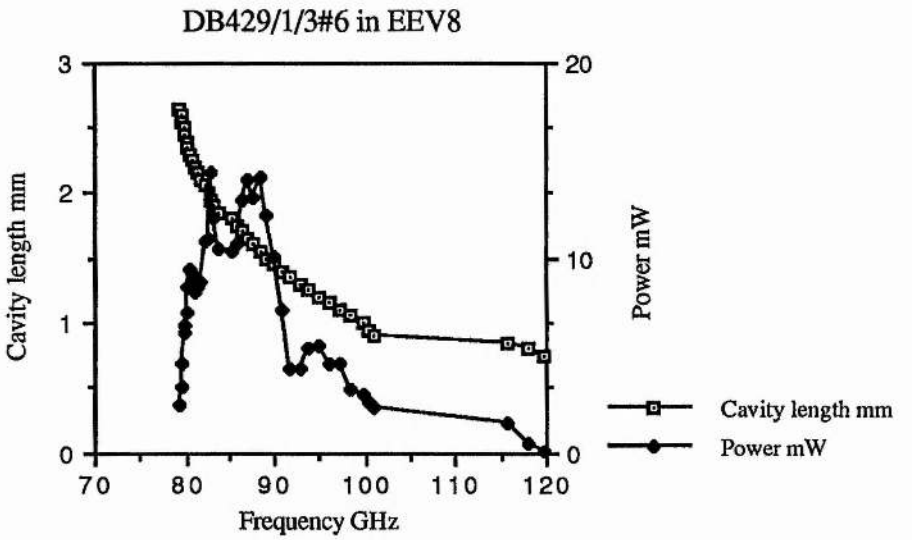

Figure 3.8.

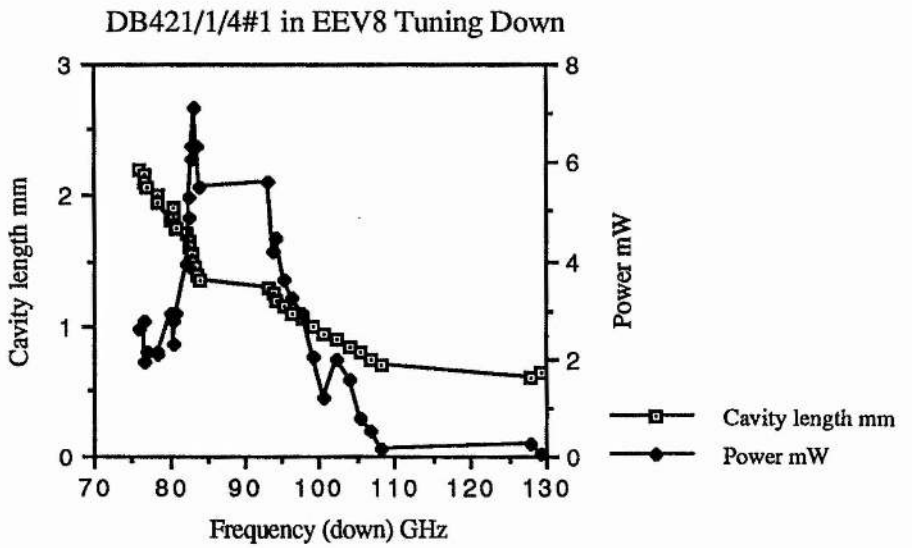

Figure 3.9.

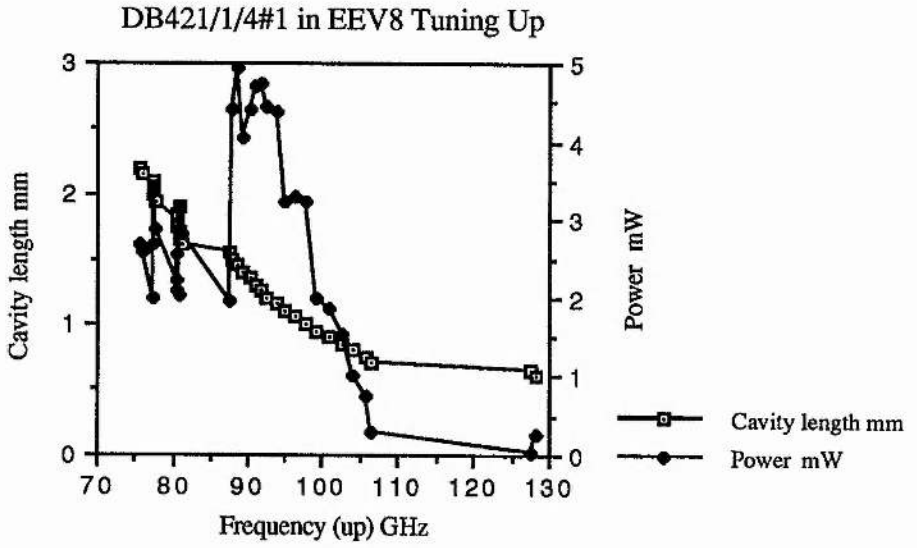

Figure 3.10.

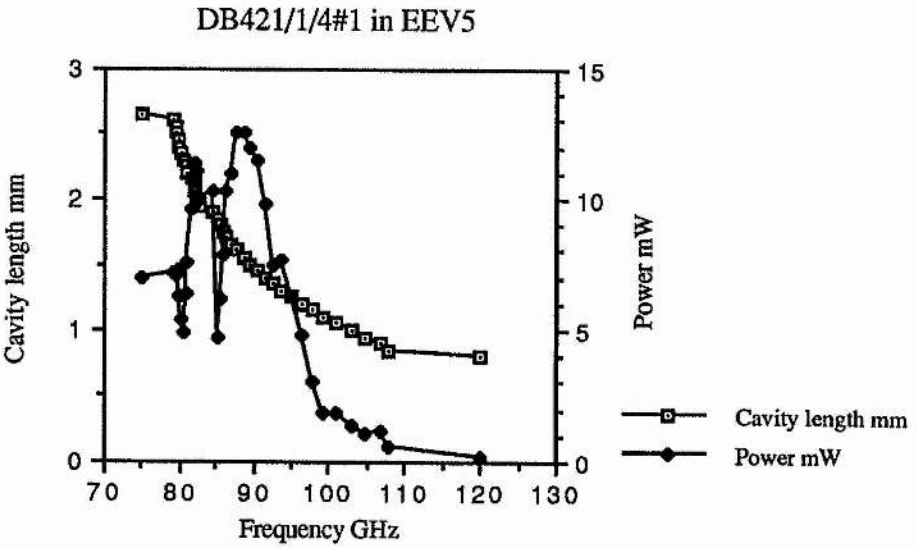

Figure 3.11.

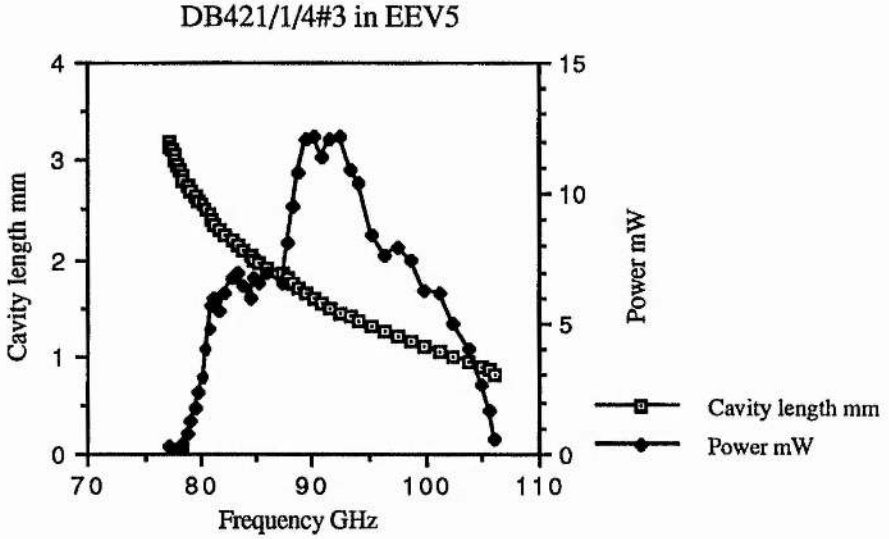

Figure 3.12.

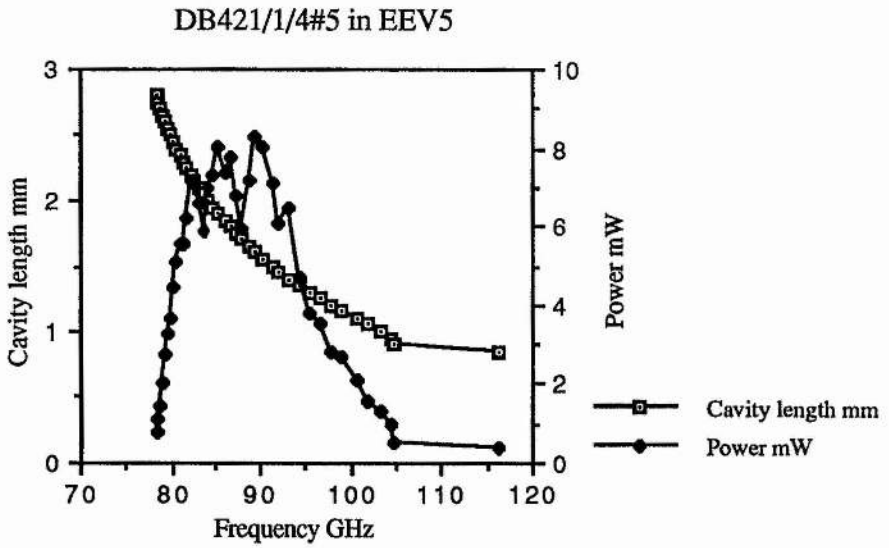

Figure 3.13.

As a general observation we may say that for a given diode, for example DB421/1/4#1, we should get most power using the largest possible size of waveguide for the particular frequency of interest. Although it was not possible to measure each diode in both sizes of waveguide, experience has shown that for our particular design of oscillator block, better coupling between the coaxial cavity and the waveguide is achieved with WG27 waveguide rather than WG28, but this will depend to some extent on the individual diode.

3.2.3. Frequency Jumps and Power Dips.

Most diodes exhibited frequency jumps during tuning, often associated with a significant dip in power. Frequency jumps and dips in power have been reported previously [1-3], a result of the admittance of the diode at the fundamental frequency changing significantly, in particular where the sign of the reactive termination of the second harmonic changes.

In the analysis performed by Smith [1] the resonant condition met when one tunes through a second harmonic resonance is given by

$$|B_c(\omega)| - 2\left(\frac{V_2}{V_1}\right)^2 |B_c(2\omega)| = B_T = 0 \qquad (3.1)$$

where $B_c(\omega)$ and $B_c(2\omega)$ are the circuit susceptances at the fundamental and second harmonic frequencies respectively, V_1 and V_2 are the terminal voltages across the diode at ω and 2ω, and B_T is the total reactance of the circuit and diode at the frequency ω.

Normally the second term in Eq.3.1 is small, and the resonant condition will be dominated by the fundamental frequency term. If the second term should become significantly large, either through V_2 becoming large (resonance of the second harmonic in the cavity), or $B_c(2\omega)$ tending towards plus or minus infinity ('anti-resonance'), frequency jumps will occur.

It should be noted that frequency jumps associated with tuning through an

'anti-resonance' are very small since the second harmonic voltage tends towards zero in this region.

A dip in power in the close vicinity of a frequency jump is to be expected since at a resonance or anti-resonance, the cavity and the waveguide are either significantly over-coupled or under-coupled. However, one should not assume from this that when not in the close vicinity of a frequency jump, the critical coupling condition is satisfied - there is usually a certain amount of under or over-coupling. A peak in the power frequency curve will indicate that critical coupling is either satisfied or very close to being satisfied.

When one compares the experimental results with the curves predicted by theory [1], we see that there is a reasonable amount of agreement, given the inevitable differences between individual diodes.

Let us now consider the large frequency jump shown by most of the diodes at the high frequency end of the tuning range. Two or three high frequencies (around 120 Ghz, typically) could usually be detected, at very low powers. At this point, the coaxial cavity is extremely short and the diode, the resonant cap and the bottom of the choke are very close to each other - in some cases, the choke may be touching the upper surface of the cap. One may suggest that in this situation some sort of radial mode is set up in place of the normal coaxial mode, causing a frequency jump. In one case, DB429/1/#2 in EEV8, there was a *drop* in frequency at the shortest cavity length. This may either have been due to mechanical stress on the top cap of the diode package, causing slight deformation of the package, or to an increase in the capacitance seen by the diode.

Frequency jumps can also be observed at very long cavity lengths. Diode DB421/1/4#1 in block EEV8 could be made to produce oscillations of 142 GHz at a long cavity length. This was noticed when tuning very close to the cut-off frequency (75 GHz for WG28 waveguide). Reducing the bias voltage to about -4.8V and carefully adjusting the cavity length produced a frequency component of 142 GHz. There was also a component of around 75.5 GHz, indicating that the higher frequency component was anharmonic. As the cavity length was shortened, the high frequency component eventually disappeared, in a transition that was quite well-defined. Care had to be taken in interpreting the trace produced by the Fast Fourier Transform as the Martin-Puplett interferometer system can be prone to standing waves at certain

frequencies. These are usually obvious, but can sometimes cause modulation of the diode itself.

3.2.4. Current-Voltage Characteristics

I-V curves for four diodes were measured at 94 GHz (Figures 3.14 -3.17). The d.c. resistance of the oscillator block is typically 2Ω, so the actual voltages across the diode will be slightly less than those shown. The current was read from a 15V bench supply feeding the diode bias supply, and the quiescent current consumed by the bias supply was subtracted from each current reading. Threshold currents varied between about 700mA and 1000mA, and threshold voltages varied between about 2.5V and 3.5V. These figures are fairly typical for GaAs devices, although the currents passed by the diodes are a little high, indicating that these diodes are large-area devices with relatively high capacitance.

The sharp upturn of each curve shows where the Zener diode, situated in the top section of the block, starts to conduct.

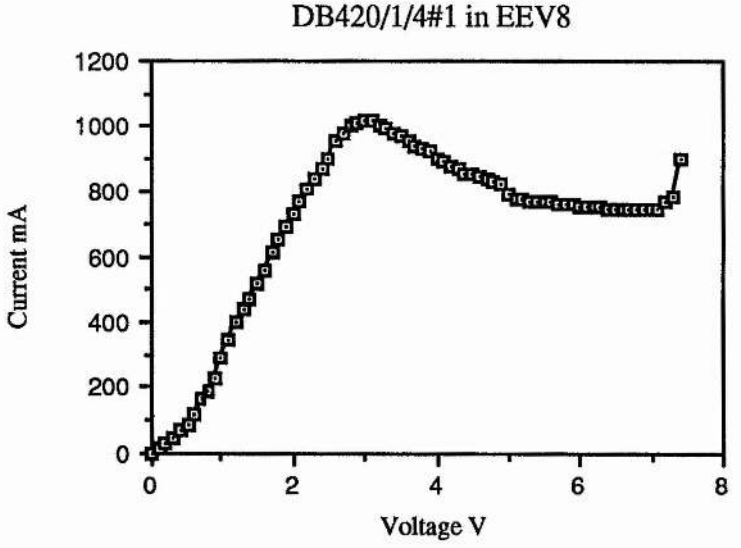

Figure 3.14.

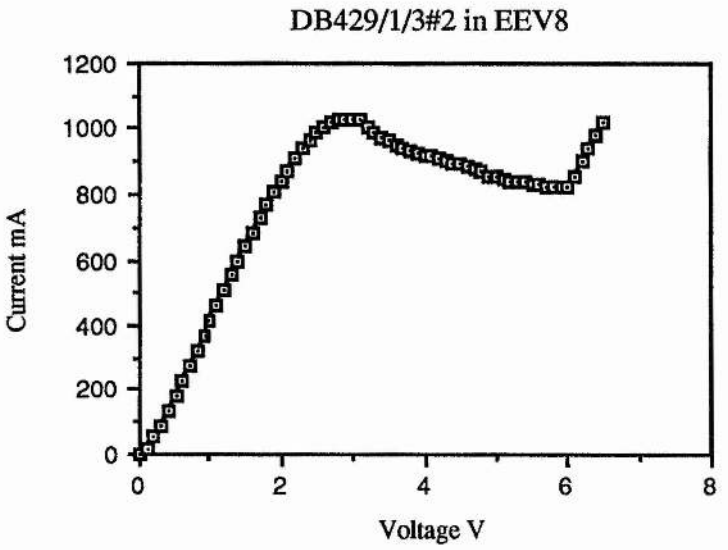

Figure 3.15.

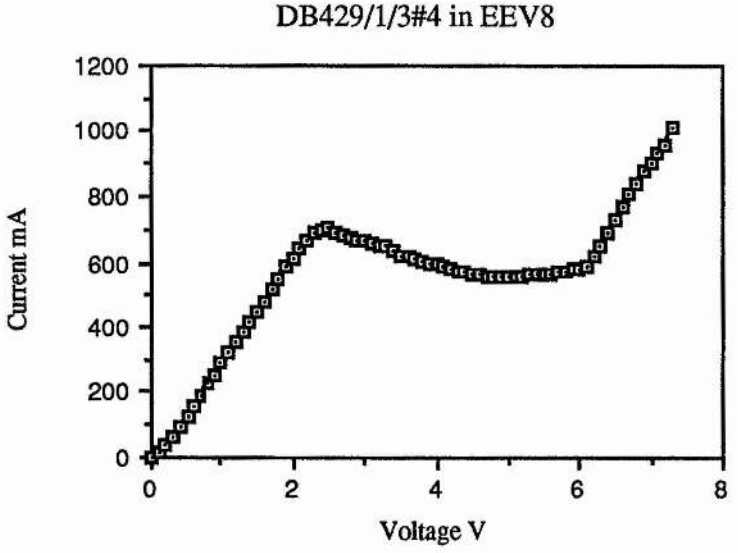

Figure 3.16.

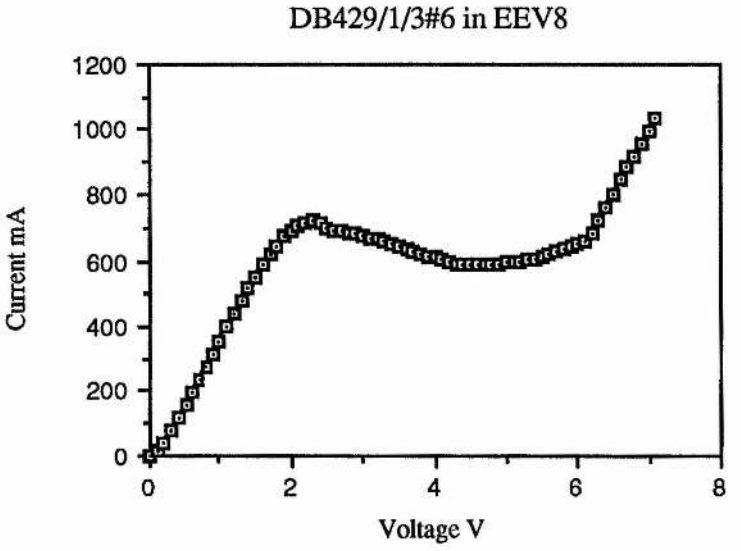

Figure 3.17.

3.2.5. Bias Oscillations

Monitoring the bias supply with an oscilloscope showed that every diode suffered from bias oscillations over some part of the negative resistance region. The frequency and amplitude of the bias oscillations varied, but typically were in the region of tens of megahertz, and between 2mV and 20mV peak-to-peak. Usually there were several frequencies present. As the bias voltage was increased to beyond about (±)4.5V, the bias oscillations disappeared.

Bias oscillations can occur with Gunn diodes if they exhibit negative resistance at low frequencies, and if the diode can see a suitable load against which it can resonate. The contacts in the choke, the protection circuit in the oscillator block, the bias lead and the bias supply can all resonate against the diode. In general it is best to try to eliminate this problem as close to the active device as possible, although there is no doubt that careful design of the bias supply can minimise the problem. Introducing lossy ferrite material into the choke structure could help to suppress bias oscillations,

but due to the current design of our chokes this has not been possible. Attention was therefore focussed on the protection circuit situated in the top section of the oscillator block (Figure 3.18).

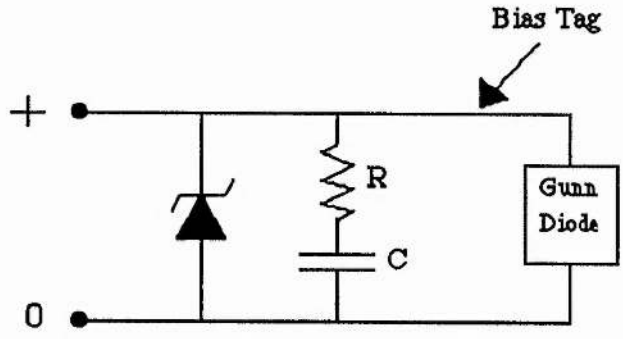

Figure 3.18. Diode protection circuit.

R is typically 22Ω and C ranges from 0.1μF to 0.01μF. These values were changed over a fairly wide range but had little or no effect. The Zener diode (usually around 6.5V) was removed and then replaced, again with no noticeable effect. Threading several ferrite beads onto the bias tag reduced the amplitude of oscillation for some, but not all, of the diodes.

All diodes operated well once they were biased above a certain level, with no further evidence of bias oscillations. In most applications, therefore, these diodes would not cause any problems. An important exception, however, is bias tuning.

3.2.6. Bias Tuning

Varying a Gunn diode's bias voltage causes the output frequency to vary as the device capacitance changes. Bias tuning is a widely-used technique in applications such as phase-locking and frequency modulation. It is convenient when measuring the variation of frequency with bias to mix the signal down to a much lower frequency, so that the frequency variations are more easily observed (Figure 3.19).

In order to monitor the change in frequency caused by varying the bias voltage, the oscillator output was mixed with the output of a low-noise, high power InP device

to produce an intermediate (IF) signal of a few hundred megahertz. Both oscillators were set separately to 94 GHz and then connected via two 10dB couplers and an isolator to prevent any modulation of one oscillator by the other. The two signals were mixed by a Flann diode mixer and the d.c. component filtered off to be used as a measure of signal strength. The diode mixer's backshort was adjusted to match impedances, and the IF signal was displayed on a Hewlett-Packard HP8558B spectrum analyzer.

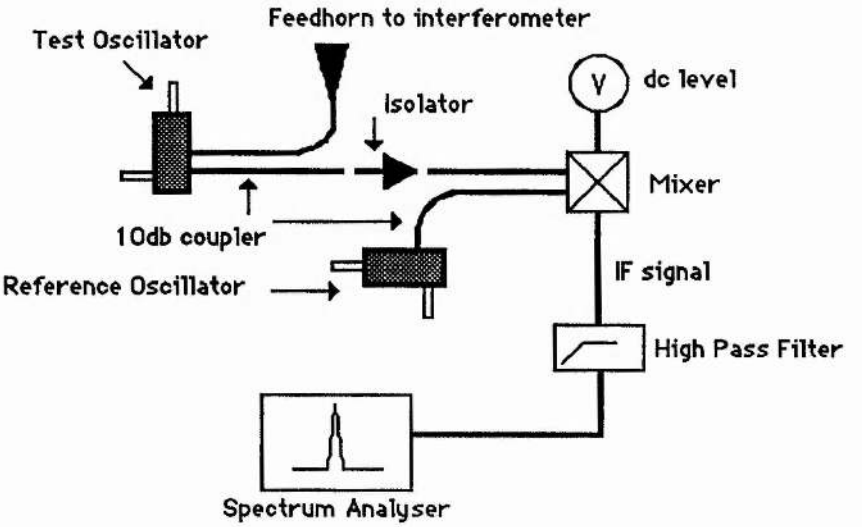

Figure 3.19. Bias Tuning

The oscillators were switched on and allowed to stabilise thermally. Bias tuning curves were obtained for the three negative top-cap devices (Figures 3.20-3.22). Unfortunately, the presence of bias oscillations made it impossible to tune at voltages below about -4.5V.

The stability of the IF signal was estimated to be 200kHz s^{-1}, 0.5MHz per 10s, with a long term drift of 10-20MHz, and the FWHM was typically a few kHz. Since the IF signal is the difference between two mm-wave frequencies, one would expect the absolute stability of either of the oscillators to be better than this.

Thermally induced frequency shifts were easily seen. Turning one oscillator off to let it cool down and then turning it back on again showed frequency shifts of tens of megahertz as the cavity warmed up. Also noted was the effect the backshort had on frequency, shifting up to 25MHz each way.

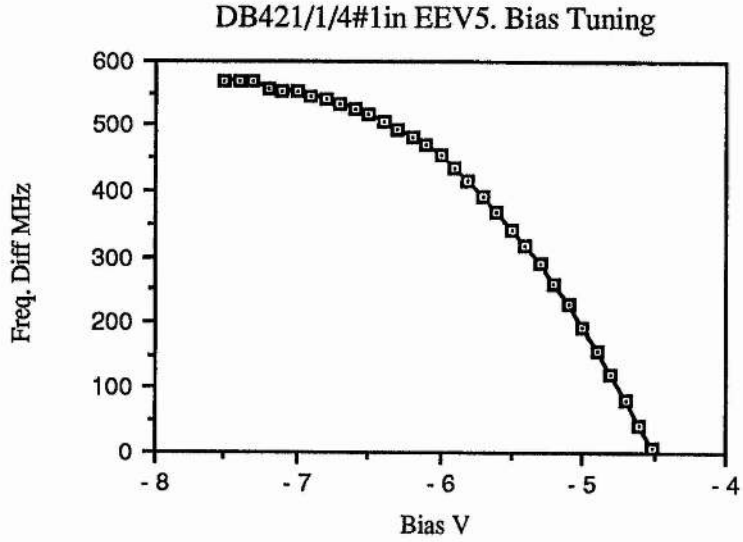

Figure 3.20.

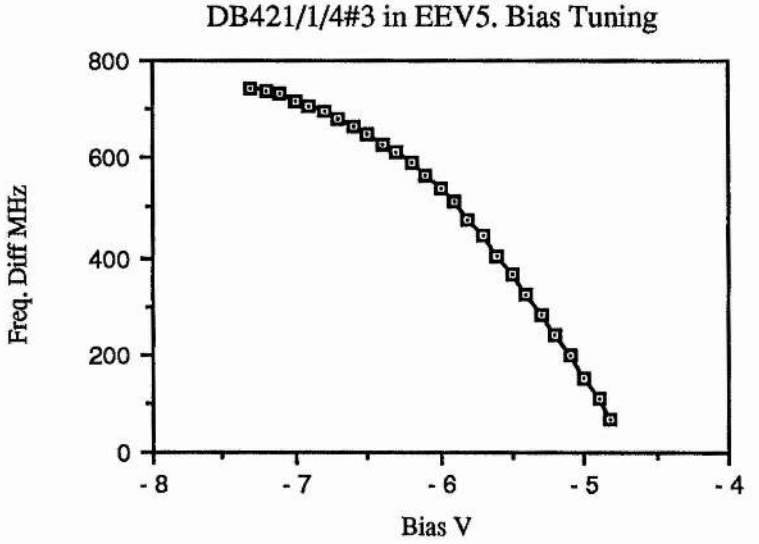

Figure 3.21.

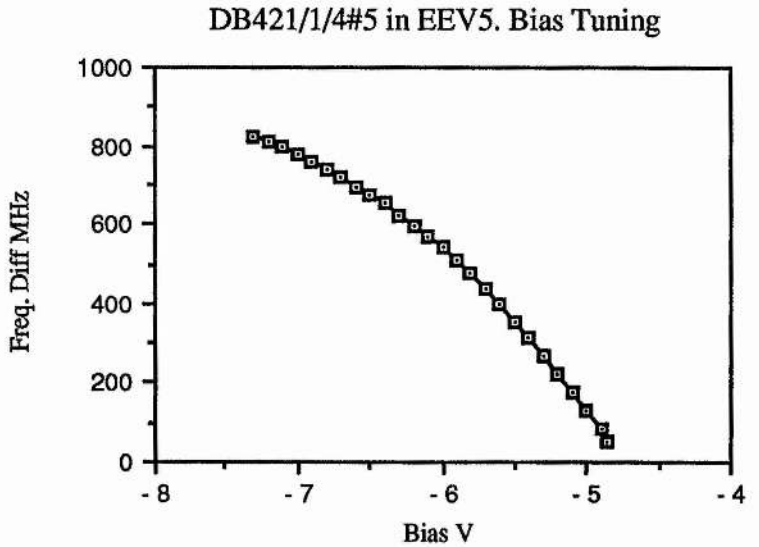

Figure 3.22.

Bias tuning is a relatively straightforward way of providing fine control over frequency, but should be treated with caution especially if one is attempting to sweep over a large (more than a few hundred MHz) frequency range. Potential problems include bias oscillations, overheating of the diode leading to premature failure, fluctuations in output power and worsened thermal stability. If fine bias control is required, for example when phase-locking the oscillator, the main requirement is that the bias supply must be stable at the millivolt level, i.e. it must have a very low noise floor.

3.3. Measurement of Thomson and Varian Gunn Diodes.

In the previous section, all of the prototype Gunn diodes were placed in nominally identical circuits in order to compare their performance. However, the more usual procedure when setting up a Gunn oscillator with a particular diode is to employ an iterative process to determine the (critical) cap and post dimensions which give the desired power/frequency characteristics. The graphs provided by Carlstrom et al [2] are a useful guide in the determination of the correct cap dimensions. A summary of their results are set out in Chapter 2.

The majority of the commercially available Gunn diodes used at St.Andrews are bought from Varian [5], with a few acquired from other sources such as Thomson [6]. While many of the oscillators built in St.Andrews are for use in our own laboratories, a number have been sold on a commercial basis to Government institutions, research laboratories of large companies, and other Universities. In such cases, the oscillator must be set up to satisfy a certain minimum specification regarding frequency range and the minimum power output over that range. This section details the cap/post dimensions, the type of diode used and other circuit parameters of some of these oscillators. The resulting power/frequency characteristics may be regarded as state of the art.

3.3.1. Wide-Band InP High-Power Oscillator .

This oscillator, supplied to the University of Kent, was required to produce at least 10mW from 72 to 92GHz. The wide-band tuning dictated the use of a second

harmonic device, and the high-power requirement led to the choice of a Varian 94GHz InP diode, type VSB9122S13. With the diode mounted in a full-height WG27 block with 3mm cavity, the optimum cap diameter was determined to be 2.32mm on a 1.0mm post. As with most oscillators, the diode was raised slightly in the cavity to help optimise the power. The power/frequency characteristics are shown in Figure 3.23.

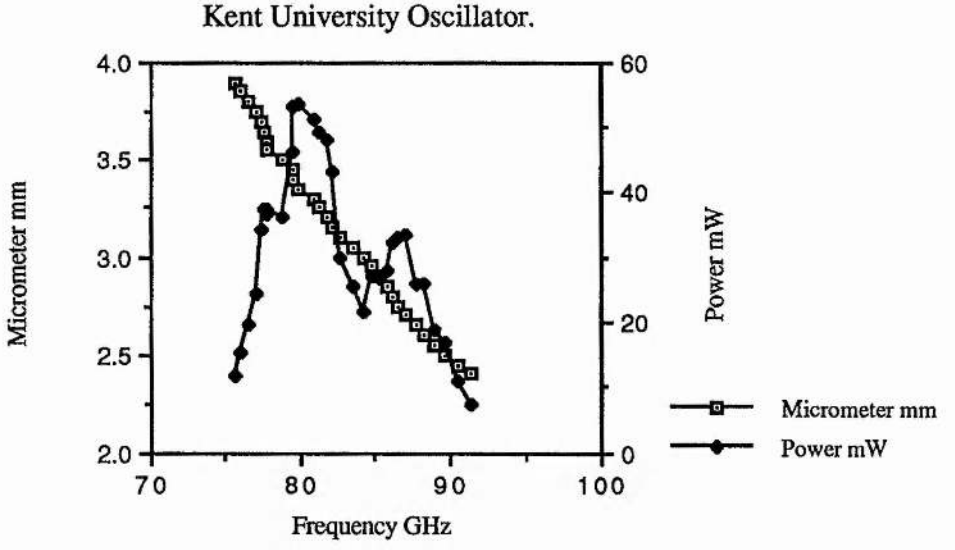

Figure 3.23

The graph shows that the actual frequency range achieved was about 76GHz to 91GHz, slightly less than specified. However, the application of the oscillator demanded that useful power at 73.5GHz be available. Consequently, a number of larger diameter caps were manufactured in an attempt to shift the frequency band downwards. This was achieved, but at the expense of the upper end of the frequency band, where 89.5GHz was also a critical frequency. In such cases, the usual course of action is to replace the diode with another nominally identical diode from the same batch. This approach exploits the small differences which always exist between diodes from the same wafer. Using the original 2.32mm diameter cap, the new diode covered a slightly wider frequency range, including 73.5GHz and 89.5GHz, but at the expense of creating a large resonance at around 77GHz and a smaller resonance at around 86GHz (Figure 3.24). Despite these (unavoidable) resonances, the oscillator was considered suitable for its application.

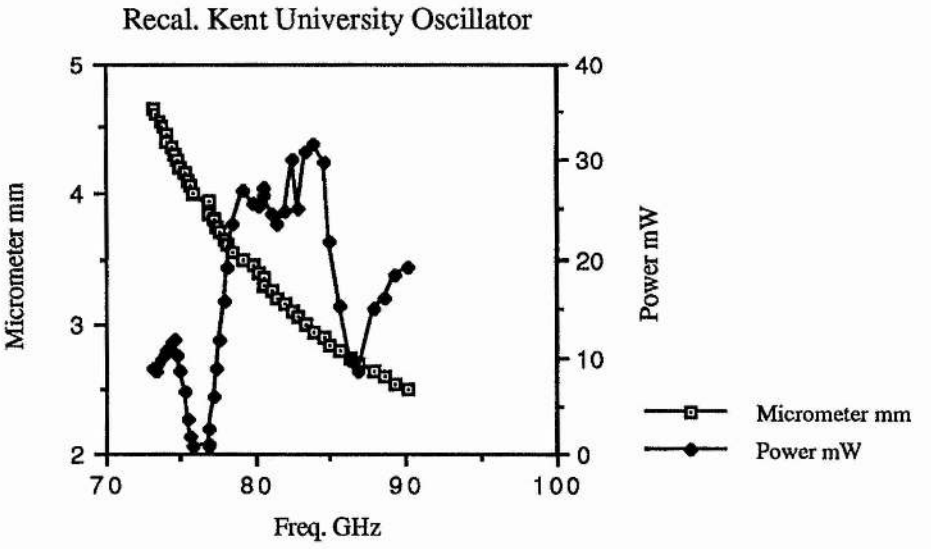

Figure 3.24.

3.3.2. Narrow-Band InP High-Power Oscillator.

The specification for this oscillator, supplied to British Aerospace Space Systems Ltd, was to provide 30mW from 73-77GHz. This combination of a narrow frequency range and high power meant that a fundamental InP diode would be a suitable choice. The diode, an 80GHz fundamental InP device from Varian, type VSB9122S4, was mounted in a standard full-height WG27 block with 3mm cavity. Impedance transformation was effected by an inductive post 1.0mm in diameter. The resulting frequency/power characteristic is shown in Figure 3.25.

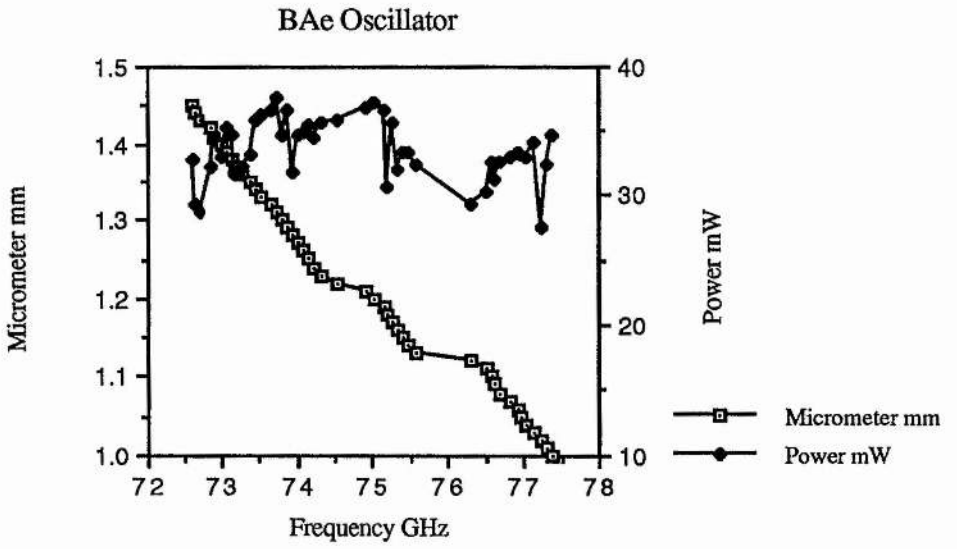

Figure 3.25.

3.3.3. Narrow-Band High-Power High-Frequency Oscillator.

Unusually, the Centre National de la Recherche Scientifique in Toulouse did not actually specify the performance they required from this oscillator. Instead, they supplied a 94GHz fundamental InP diode made by Thomson for incorporation into an oscillator. Using an identical circuit to that used for the BAe oscillator yielded the characteristics shown in Figure 3.26. In common with other fundamental oscillators, this oscillator tunes over a rather narrow frequency range (compared with second harmonic devices).

Since the operating frequency of fundamental oscillators is prone to load-pulling, it is normal practice to mount a waveguide isolator on the oscillator block. The position of the backshort can also pull the frequency much more than with second harmonic oscillators (see Chapter 2). In all the power/frequency curves presented here, the backshort was adjusted to give the maximum power at each frequency setting.

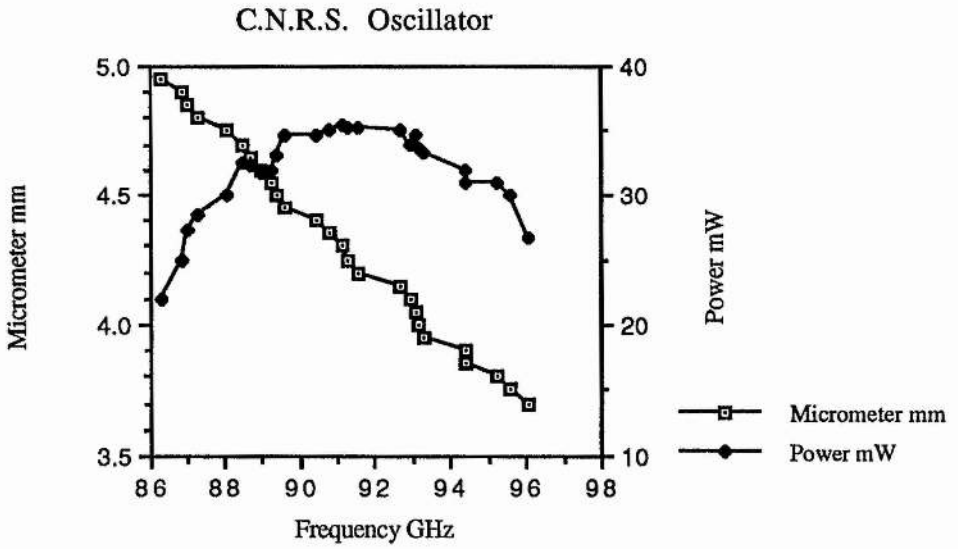
C.N.R.S. Oscillator
5.0
4.5
4.0
3.5
Micrometer mm
40
30
20
10
Power mW
86
88
90
92
94
96
98
Frequency GHz
Micrometer mm
Power mW

Figure 3.26

Chapter 3 References.

[1] G.M.Smith, "Transferred Electron Oscillators at MM Wave Frequencies And Their Characterisation Using Quasi-Optical Techniques", PhD Thesis, St.Andrews University, 1990.

[2] J.E.Carlstrom, R.L.Plambeck and D.D.Thornton, "A Continuously Tunable 65-115 GHz Gunn Oscillator", *IEEE Trans. Microwave Theory Tech.*, vol. MTT-33, no.7, pp. 610-619, 1985.

[3] W.H.Haydl, "Fundamental and Harmonic Operation of Millimeter-Wave Gunn Diodes", *IEEE Trans. Microwave Theory Tech.*, vol. MTT-31, no.11, pp.879-889, 1983.

[4] D.H.Martin, "Martin-Puplett Interferometric Spectrometers", *Infrared and Millimeter Waves*, vol.6, K.Button, ed., New York: Academic Press 1982.

[5] Varian, Solid State Microwave Division, 3251 Olcott Street, Santa Clara, CA 95054.

[6] Thomson-CSF Division Composants Hybrides et Microondes, 29, Avenue Carnot, B.P. 58, 91302 Massy Cedex, France.

4. Theory of Quantum Well Devices

4.1. Low Dimensional Structures

Recent advances in the techniques of molecular beam epitaxy (MBE) and metal-organic chemical vapour deposition (MOCVD) have enabled physicists to fabricate single crystals of metals, insulators or semiconductors with interfaces smooth to the atomic layer limit. In addition, the ability to grow extremely thin layers (<100Å) results in the quantum mechanical restriction of the degrees of freedom of electrons, giving rise to novel electronic, magnetic, optical and vibrational properties. Such systems are known as low dimensional structures (LDS).

One of the first low dimensional structures to be proposed and modelled was a finite 'superlattice' consisting of alternate layers of GaAs and $Ga_{1-x}Al_xAs$. Figure 4.1 shows the spatial variation of the conduction and valence band edges perpendicular to the layer planes.

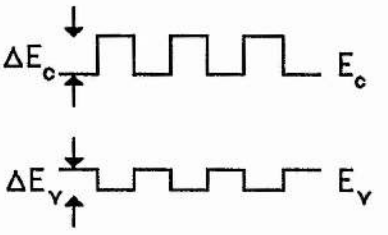

Figure 4.1

GaAs has a smaller band gap than $Ga_{1-x}Al_xAs$, hence the periodic square-well potential of the conduction band. Such a structure, with a large superlattice period, lends itself particularly well to the application of the Kronig-Penney model, originally developed to calculate the band structure of bulk semiconductors. (See, for example, C.Kittel, Introduction to Solid State Physics, 5th Edition, Wiley.) The square-well periodic potential introduced by Kronig and Penney allows the wave equation to be solved in terms of simple analytic functions, resulting in allowed energy bands separated by forbidden energy gaps (Figure 4.2). This can also be regarded as the reduction of the Brillouin zone into a series of minizones due to the introduction of a

large superlattice period which must, nonetheless, be small when compared with the electron mean free path.

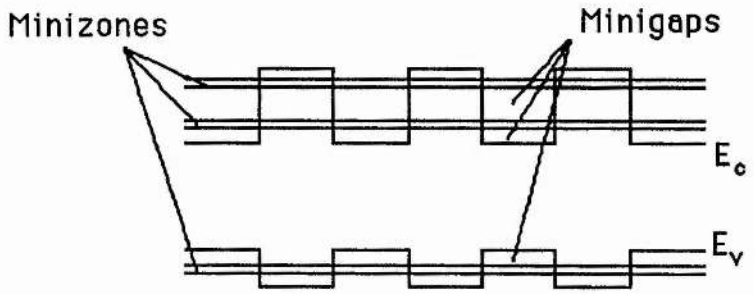

Figure 4.2. Minizones in a superlattice.

4.2. Vertical Transport - Electron Tunneling.

Vertical transport through a superlattice refers to electron transport perpendicular to the lattice layers. In this regime, the important transport mechanism is electron tunneling through the potential barriers in the conduction band, where the periodic structure of the superlattice serves as a filter to the electron energy through the superlattice, giving rise to regions of negative differential conductivity (NDC) in the current - voltage (I-V) characteristic of the device. NDC can be exploited for a number of uses in, for example mixers and detectors, (where strictly speaking any non-linear I-V characteristic will do) and in the construction of oscillators for operation in the millimetre and sub-millimetre bands.

Tsu and Esaki [1] first calculated the transport properties of a finite superlattice by applying the formalism of multibarrier tunneling to the system. By writing the total energy E as the sum of the longitudinal and transverse energies, i.e.

$$E = E_l(V) + \hbar^2 k_t^2 / 2m^* \qquad (4.1)$$

one can separate the three-dimensional Schrödinger equation for the one-dimensional periodic potential V(x), where x is along the direction of the

multibarriers, into transverse and longitudinal parts.

The wave equation is expressed by the product

$$\psi = \psi_l \psi_t \qquad (4.2)$$

The electron wave-functions in the left and right contacts of an n-period superlattice are respectively

$$\psi_1 = \psi_t[\exp(ik_1 x) + R\exp(-ik_1 x)] \qquad (4.3)$$

$$\psi_n = \psi_t[T\exp(ik_n x)] \qquad (4.4)$$

where R and T are the reflection and transmission amplitudes. By matching the derivatives and values at each discontinuity, Tsu and Esaki were able to calculate the transmission coefficient T*T versus the electron energy for the cases of two, three and five barriers. Due to a separation of variables, T*T is a function only of the longitudinal energy. In theory the calculations may be applied to any number of barriers though in practice the extent of the electron mean free path is only a few superlattice periods. Figure 4.3 shows the transmision coefficient T*T for the cases of two (20Å - 50Å - 20Å), three and five barriers. In the case of two barriers, the transmission curve is very similar in shape to the I-V curve which shows peaks in the tunnelling current corresponding to peaks in the transmission probability.

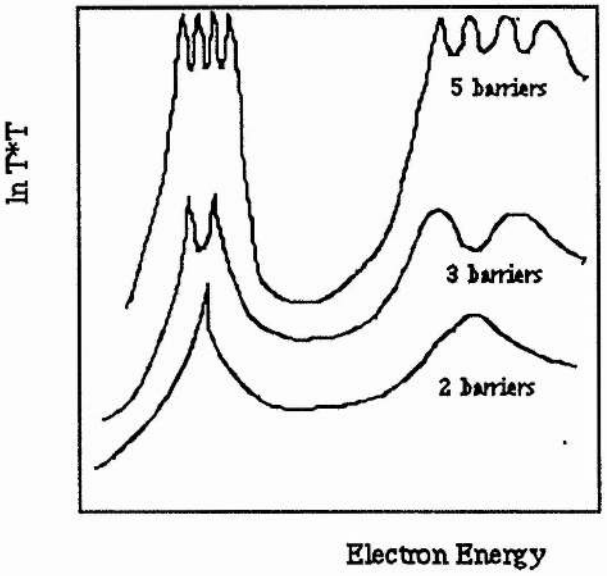

Figure 4.3. Transmission Coefficient T*T.

4.3 . The Double Barrier Diode .

The double barrier diode, the 'two-barrier' case above, consists of a single thin layer of normally undoped GaAs sandwiched between two layers of the larger band-gap $Ga_{1-x}Al_xAs$, and as such resembles a small portion of a superlattice (Fig 4.4). In the case of the superlattice, electron transport depended on tunneling from one minizone to another through a potential barrier. The double barrier diode, however, does not have minizones separated by minigaps; rather, electron transport depends on the presence of allowed states in the central quantum well.

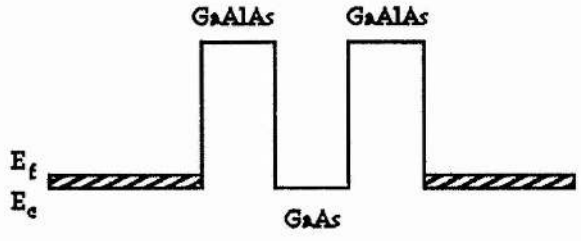

Figure 4.4. Double Barrier Diode.

To show how these allowed states arise, let us refer to the paper by Ricco and Azbel [2]. They considered the case of a generalised double barrier structure (Figure 4.5) which is straightforward to solve and has exact analytical solutions. Following their working, one can write the global transmission coefficient of the whole barrier as

$$T_G = \frac{C_0}{C_1 T_l T_r + C_2 \frac{T_l}{T_r} + C_3 \frac{T_r}{T_l} + \frac{C_4}{T_l T_r}} \qquad (4.5)$$

where T_l and T_r are the transmission coefficients of the left and right barriers respectively, and are exponentially dependent on energy. The C's are phase factors depending much more weakly on energy and may be regarded as constants (of the same order of magnitude). T_l and T_r are small (<<1), so equation 4.5 becomes

$$T_G \approx \frac{C_0}{C_4} T_l T_r \approx T_l T_r \qquad (4.6)$$

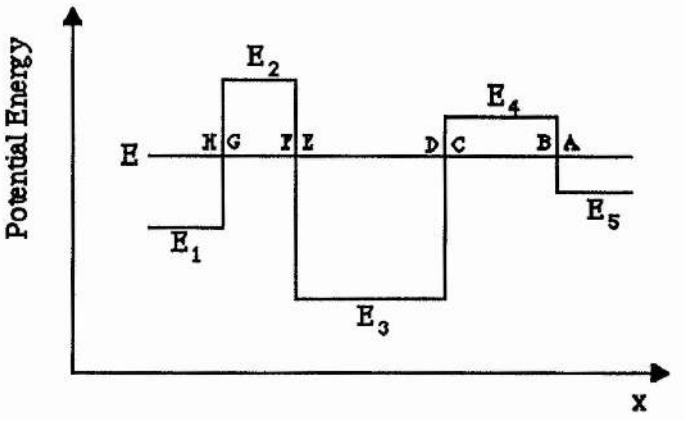

Figure 4.5

For some particular energies, however, C_4 vanishes, leading to strong resonances:

$$T_{G\,res} \approx C\frac{T_{min}}{T_{max}} \approx \frac{T_{min}}{T_{max}} \qquad (4.7)$$

where T_{min} and T_{max} represent the smaller and larger of T_l and T_r, respectively, and C is either C_0/C_2 or C_0/C_3, depending on whether $T_{max}=T_l$.

By comparing equations 4.6 and 4.7 we see that

$$\frac{T_{G\,res}}{T_G} = \frac{1}{T_{max}^2} \qquad (4.8)$$

The expressions in 4.6, 4.7 and 4.8 illustrate that while the presence of the quantum well has virtually no effect off resonance, the transmission coefficient can increase dramatically with very small energy changes which produce resonance.

The condition for resonance to occur, that C_4 must vanish, is satisfied by the energy E of the tunneling carriers matching the energies of the well (quasi) eigenstates. This is written mathematically as

$$k_3 d_3 = \tan^{-1}\frac{\alpha_2}{k_3} + \tan^{-1}\frac{\alpha_4}{k_3} + (n-1)\pi \qquad (4.9)$$

where

$$k_i = \hbar^{-1}[2m^*(E-E_i)]^{\frac{1}{2}}$$

and

$$\alpha_i = \hbar^{-1}[2m^*(E_i-E)]^{\frac{1}{2}}$$

E_i denotes the potential energy, k_i refers to the classically allowed regions and α_i refers to the classically forbidden regions. The subscript numbering goes as Figure 4.5.

If we assume that the device has symmetrical barriers (Figure 4.6), equation 4.9 can be expressed as (using the notation of Figure 4.6)

$$\hbar^{-1}\sqrt{2m^*E}\,w = 2\tan^{-1}\frac{(\phi_0-E)^{\frac{1}{2}}}{E^{\frac{1}{2}}} + (n-1)\pi \qquad (4.10)$$

Solving equation 4.10 yields the values of the eigenstates within the quantum well, for the the case of no applied field. The solutions agree with those obtained by Chang, Esaki and Tsu [3], from the transmission expression derived by Tsu and Esaki.

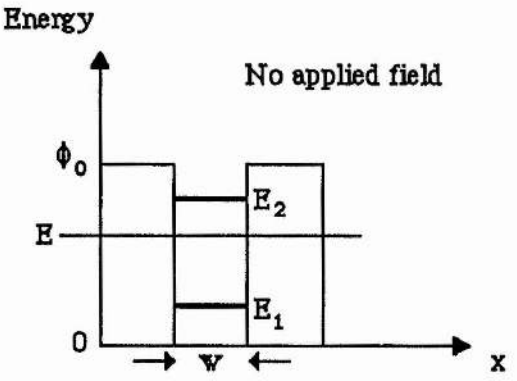

Figure 4.6

4.4 . Negative Resistance

The origins of negative resistance are depicted in the energy band diagrams of Figure 4.7. The electrons originate near the Fermi level to the left of the first barrier, tunnel into the well and then tunnel out through the second barrier. Resonance occurs when the energy of the injected carriers becomes approximately equal to the energy

level E_1 of the electrons confined within the well, and the current rises rapidly. As one increases the bias further so that the range of electron energies in the contact layer is higher than E_1, the current falls to its lower, non-resonant value. The result is that the current-voltage characteristic shows pronounced negative resistance. Increasing the bias voltage still further can result in a second resonance at the second energy level within the well [3, 4], though in many cases thermal excitation of electrons over the barriers can obscure this effect.

4.5 . The mechanism of tunneling, and theoretical frequency limits.

The theoretical frequency limit of a double barrier diode (DBD) is directly related to the speed of transport of carriers through the device. Any attempt to predict the frequency limit of a DBD will also involve modelling the transport processes through the structure.

Ricco and Azbel [2] examined in detail the mechanism of tunneling and in particular highlighted some phenomena which until then had been largely overlooked. Two important points were identified - first, any non-negligible applied field will destroy the symmetry of the double barrier, as can be seen in Figure 4.7. This alters the transmission coefficients through each barrier and causes the resonance effect to be reduced. Recalling that, from equation 4.7, the global transmission coefficient at resonance, $T_{G\,res}$, is maximised when $T_l=T_r$, we see that there will be a reduction in the global transmission coefficient if $T_l< T_r$. If one were to make the left-hand barrier thinner than the right-hand barrier, one might hope to be able to recreate the optimal condition of $T_{G\,res}\approx 1$. However, such optimum conditions do not always exist, they require some non-trivial engineering, and are specific of a given resonance peak.

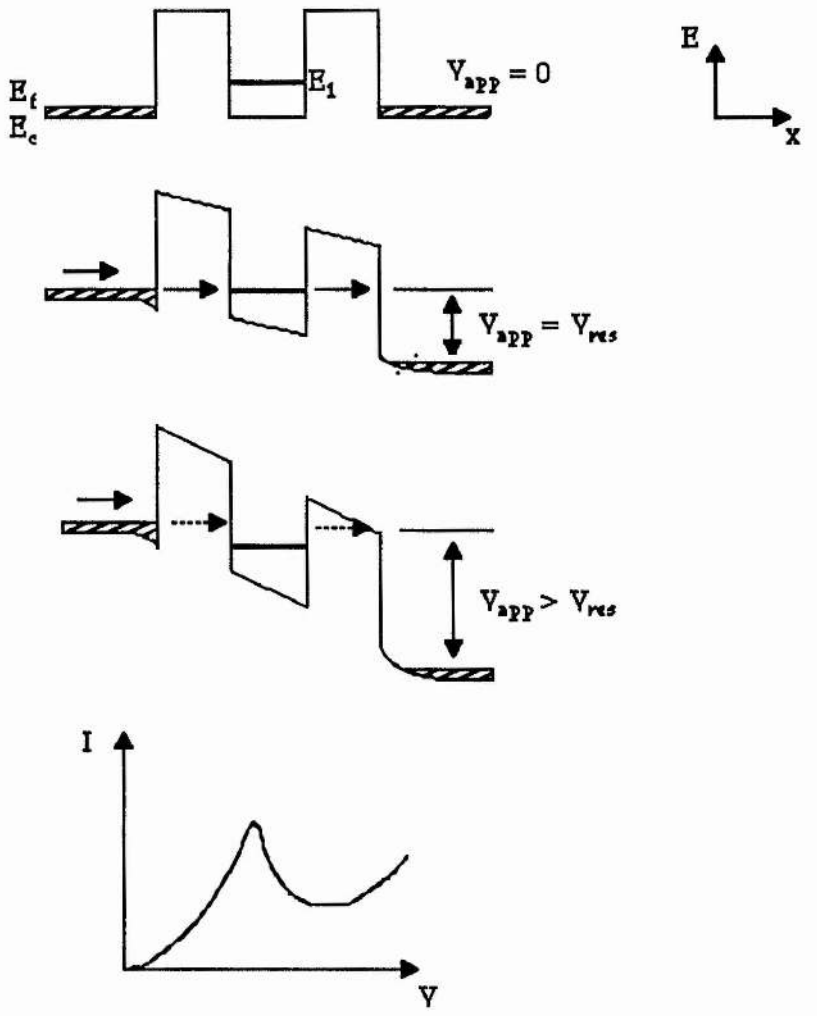

Figure 4.7.

The second point which is made is that in some cases there may be a non-negligible time required in order to establish fully a resonant state. Equation 4.10 is based on the solutions of the time-*independent* Schrödinger equation, so this requires the wave equation at resonance to be strongly localised. Physically, this means that the quantum well must be 'filled up' with electrons before resonant tunneling can be fully established. A time constant τ_0 is associated with this process, which is assumed to be the resonant state lifetime, i.e.

$$\tau_0 \approx \frac{\hbar}{\Gamma} \propto \frac{1}{T_{max}} \qquad (4.11)$$

where Γ is the resonance width which can be estimated from [5]

$$\Gamma \approx E_k e^{-2d\kappa} \qquad (4.12)$$

and is also related to the magnitude of the NDR by

$$R_n = \frac{4\pi^2\hbar^3}{e^2 m^* A} \quad \frac{1}{E_f - \frac{\pi\Gamma}{2}} \qquad (4.13)$$

This time constant τ_0, say Ricco and Azbel, can have non-negligible and even quite large values. In the case of references 3 and 9 they calculated $\tau_0 \approx 10^{-11}$ seconds which is acceptably fast, but calculated $\tau_0 \approx 10^6$ seconds from a paper in the Japanese Journal of Applied Physics which, unfortunately, was incorrectly referenced. Apparently the barrier height used was large which made T_{max} too low. (Incidentally, 10^6 seconds is about 11.5 days!) However, once the eigenstate is filled up with all the carriers it can accommodate, a much shorter time becomes important. This is the time required for a carrier to cross a single barrier, since we can imagine an incoming electron 'pushing out' other electrons through the second barrier [2], and is of the order of 10^{-13} to 10^{-15} seconds.

In considering the time constant τ_0 to be the fundamental limitation on speed for most practical devices, Luryi [6] proposed that a simple estimate of τ_0 could be the RC time constant of the 'quantum capacitor' formed between the QW and the controlling electrodes. Basing his calculations on a WKB expression [7] for the current density [8], Luryi found, for the DBD's used in references 9 and 10, that $f_{max} \approx$ 4GHz. Although not inconsistent with the 18GHz oscillations acheived by Sollner et al [10], it was almost three orders of magnitude lower than the frequency of the same group's detector experiments [9]. In attempting to explain this high frequency behaviour Luryi proposed that, instead of relying on a resonant Fabry-Perot type effect, NDR could arise solely out of electrons tunneling from a three-dimensional system of states to a two-dimensional system of states such as a QW.

To see how this happens, consider Figure 4.8 which illustrates in k-space the Fermi sea of electrons in a degenerately doped emitter. During the tunneling process, the lateral electron momentum (k_x, k_y) is conserved. Thus for $E_c<E_1<E_f$ tunneling is only possible for electrons whose momenta lie in the shaded disc in the figure, i.e. for $k_z=k_1$. As the emitter potential rises, the disc moves downwards in the direction of the equatorial plane of the Fermi sphere and more and more electrons are able to tunnel through the barrier. When E_c rises above E_1 then (assuming T=0, no thermal excitation) no electrons can tunnel into the QW *and* conserve their lateral momentum, so the tunneling current falls. Luryi also commented that should this mechanism be operating, then the symmetry of the barriers should not be important. This type of tunneling is known as *sequential* tunneling - the carriers tunnel into the QW and subsequently tunnel out again through the right-hand barrier.

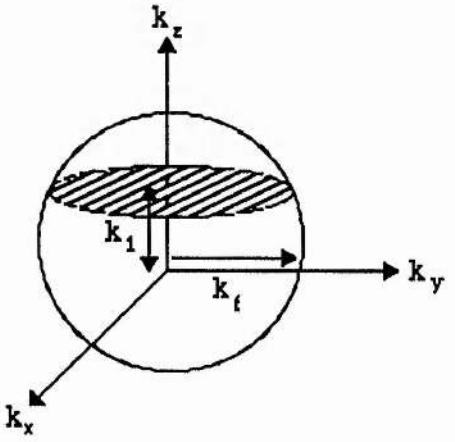

Figure 4.8.

The oscillation frequencies of 56 GHz [11] and 108 GHz [4] obtained by Brown et al and Sollner et al respectively, cast doubt on the validity of the WKB approximation as a means of calculating f_{max}. The WKB approximation is valid for slowly varying functions (or potentials), which, on the scale of the carrier wavelength, is not the case for the potential in the DBD structure. One must also be aware that the carrier is contained between two barriers which are separated by less than the carrier wavelength, hence the carrier is located partially outside both barriers at any time. This has the effect of increasing the probability of escape.

A useful comparison of methods of estimating f_{max} was set out by Sollner et al [12]. By examining parts of the problem separately they were able to calculate a characteristic time for each part, thus setting bounds for the maximum frequency of response. Although not a complete solution, it nonetheless gives an idea of the maximum oscillation frequencies one could expect, limited by: the device equivalent circuit (Figure 4.9); the transit time across the depletion region on the collector side; the WKB estimate of charge storage within the well; Luryi's estimate of charge storage within the well; Kundrotas and Dargys' estimate of electron lifetime in a well with infinitely thick barriers [13]; and the calculation of the energy width of the transmission through the DBD (equation 4.11). For clarity, Sollner's table of measured and calculated parameters is reproduced in Table 4.1.

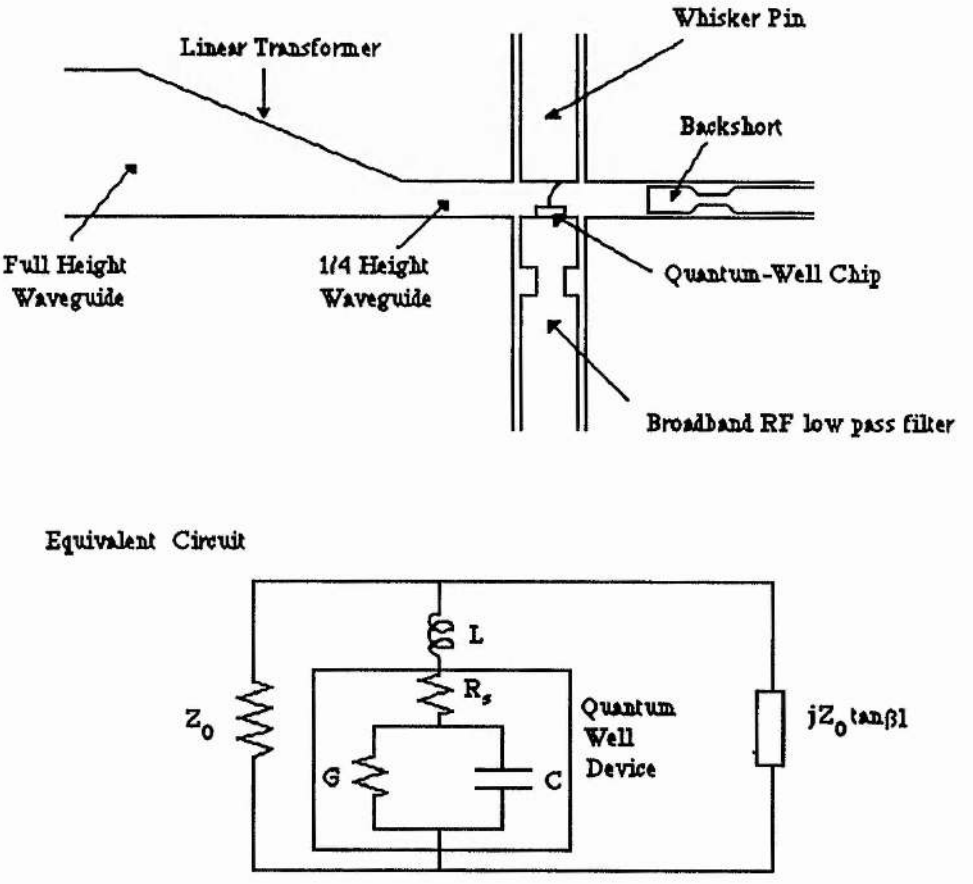

Figure 4.9. Device equivalent circuit.

Table 4.1. Measured and calculated parameters for three different wafers of DBD's.

	Sample		
	1	2	3
Material Parameters			
Barrier material	AlAs	$Ga_{0.7}Al_{0.3}As$	AlAs
Barrier thickness (nm)	2.5	3.0	1.5
Well thickness (nm)	4.5	4.5	4.5
Doping outside barriers (cm^{-3})	$1x10^{18}$	$2x10^{17}$	$2x10^{17}$
Electrical Parameters			
Peak-valley ratio, 300K	1.7/1	1.3/1	3.5/1
Peak current density ($x10^4 A\ cm^{-3}$)	0.8	1.2	4.0
Depletion layer at bias (nm)	15	30	70
Capacitance (fF)[a]	100	50	20
Max. neg. conductance (mS)[a]	5.0	8.0	13.0
Series resistance (Ω)[a]	10	15	15
Oscillation Characteristics			
dc bias I_B, V_B (mA,V)	0.7,0.40	2.7,0.32	3.0,0.95
f_{osc}(GHz)[b]	20.7	43.7	56.4
Theoretical			
Max. oscillation frequency			
f_{circ}(GHz)[c]	35	70	200
f_{depl}(GHz)[d]	1000	500	230
f_{WKB}(GHz)[e]	0.01	220	6.0
f_L(GHz)[f]	0.01	60	6.0
f_{KD}(GHz)[g]	130	300	100
$f_{\Delta E}$(GHz)[h]	80	2100	800

[a] Typical values for a circular mesa of 4μm diameter.
[b] Maximum observed fundamental oscillation frequency.
[c] $f_{circ}=(2\pi C)^{-1}(-G_{max}/R_s - G^2_{max})^{1/2}$
[d] From depletion layer drift time.
[e] WKB estimate of charge storage time in well.
[f] From ref.6 for charge storage time in well.
[g] From ref.13, for electron lifetime in well with infinitely thick barriers.
[h] From calculation of energy width of transmission through double-barrier structure.

It is clear that the WKB method is not suitable as a means of calculating the maximum frequency of oscillation of QW devices. Sollner et al suggested that a consideration of the transmission energy width, bearing in mind transit time effects and the device equivalent circuit, would give the best estimate of f_{max}.

Jogai, Wang and Brown [14] discussed the problem of maximum frequency of QW oscillators and estimated that for a double-well device, an upper limit of a few hundred GHz would be expected. Single-well devices would be much faster say the authors, although they express some doubt that Sollner's detection of NDR at 2.5THz actually depended on the origin of the NDR. Their estimate of the tunneling time was based on the time evolution of a Gaussian wave packet in the vicinity of a double-well, triple-barrier device, and required a numerical solution of the time-dependent Schrödinger equation. (Recall that Ricco and Azbel solved the time-*independent* Schrödinger equation, with the associated concept of strong localisation.) It is not clear why Jogai et al should have chosen to examine a double-well device rather than the more usual single-well device.

Coon and Liu [5] had pointed out that small NDR (or alternatively, large NDC) is desirable for high-frequency operation and calculated that if Sollner's device [10] had had the theoretical minimun R_n of 0.5Ω instead of the measured R_n of 400Ω, f_{max} would rise to about 1THz. It is interesting to note that the minimum R_n is not practically obtainable since there is a trade-off between small R_n and small Γ, the resonance width. We see from equation 4.13 that NDR is directly related to the resonance width. If the resonance width is reduced to zero then we have

$$\text{Minimum } R_n = \frac{4\pi^2\bar{h}^3}{e^2 m^* A}\ \frac{1}{E_f} \qquad (4.14)$$

However, the time delay associated with zero Γ is, from equation 4.11, infinite, so reducing Γ indefinitely will eventually degrade the maximum oscillation frequency. For $f_{max} \approx$ 1THz then Γ should not be less than about 1meV.

A different approach was adopted by Frensley [15] who used quantum transport theory to evaluate the linear and lowest order non-linear response of a QW resonant tunneling diode. He considers the Liouville equation

$$\frac{\partial f}{\partial t} = \frac{L}{i\hbar} f \qquad (4.15)$$

where L is the Liouville (super)operator and f is the Wigner function [16], a single particle distribution function. By applying perturbation theory to L and f, Frensley was able to calculate the admittance of the device as a function of frequency and found the real conductance to be negative up to the terahertz region, becoming positive at around 6THz. This result is encouraging in that it appears to confirm that Sollner's detection of radiation at 2.5THz was indeed due to the the presence of NDR. However, Frensley calculated that a practical limit on the oscillation frequency would be around 40GHz, due to the 'circuit limit' (see Table 4.1), which is reached when the device negative resistance can no longer cancel the series resistance R_s.

Frensley, in his conclusion, remarks that Luryi's RC model is not the correct way to calculate the response time of the device and that the quantum transport approach accurately describes the process of carriers filling up the QW, with associated response times of the order of 10^{-13} seconds. He also refers to Luryi's sequential tunneling theory in stating that *"there appears to be no compelling reason to invoke incoherent processes to explain the behaviour of a normal resonant tunneling current near the peak of the I-V curve"*, although he does admit that such processes may become significant in the case of a very small current, such as in the valley of the I-V curve and in wide-barrier devices. In fact, it is now widely accepted that coherent and sequential tunneling processes occur simultaneously.

In 1988, Brown et al measured oscillations in the range 102 - 112 GHz in a WR-6 waveguide resonator, with a peak power of about 5μW [17]. The same diodes produced oscillations between 192 and 201 GHz in a WR-3 resonator and generated about 0.2μW peak power. Since the previous esimate of f_{max} for their fastest device was 186GHz [11], they found it necessary to make a more detailed analysis of the double-barrier diode.

The diodes in question were from wafer number 3 (see Table 4.1) and had been the best samples up till then, having oscillated at 56GHz. These diodes had thin (1.7nm) undoped AlAs barriers separated by a 4.5nm thick undoped GaAs quantum well. AlAs was the material of choice for the barriers since it had previously been identified as producing a large room-temperature peak to valley current ratio [18]. The large Γ-point discontinuity in the conduction band at the interface between the GaAs

and the AlAs helps to reduce the effects of thermionic emission of carriers over the barrier, but requires the barriers to be made thin. Thin barriers also allow large current densities, and decrease the lifetime of the carrier in the quantum well, thus increasing the frequency limit dictated by this lifetime. It is interesting to note that direct Γ-valley tunneling processes take place in the thin AlAs region rather than indirect, phonon assisted tunneling, because the time the wave packet spends in this narrow barrier is too short to allow the creation or absorbtion of phonons. Evidence of direct tunneling was confirmed by calculation of the Γ-point discontinuity (assuming 65% of the discontinuity occurs across the conduction band, 35% across the valence band) which gave a figure of 1.036eV. Measured I-V curves agreed best with theoretical I-V curves which assumed a conduction band discontinuity of 1.0±0.1eV.

Figure 4.10 shows the resonator circuit used to obtain high-frequency oscillations.

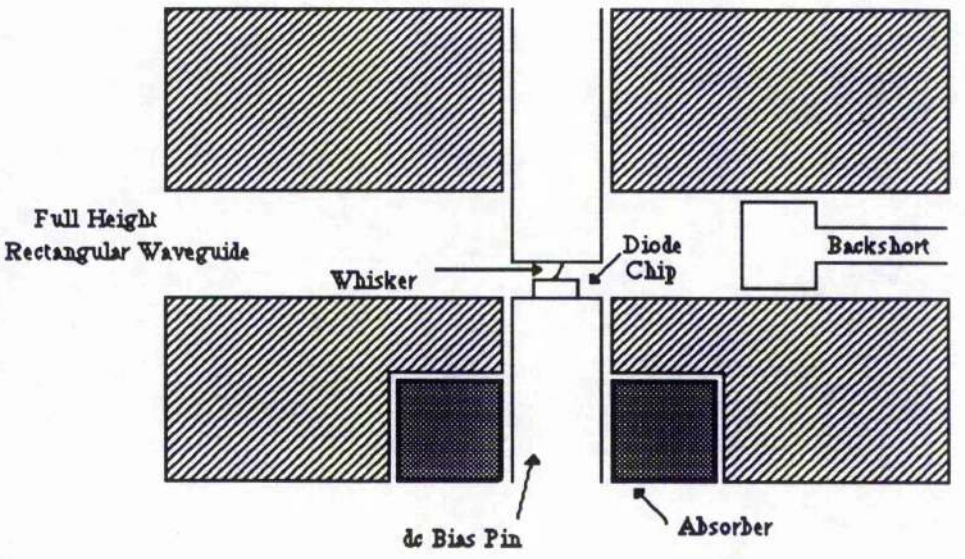

Figure 4.10. Waveguide resonator circuit.

The lumped equivalent circuit shown in Figure 4.9 was again used to find an upper bound on f_{max}. Assuming that all the elements of the circuit are independent of frequency, then the real part of the terminal impedance of this circuit is negative up to a frequency

$$f_R = (2\pi C)^{-1} (- G/R_s - G^2)^{1/2} \qquad (4.16)$$

R_s, the parasitic series resistance and the capacitance C are assumed to be nearly independent of bias voltage, but G varies rapidly from a maximum negative value G_{max} at the centre of the NDC region to zero at the peak and valley points; thus f_R may be considered as a function of G only.

The series resistance R_s may be written as

$$R_s(f) = \frac{\rho_c + \rho_e L_e}{A} + \frac{\rho_s}{\pi\delta} \left[0.5 \ln(b/d) + h/b\right] \qquad (4.17)$$

where A is the mesa area, ρ_c is the specific contact resistance, ρ_e is the epilayer resistivity and L_e is the total thickness of the undepleted epilayers on both sides of the heterostructure. The second, frequency-dependent term, relates to spreading resistance in the surrounding substrate where ρ_s is the substrate resistivity, b is the effective diameter of the chip, h is the chip thickness and δ is the skin depth in the substrate, given by

$$\delta = [2\rho/(\mu\omega)]^{1/2} \qquad (4.18)$$

where μ is the permeability and ω is the angular frequency. The assumptions are that the frequency is high enough that $\delta \ll b$ and also that $\delta \ll h$, but δ is much greater than the mesa diameter. Substituting equation 4.17 into equation 4.16, the lumped-circuit model, gives us the lumped-circuit model modified by the skin effect.

The third theoretical model proposed by Brown et al is a combined transit-time (across the depletion layer on the anode side) and skin-effect model. The real part of the terminal impedance is given by

$$R_T = \frac{1}{\omega C_D} \cdot \frac{\sigma}{\sigma^2 + \omega^2\varepsilon^2} \cdot \frac{\sigma(1-\cos\vartheta) + \omega\varepsilon \sin\vartheta}{\vartheta} + R_s(f) \qquad (4.19)$$

where σ is the injection conductance (dJ/dF) of the double-barrier structure, F is the electric field across the structure, ϑ, the transit angle equals $\omega D/v_d$ where v_d is the average drift velocity across the depletion layer of width D, $R_s(f)$ is given by equation 4.17 and $C_D = \varepsilon A/D$. The injection conductance was written, assuming the structure to be uncharged, as

$$\sigma = (D + W)\frac{dJ}{dV_J} = (D + W)\frac{G}{A} \qquad (4.20)$$

where W is the width of the well, V_J is the voltage across the structure and J, the current density, was given as a modified version of the expression used by Tsu and Esaki. The zero-resistance frequency in this case is defined by the frequency at which R_T vanishes. G may be calculated from $G = dJ/dV_J$ or it may be estimated from $G_{max} = -2.1\Delta I/\Delta V$, where ΔI and ΔV are the ranges of the negative part of the I-V curve.

f_{max} was calculated for each of the three theoretical models, denoted by $(f_{max})_L$ for the lumped-circuit model, $(f_{max})_S$ for the lumped-circuit plus skin-effect model, and $(f_{max})_T$ for the combined transit-time and skin-effect model. Since C_A, the capacitance due to the accumulation layer was expected to exceed C_{DW}, the capacitance of the well and depletion region by a factor of about ten, the device capacitance was calculated from $C_{DW} = \varepsilon A/(D+W)$. The dielectric constant ε was assumed to be constant over the whole of the active region. Three different mesa diameters were considered - 4, 2 and 1μm. In addition, two different drift velocities were considered for the transit-time model, since the exact drift velocity was not known. However, the two values chosen, 2×10^7 cm s^{-1} and 4×10^7 cm s^{-1}, were thought to be within the range of possible values. Table 4.2 shows the values of f_{max} calculated for each model.

The range of $(f_{max})_T$ for the 4μm device actually used is higher than that observed experimentally, but the transit-time delay does significantly reduce f_{max} compared with the other models. The authors point out that the increase in f_{max} as one decreases the mesa diameter is due to the spreading resistance becoming a smaller fraction of R_s in the smaller devices.

Table 4.2. Values of f_{max} for three models under consideration.

Mesa diameter (μm)	$(f_{max})_L$ (GHz)	$(f_{max})_S$ (GHz)	$(f_{max})_T$ (GHz) ($v_d = 2 - 4\times10^7$ cm s^{-1})
4	293	274	214 - 244
2	310	310	237 - 275
1	317	317	244 - 283

In seeking to increase f_{max}, the proposal to try to increase G_{max} was not seriously considered, since the G_{max} which had been calculated for their present devices was close enough to that value of G which produces the highest f_{max}. Rather, the authors suggested that R_s should be decreased by means of an altered doping profile (Figure 4.11).

By rapidly increasing the doping concentration to about 2×10^{18} cm^{-3} after a few accumulation-layer lengths on the cathode side and to the same level after about 100nm on the anode side, the contact specific resistance should be reduced and the epilayer resistance cut by a half. The values of f_{max} for the proposed devices are shown in Table 4.3.

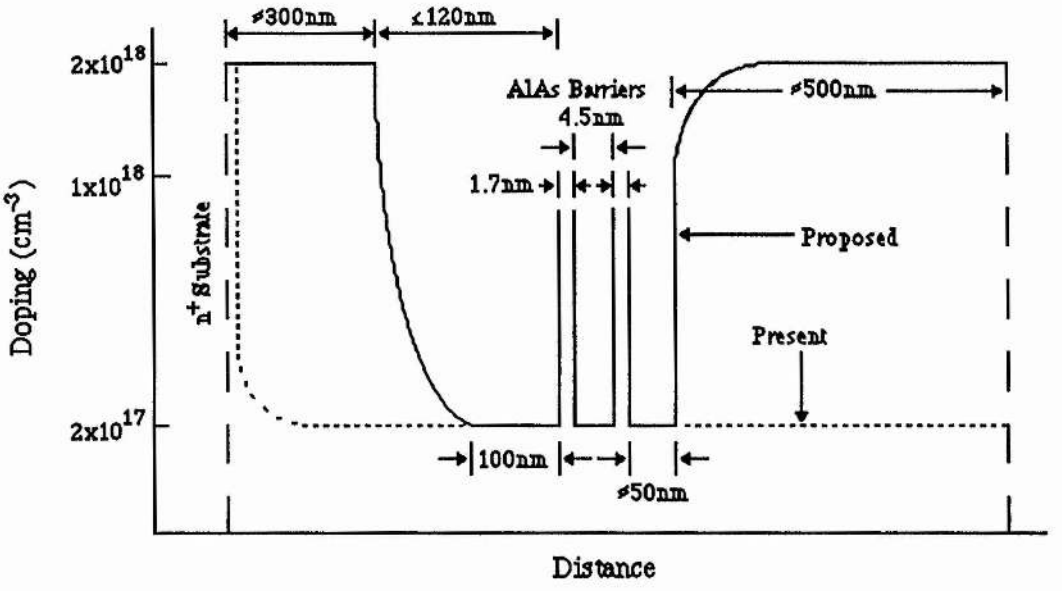

Figure 4.11. Proposed doping profile.

Table 4.3. Values of f_{max} for proposed devices.

Mesa diameter (μm)	$(f_{max})_L$ (GHz)	$(f_{max})_S$ (GHz)	$(f_{max})_T$ (GHz)
	(v_d= 2 - 4×10^7 cm s^{-1})		
4	593	467	369 - 426
2	676	634	475 - 568
1	758	730	535 - 641

It is claimed that a further increase in f_{max} of around 10% may also be possible if the current density could be increased without significantly reducing the peak to valley current ratio.

This analysis by Brown et al does not include the finite lifetime of electrons in the well, given in equation 4.11. The authors remind us that this lifetime has often been

thought to determine the zero-resistance frequency, but cautiously suggest that while there will definitely be a slowing down of the tunneling process, the exact effect on f_{max} is unclear. One would expect that the lifetime in the well will cause an inductive effect since the ac current will lag behind the ac voltage.

This new element, the "quantum-well inductance", was included in a revised model by Brown et al to explain the observed effect of the oscillation power rolling off at a lower frequency than predicted by a model containing only resistive and capacitive elements [19]. The model proved to be consistent with their observed result of 420GHz, the highest oscillation frequency from a GaAs/AlAs diode to date. The diode was a 4μm diameter device with 1.1nm barriers separated by a 4.5nm well. The peak current density of the device was $1.5x10^5 Acm^{-2}$, compared with $4x10^4 Acm^{-2}$ for the previous device which had oscillated at 200GHz. This dramatic increase in current density was due primarily to the increased doping on the cathode side. The layers on the substrate side were also doped to a higher level than previous devices, resulting in a calculated series resistance of 4Ω at dc and 6Ω at 600GHz, compared to the previous figure of 15Ω. The maximum theoretical oscillation frequency predicted by the model which takes into account both the transit-time and inductance effect was 457GHz, a figure which was felt to be limited once more by the series resistance R_s.

The question of power output of quantum well devices is one which many authors tend to ignore. The theoretical maximum output power of such devices can be estimated from $P=3/16\Delta I\Delta V$ where ΔI (ΔV) is the range of current (voltage) in the NDR region. For the device investigated in [17] this figure is about 7μW and the actual figure is 0.2μW. One of the requirements for fast diodes is a steep negative resistance slope and this alone will rule out the possibility of power being generated at, say, the milliwatt level. Also, an increase in the device area intended to increase the current density and thus the power output would also have the effect of increasing G_{max} to the point of making the device unstable at lower frequencies (instability at lower frequencies is a problem sometimes encountered with Gunn diodes), and may increase the device capacitance unduly. Brown et al suggest that an array of independently biased diodes, each with its own resonator circuit and planar antenna could be one approach to increasing the power, while another could be that of the quantum-well injection transit-time device (QWITT), discussed in the next section.

4.6. Novel Tunneling Structures.

Apart from the by now familiar GaAlAs-GaAs double barrier diode and the uniform superlattice, there exist, by virtue of the ever-improving crystal growth techniques, a number of new tunneling structures. This section aims to give a brief description of some of these devices.

Several groups have constructed double barrier, single quantum well devices with different materials from the usual GaAlAs-GaAs. Vuong et al [20] constructed a device with an InGaAs well flanked by InP barriers and InGaAs epilayers either side of the DBD structure. Resonant tunneling was observed at 77K and 4.2K, and the measured I-V curves were symmetric about zero bias, a feature not usually seen with GaAlAs-GaAs structures. The peak to valley ratios were small, due, it was thought, to a large leakage current at the edges of the devices.

Resonant tunneling has also been observed in a GaAlAs-InGaAs structure [21], where the central QW of InGaAs has a negative conduction band offset with respect to the contact material. It was calculated that the conduction band offset was nearly 100%. The device exhibited NDR at low temperatures, which started to degrade at about 100K and ceased to exist at around 275K.

An outstanding result was recently obtained by Brown et al [22], in which oscillations up to 712GHz at room temperature, at a maximum power level of 0.3μW, were measured from a diode grown from InAs/AlSb. This material has three main advantages over the GaAs/AlAs system for making high-speed resonant-tunneling diodes. Firstly, the band offset allows an electron to tunnel through an AlSb barrier with a smaller attenuation coefficient than through an AlAs barrier in a GaAs/AlAs system, which leads to a higher available current density $\Delta J=J_P-J_V$, where J_P and J_V are the peak and valley current densities respectively. A high ΔJ generally leads to a lower RC time constant. The drift velocity in InAs is also higher than in GaAs, leading to a reduced depletion-layer time-delay, which raises the f_{max}. Finally, the higher mobility of electrons in InAs reduces the series resistance R_s, which also increases f_{max}. This result represents the highest room-temperature oscillations from a solid-state oscillator to date.

A recent paper by Zaslavsky et al [23] examined the property of bistability in a DBD which can occur if the build-up of space-charge within the well alters the bias

distribution across the structure, resulting in the existence of two current states in the bistable region. To exaggerate this effect and increase the well charge density the collector barrier was made significantly higher than the emitter barrier, so that in forward bias the electrons would spend more time than normal in the well. Under these conditions V_{peak} is shifted upwards. It was found that in this region the device could exist in either a high- or low-current state, depending on the direction of sweep of the bias voltage. This hysteresis-like behaviour can in some cases be due to bias-circuit oscillations but the authors were confident that the high impedance of their device at lower frequencies suppressed any such oscillations. The application of a magnetic field parallel to the layers induced Landau quantization of the electrons within the well and clearly showed different oscillatory behaviour between the high- and low-current states, since the tunneling mechanisms are different. Tunneling in the high-current state is due to the familiar 'lining-up' of the emitter energy level with an energy level within the well, whereas the low-current state relies largely on phonon-assisted tunneling.

Moving on from double barrier, single well structures, we find that resonant tunneling has been observed in a multi-quantum well (35 periods) structure at low temperatures, dubbed sequential resonant tunneling [24], and a new hybrid device has been proposed and analysed [25]. Already mentioned briefly in the previous section, this is the quantum-well injection transit-time device (QWITT), which can be regarded as transit-time device with a DBD injector. It is a deliberate exploitation of the depleted layer found on the anode side of a normal DBD structure, in which the material parameters of both the QW and the depletion layer, or transit region, are tailored to give the desired negative resistance. The QW structure need not itself operate in the negative resistance region: indeed, if the device is biased in the positive resistance region and the transit angle ϑ of the depletion layer lies between π and 2π in the frequency range of interest, then an increase in the device area should improve the ouput power without causing low frequency stability problems.

Devices based on superlattices include a double barrier, single quantum well device in which the barriers are replaced by thin, short period superlattices (three 7Å layers of AlAs separated by two 7Å layers of GaAs) [26], the superlattice tunnel diode which is similar to the above but has a central barrier instead of a central QW [27], and the graded parameter superlattice [27]. All show NDR to a greater or lesser extent.

Finally, novel applications proposed for tunneling devices include self-oscillating mixers, series arrays with memory capability, frequency quintuplers with total suppression of even harmonics [4], and the use of DBD's for logic elements [28]. We await developments with interest.

Chapter 4 References

[1] R.Tsu and L.Esaki, "Tunneling in a finite superlattice", *Appl. Phys. Lett.*, vol. 24, no. 11, p.562, 1973.

[2] B.Ricco and M.Ya.Azbel, "Physics of resonant tunneling. The one-dimensional double barrier case", *Phys. Rev. B*, vol. 29, no. 4, p.1970, 1984.

[3] L.L.Chang, L.Esaki, and R.Tsu, "Resonant tunneling in semiconductor double barriers", *Appl. Phys. Lett.*, vol. 24, no. 12, p.593, 1974.

[4] T.C.L.G. Sollner, E.R.Brown, and W.D.Goodhue, "Microwave and millimeter-wave resonant tunneling diodes", *International Workshop on Future Electron Devices - Superlattice Devices*, Tokyo, 9-11 February 1987.

[5] D.D.Coon and H.C.Liu, "Frequency limit of double barrier resonant tunneling oscillators", *Appl. Phys. Lett.*, vol. 49, no. 2, p.94, 1986.

[6] S.Luryi, "Frequency limit of double-barrier resonant-tunneling oscillators", *Appl. Phys. Lett.*, vol. 47, no. 5, p.490, 1985.

[7] See, for example, L.I.Schiff, "Quantum Mechanics", (McGraw-Hill Kogakusha), 2nd edition, 1955.

[8] J.G.Simmons, "Generalized Formula for the Electric Tunnel Effect between Similar Electrodes Separated by a Thin Insulating Film", *J. Appl. Phys.*, vol. 34, no. 6, p.1793, 1963.

[9] T.C.L.G.Sollner, W.D.Goodhue, P.E.Tannenwald, C.D.Parker, and D.D.Peck, "Resonant tunneling through quantum wells at frequencies up to 2.5THz", *Appl. Phys. Lett.*, vol. 43, no. 6, p.588, 1983.

[10] T.C.L.G.Sollner, P.E.Tannenwald, D.D.Peck, and W.D.Goodhue, "Quantum well oscillators", *Appl. Phys. Lett.*, vol. 45, no. 12, p.1319, 1984.

[11] E.R.Brown, T.C.L.G.Sollner, W.D.Goodhue, and C.D.Parker, "Millimeter-band oscillations based on resonant tunneling in a double-barrier diode at room temperature", *Appl. Phys. Lett.*, vol. 50, no. 2, p.83, 1987.

[12] T.C.L.G.Sollner, E.R.Brown, W.D.Goodhue, and H.Q.Le, "Observation of millimeter-wave oscillations from resonant tunneling diodes and some theoretical considerations of ultimate frequency limits", *Appl. Phys. Lett.*, vol. 50, no. 6, p.332, 1987.

[13] J.Kundrotas and A.Dargys, "Electron Tunneling from an Ultrathin Quantum Well in Constant and Alternating Electric Fields", *Phys. Status Solidi B*, vol. 134, p.267, 1986.

[14] B.Jogai, K.L.Wang, and K.W.Brown, "Frequency and power limit of quantum well oscillators", *Appl. Phys. Lett.*, vol. 48, no. 15, p.1003, 1986.

[15] W.R.Frensley, "Quantum transport calculation of the small-signal response of a resonant tunneling diode", *Appl. Phys. Lett.*, vol. 51, no. 6, p.448, 1987.

[16] E.Wigner, "On the Quantum Correction For Thermodynamic Equilibrium", *Phys. Rev.*, vol. 40, p.749, 1932.

[17] E.R.Brown, W.D.Goodhue, and T.C.L.G.Sollner, "Fundamental oscillations up to 200 GHz in resonant tunneling diodes and new estimates of their maximum oscillation frequency from stationary-state tunneling theory", *J. Appl. Phys.*, vol. 64, no. 3, p.1519, 1988.

[18] W.D.Goodhue, T.C.L.G.Sollner, H.Q.Le, E.R.Brown, and B.A.Vojak, "Large room-temperature effects from resonant tunneling through AlAs barriers", *Appl. Phys. Lett.*, vol. 49, no. 17, p.1086, 1986.

[19] E.R.Brown, T.C.L.G.Sollner, C.D.Parker, W.D.Goodhue, and C.L.Chen, "Oscillations up to 420GHz in GaAs/AlAs resonant tunneling diodes", *Appl. Phys. Lett.*, vol. 55, no.17, p.1777, 1989.

[20] T.H.H.Vuong, D.C.Tsui, and W.T.Tsang, "Tunneling in $In_{0.53}Ga_{0.47}As$-InP double-barrier structures", *Appl. Phys. Lett.*, vol. 50, no. 4, p.212, 1987.

[21] M.A.Reed and J.W.Lee, "Resonant tunneling in a GaAs/AlGaAs barrier/InGaAs quantum well heterostructure", *Appl. Phys. Lett.*, vol. 50, no. 13, p.845, 1987.

[22] E.R.Brown, J.R.Söderström, C.D.Parker, L.J.Mahoney, K.M.Molvar, and T.C.McGill, "Oscillations up to 712GHz in InAs/AlSb resonant-tunneling diodes", *Appl. Phys.Lett.*, vol. 58, no.20, p.2291, 1991.

[23] A.Zaslavsky, V.J.Goldman, D.C.Tsui, and J.E.Cunningham, "Resonant tunneling and intrinsic bistability in asymmetric double-barrier heterostructures", *Appl. Phys. Lett.*, vol. 53, no. 15, p.1408, 1988.

[24] F.Capasso, K.Mohammed, and A.Y.Cho, "Sequential resonant tunneling through a multiquantum well superlattice", *Appl. Phys. Lett.*, vol. 48, no. 7, p.478, 1986.

[25] V.P.Kesan, D.P.Neikirk, P.A.Blakey, B.G.Streetman, and T.D.Linton, Jr., "The Influence of Transit-Time Effects on the Optimum Design and Maximum Oscillation Frequency of Quantum Well Oscillators", *IEEE Trans. Elec. Dev.*, vol. 35, no. 4, April 1988.

[26] M.A.Reed, J.W.Lee, and H-L.Tsai, "Resonant tunneling through a double GaAs/AlAs superlattice barrier, single quantum well heterostructure", *Appl. Phys. Lett.*, vol. 49, no. 3, p.158, 1986.

[27] M.J.Kelly, R.A.Davies, N.R.Couch, B.Movaghar, and T.M.Kerr, "Novel Tunneling Structures: Physics and Device Implications", GEC Hirst, unpublished.

[28] H.C.Liu and D.D.Coon, "Heterojunction double-barrier diodes for logic applications", *Appl. Phys. Lett.*, vol. 50, no. 18, p.1246, 1987.

5. Frequency Multiplication.

5.1. Introduction

Frequency multipliers are widely used to provide a reliable source of local oscillator power for heterodyne receivers and laboratory measurement systems in the millimetre and submillimetre wavelength regions. The essential operation of a frequency multiplier is for a non-linear device to be driven by a sinusoidal waveform, which results in the generaton of higher harmonics. The harmonic numbers and their relative amplitudes will depend on the exact nature of the non-linearity of the device being driven.

Since direct generation of power by room-temperature solid-state devices above about 150GHz is normally quite difficult, the use of costly and delicate vacuum devices such as klystrons and carcinotrons (backward-wave oscillators) has been widespread. Solid-state frequency multipliers offer a relatively inexpensive and more robust source of LO power, operating from bias supplies of just a few volts. The availability of high cut-off frequency Schottky-barrier diodes has enabled the design of a number of efficient multipliers (e.g.[1 to 4]), which produce sufficient power to drive SIS mixers and detectors.

5.2. The Varactor Diode

The non-linear element of a varactor diode is its back-biased junction capacitance. A varactor can be represented most simply as a non-linear capacitance with a constant series resistance (Figure 5.1).

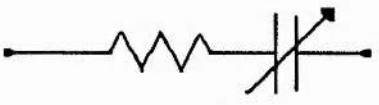

Figure 5.1. The Varactor Model.

Note that this model does not take into account any effects due to lead inductance, capacitance due to the diode package, or conductance over the surface of the varactor.

The dc current-voltage characteristic of a varactor diode is shown in Figure 5.2. The reverse bias voltage at which breakdown occurs is known as the reverse breakdown voltage V_B, and it is assumed that V_B cannot be exceeded.

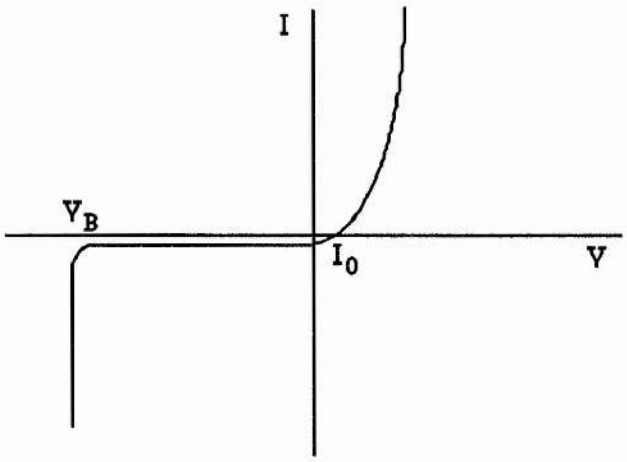

Figure 5.2. Varactor diode dc characteristic.

For the purpose of analysis, we shall consider the ideal p-n abrupt-junction varactor. Practical Schottky-barrier varactors are optimised in such a way as to exhibit very closely the characteristics of the abrupt-junction varactor.

The abrupt-junction varactor is so named because the doping changes abruptly from an excess of donors to an excess of acceptors (Figure 5.3).

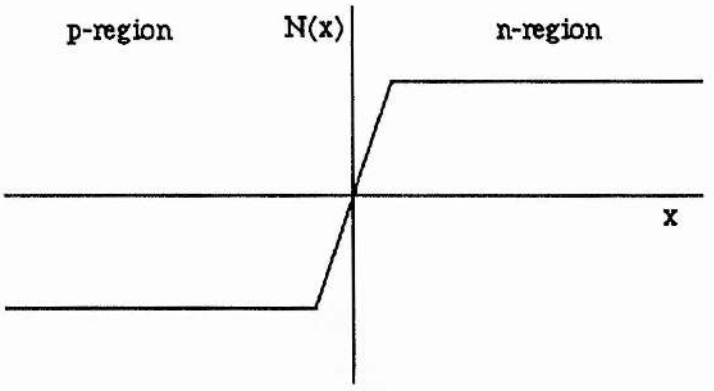

Figure 5.3. The fixed-charge density of the abrupt-juncton varactor

On the p-side of the junction there are free holes and an equal concentration of (-) ionized acceptor impurity atoms, and on the n-side there are free electrons and an equal concentration of (+) ionized donor impurity atoms. Initially, a small amount of diffusion of carriers occurs across the junction which leaves an excess of acceptor ions on the p-side and an excess of donor ions on the n-side. The electric field so produced inhibits further diffusion of carriers across the junction, giving rise to a depletion region of thickness D. The built-in voltage drop associated with the depletion region is known as the contact potential ϕ. If reverse bias is applied to the junction, the depletion layer becomes wider as more mobile charges are removed from the region (Figure 5.4). The amount of charge removed is a function of the voltage applied across the junction, and the device can be regarded as a capacitor with a non-linear charge-voltage curve. (Note that we are talking about the junction voltage only, and not the voltage across the whole device. This latter voltage will of course include a voltage drop across the series resistance.)

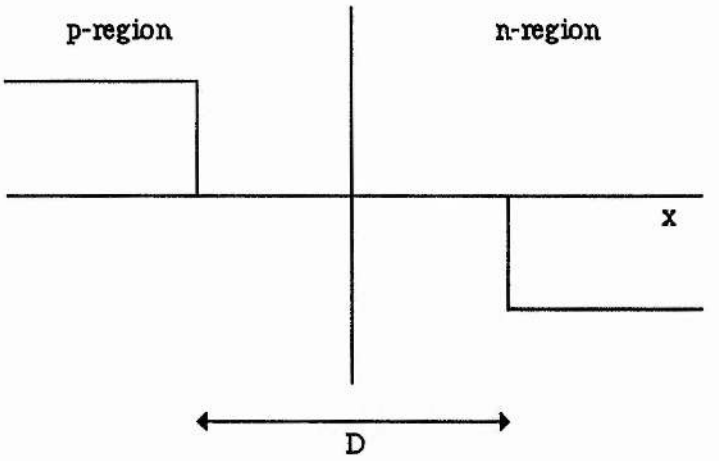

Figure 5.4. The mobile charge density of the abrupt-junction varactor.

If the voltage is changed by some small amount Δv, the charge will change by a small amount Δq. We can then define the incremental elastance (reciprocal of capacitance) as

$$S = \frac{\Delta v}{\Delta q} \qquad (5.1)$$

We can also note that, from the parallel-plate capacitor analogy,

$$S = \frac{D}{\varepsilon A} \qquad (5.2)$$

where D is the depletion layer width, ε is the dielectric constant of the semiconductor, and A is the junction area. S varies from S_{max} at $v = V_B$, the reverse breakdown voltage, to zero when $v = -\phi$, the contact potential (v measured in the negative direction).

To find the elastance as a function of the voltage, we integrate

$$dv = S\, dq \qquad (5.3)$$

From Figure 5.3 we see that the charge q which is removed is proportional to D: therefore, from equation 5.2, the elastance is proportional to the charge. Integrating equation 5.3 gives

$$S = S_{max}\left(\frac{v+\phi}{V_B+\phi}\right)^{\frac{1}{2}} \qquad (5.4)$$

which can be expressed as

$$v \propto \frac{1}{C^2} \qquad (5.5)$$

If we now plot elastance as a function of (reverse) voltage, we get (Figure 5.5). Note that the curve is more non-linear at lower values of reverse voltage, i.e. the second derivative of the elastance-voltage curve is larger (and negative).

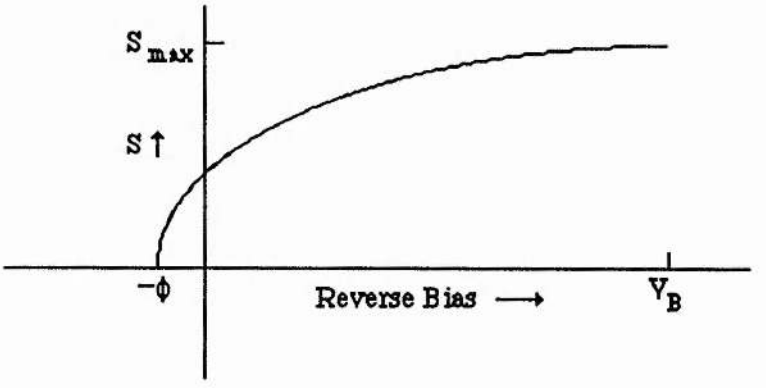

Figure 3.5. Elastance as a function of reverse bias for the abrupt-junction varactor.

5.3 . General Multiplier Equations.

If we rearrange equation 5.3 and integrate, using the expression for S given in equation 5.4, we get

$$\frac{v+\phi}{V_B+\phi} = \left(\frac{q+q_\phi}{Q_B+q_\phi}\right)^2 \qquad (5.6)$$

where the charge $(-q_\phi)$ is the charge at voltage $-\phi$, and Q_B is the charge at the breakdown voltage V_B. Let us assume that there are only two currents flowing in the varactor; the input current at frequency ω_0 and the output current at frequency $n\omega_0$. We can write down the instantaneous charge as

$$q = Q_0 + Q_1 \sin \omega_0 t + Q_n \sin n\omega_0 t \qquad (5.7)$$

where Q_0 is the average value of the stored charge. Substituting equation 5.7 into equation 5.6 and gathering like terms [5] yields an expression for the instantaneous voltage over the junction, with ac voltage terms in $2\omega_0$, $2n\omega_0$, $(n+1)\omega_0$ and $(n-1)\omega_0$. Bearing in mind that we specified that the output current should flow at a frequency of $n\omega_0$, we see that unless n=2, there is no voltage source of frequency $n\omega_0$. Therefore, for the back-biased abrupt-junction varactor, it is impossible to construct a multiplier other than a doubler with currents flowing only at the input and output frequencies. To generate higher harmonics, it is necessary to allow intermediate harmonic currents, known as idlers, to flow in the varactor. In constructing a tripler, for example, it is necessary to allow current to flow at $2\omega_0$, which then mixes with the fundamental, ω_0, to produce $3\omega_0$. The idler at $2\omega_0$ must be terminated by a short-circuit to ensure maximum conversion to the third harmonic. A tripler such as this would be termed a 1-2-3 tripler. Similarly, a quadrupler can have either one (1-2-4) or two (1-2-3-4) idlers, depending on the particular varactor and the choice of external circuit.

It is worth noting briefly that varactors with different doping profiles such as the graded-junction varactor, which has a cube-law rather than a square-law characteristic, may be capable of generating high harmonics without the use of idlers. However, since we will be concerned with Schottky-barrier varactors whose voltage-charge characteristics approximate well to the ideal square law, we will not be considering other doping profiles.

5.4. Varactor Figures of Merit.

Theoretically, a varactor is capable of 100% conversion efficiency. Intuitively, we may see how this can be - if there are no (resistive) loss mechanisms at all in our varactor and its circuits, then we should see the same amount of power at the output as at the input, but at a different frequency. This argument is merely another way of presenting the Manley-Rowe formulas [6], which state that the sum of all powers flowing into a non-linear reactance must be zero. To illustrate this, imagine that we introduce power at a frequency ω_0 via a lossless bandpass filter to a non-linear capacitance, and extract power at a frequency $n\omega_0$ via another lossless bandpass filter to a load (Figure 5.6).

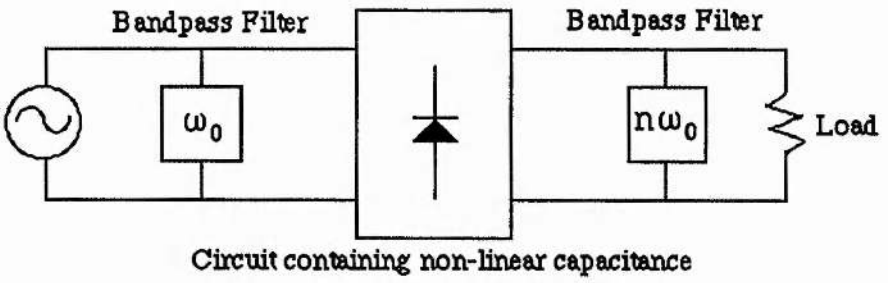

Figure 5.6. Ideal lossless multiplier circuit.

In this circuit, power can *only* be introduced at frequency ω_0 and can only be passed to the load at frequency $n\omega_0$, so, by the Manley-Rowe relations, conversion efficiency is 100%. However, in all practical varactors, the series resistance R_s reduces the efficiency as do various losses associated with the input, output and idler circuits. For an ideal varactor, the diode conversion efficiency may be written as [5]

$$\eta_d = \exp(-\alpha f_{out}/f_{cd}) \qquad (5.8)$$

where f_{out} is the output frequency and f_{cd} is the dynamic cut-off frequency given by

$$f_{cd} = \frac{S_{max} - S_{min}}{2\pi R_s} \qquad (5.9)$$

α is the efficiency parameter which depends on the harmonic order and on the input drive level. Burckhardt [7] uses an iterative technique to find the Fourier components of the diode voltage and then calculates the diode efficiency as the ratio of output to input power. α is then calculated from equation 5.8. However, it is important to note that the values of α given in [7] assume an input frequency to output frequency ratio of 1:100, clearly inappropriate for diodes operating at mm-wave frequencies. For an input drive level which swings the voltage between V_B and zero volts, Archer [8] quotes values of α of about 10 for a doubler and about 16.5 for a tripler with second harmonic idler.

Some manufacturers will quote a zero-bias cut-off frequency f_c, where

$$f_c = \frac{1}{2\pi R_s C_0} \qquad (5.10)$$

and C_0 is the capacitance of the junction measured at zero applied bias. Since C_0 is close to the maximum value of junction capacitance, equation 5.10 yields a lower value of cut-off frequency than does equation 5.9. The dynamic cut-off frequency f_{cd} is however a more realistic parameter because it takes into account the fact that the varactor is being driven.

It can be seen from equation 5.8 that a high dynamic cut-off frequency is desirable for good conversion efficiency, so R_s should be as small as possible and S_{max}-S_{min} should be as large as possible. This latter requirement presents us with a choice - increasing the elastance, (i.e. decreasing the capacitance) would be achieved by reducing the device area, but this will in turn limit the power handling capability of the varactor. Therefore a compromise must be found between good high-frequency performance and good power capability. Gewartowski [5] and Penfield and Rafuse [9] have carried out detailed analyses of varactor design and applications, with examples. It will be noted that the efficiencies and power levels quoted in these examples are high, but the frequencies of operation are typically only a few GHz, so acheiving a high f_{cd} to f_{out} ratio (for example) is not too difficult. An example of a typical GaAs Schottky barrier varactor required to produce power in the range 110-170 GHz may have $R_s \approx 10\Omega$, $C_0 \approx 20$pF and $f_c = 800$GHz. The maximum input power would be around 50mW and the efficiency, provided the diode is mounted in a suitable circuit, may be around 20% (doubler) and 10% (tripler).

5.5. Circuit Design.

At millimetre-wave frequencies, a varactor diode is normally mounted in a microwave cavity which should satisfy a number of criteria. Firstly, the input and output ports should be properly matched to the the dynamic impedance of the varactor at their respective frequencies. Also, if idlers are present, then they should be short-circuit terminated. Finally, only input, output and idler currents should flow in the varactor - all other frequencies should be presented with an open circuit.

The type of circuit normally used to construct millimetre-wave multipliers is of the crossed-waveguide design. Figure 5.7 is one example of a crossed-guide frequency multiplier.

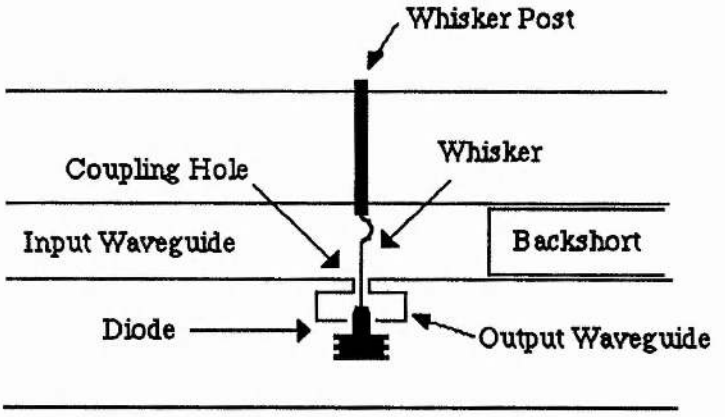

Figure 5.7. Crossed-guide multiplier with whisker contact.

Power at the pump frequency enters the block via the input waveguide and is coupled to the diode by the whisker, which also carries the dc bias. The diode is situated in the output guide and the harmonic frequency exits the block via the output waveguide. As with any other type of microwave circuit, it is essential that the input and output circuits are correctly matched to the diode at their respective frequencies. In general, one has the problem of matching the waveguide characteristic impedance, which is around a few hundred ohms (depending on the waveguide size and the frequency) to a considerably different device impedance. In the above example the input waveguide impedance has to be matched to the (inductive) whisker across the waveguide. If we write the impedance of the whisker as $Z_W = R_W + jX_W$, and assume

that the resistive part of the whisker's impedance is much less than Z_0, the waveguide characteristic impedance, then it can be shown that [10]

$$X_W \approx (Z_0 R_W)^{\frac{1}{2}} \qquad (5.11)$$

Therefore, if R_W is small then X_W, the whisker's inductance must also be small. At high frequencies it is sometimes difficult to make the inductance low enough to match properly. Lowering the height of the waveguide to reduce the inductance will, however, reduce the value of Z_0 and by equation 5.11, the required value of X_W will also be reduced, although at a slower rate. The same considerations are also applicable in the output circuit. Inductances must be kept low, so the diameter of the coupling hole through which the whisker passes must be kept small. The combination of whisker and coupling hole also acts as a low pass filter, with its cut-off frequency falling between the input and output frequencies.

Filtering between the input and the output can also be acheived with a stripline probe and filter on a quartz substrate (Figure 5.8). The filter structure may be of the high-Z - low-Z low-pass design [8], or, for single-frequency operation, band-reject shunt stubs may be used [11]. Stripline filter designs have the advantage of ease of design and construction. For a given response, either maximally flat or equal-ripple Tchebyshev, and a given number of sections, there exists a set of G-values, or normalised inductance and capacitance values corresponding to lumped circuit elements of the filter. The lengths of the high-Z - low-Z sections can then be calculated in a straightforward manner [12]. This type of filter gives the designer much more control over the performance of the multiplier, but it is not without its problems: the quartz substrate is quite delicate, and bonding of diode chips, whiskers and bias wires to the thin copper tracks can be tricky.

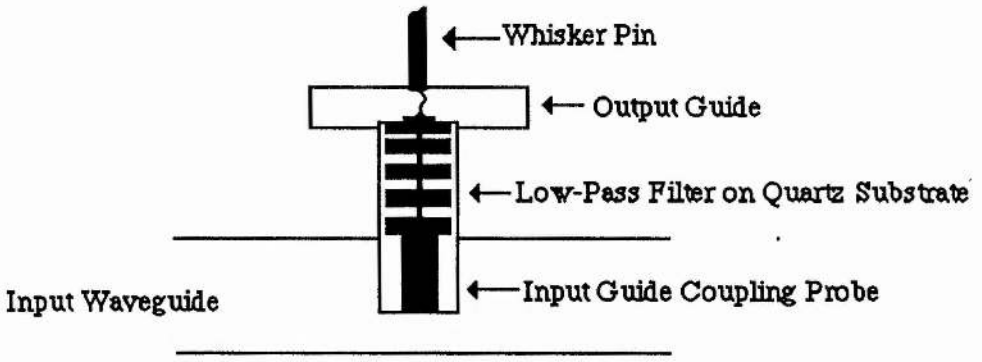

Figure 5.8. Stripline low-pass filter coupling.

An alternative type of filter is the coaxial filter used, for example, by Erickson in a 230GHz tripler [1]. Figure 5.9 shows a typical multiplier block with coaxial filter.

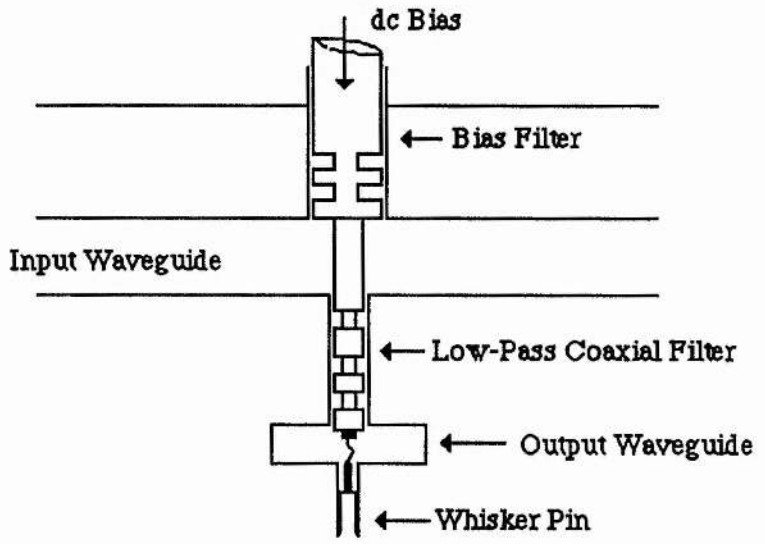

Figure 5.9. Section through multiplier with coaxial filtering.

The coaxial filter is designed to transmit power to the diode at the pump frequency, while presenting a short circuit to higher frequencies at the top of the ouput waveguide wall. Design procedures are similar to those employed in the design of stripline filters because the same sets of G-values can be used. The formulae given by Brewer and Räisänen [13] can be solved by an iterative technique to find the lengths of the various sections. The bias filter shown in Figure 5.9 is designed in exactly the same way as the low-pass filter, the difference being that the bias filter must reject the

pump frequency. The cut-off frequency in this case will be chosen to lie somewhere between dc and the pump frequency.

Coaxial line filters must be electrically isolated from the rest of the block, i.e. they must be non-contacting. Common methods of acheiving electrical isolation at dc are anodising, either of the cavity or of the filter structure; inserting a small Teflon sleeve into the cavity; or wrapping the filter structure in a low-loss dielectric such as Mylar. The method chosen will depend to a large extent on the relative physical sizes of the cavity and the filter structure. Since one needs to make the gap between the filter structure and the cavity wall quite small in order to reduce inductance, the fitting of a thin Teflon sleeve would be extremely difficult. Likewise, if the desired output frequency is, say, between 150 GHz and 200 GHz, the coaxial filter would have an outside diameter of a millimetre or less and the inner structure would therefore be rather delicate. It would seem in those circumstances that wrapping the structure in a suitable dielectric such as Mylar may place too much mechanical strain on the structure; in other words it could easily be bent. Possibly the best and safest method is to make the block from aluminium and anodise the inner walls of the coaxial cavities, or to anodise the filter structure itself.

The method of contacting the varactor diode in the three types of block described above is whisker contacting. Whisker contacting is popular at millimetre and submillimetre wavelengths because the parasitics associated with a whisker contact are low. The contacting surface of the varactor chip is a honeycomb array of many hundreds of contacts situated in pits etched into a passivation layer. The whisker itself is a thin wire of phosphor bronze or platinum which is etched or spark-eroded into a fine point with a radius of a few microns, and is mounted onto the end of a larger pin. Before forming the point on the whisker, the wire is bent into an approximate S-shape to give some degree of spring to the whisker. Actually forming the contact to the diode chip is a skilled job which involves the whisker pin being pushed through an interference-fit hole by a micrometer or non-rotating chuck. A curve tracer is attached to the whisker (or the diode) and the instant that contact is seen to be made, the micrometer is withdrawn. The contact is then maintained by the force of the spring of the S-shape of the whisker. Should that particular contact fail, the whisker is withdrawn and a new one mounted: the chances of recontacting the damaged junction are minimal.

If a varactor multiplier is to operate with idlers, for example as a tripler, then the circuit design should take this into account. Idlers must be terminated ideally in a short-circuit: if, for example, one uses a backshort to effect the termination then the backshort should be a whole number of half guide-wavelengths from the plane of the diode. The simplest way of terminating an idler at the second harmonic is to choose the output guide to be cut-off at the second harmonic [1]. The idler circuit impedance in this case depends on the whisker-pin geometry (see Figure 5.9). A similar approach is to make the output guide large enough to pass the second harmonic but then to place a waveguide transformer approximately half a guide wavelength (at the second harmonic) from the diode plane. The transformer may be either a taper or a series of step discontinuities [2], which reduces the guide to a size which will pass the desired output frequency but will be cut-off at the second harmonic. Both of the above circuits will normally have a backshort behind the diode. In the first case, the backshort will have an effect on the impedance at the output frequency only. In the second case, the backshort will affect both the impedance at the second harmonic and the impedance at the output frequency, and as a result it may not be possible to optimise both circuits simultaneously. Archer [3] has solved this problem by tuning the idler and output circuits with quasi-optical components. The output waveguide is made large enough to pass the second harmonic, via a feedhorn and collimating lens, onto a dichroic plate. The dichroic plate acts as a high pass filter, and comprises a flat aluminium sheet drilled through with an array of circular holes. The circular holes are regarded as short lengths of circular waveguide whose diameter is small enough to be cut-off at the second harmonic. The transmission curve of the dichroic plate is a function of the thickness of the plate, the diameter of the holes, and the spacing between the holes. As the plate looks like a plane mirror at the second harmonic, moving the plate axially with respect to the plane of the diode tunes the idler frequency termination. With the multiplier working as a tripler, the third harmonic is tuned with a pair of fused quartz plates. The reactive part of the third harmonic impedance is tuned by moving these plates relative to the diode, and the transmission peak depends on their spacing - similar to a Fabry-Perot resonator. A second dichroic plate which reflects the third harmonic but passes the fourth was placed behind the first dichroic plate so that the system worked as a quadrupler. Quasi-optical circuit terminations of this type have virtually no resistive loss and are relatively broad-band, and thus have considerable advantages over waveguide or stripline circuits at sub-millimeter wavelengths.

At the beginning of this section it was mentioned that only input, output and idler

currents should be allowed to flow in the varactor, and that all other frequencies should be presented with an open circuit. In the context of millimeter-wavelength frequency multipliers there is usually no need to make any special provision for these other frequencies. Sub-harmonic generation is not a problem in waveguide blocks because of the high-pass characteristics of waveguide, and unless frequencies higher than the output frequency are presented with a properly matched circuit, additional currents will tend not to flow.

5.6. Multiplication in Non-Linear Resistances.

Since any non-linear device will generate harmonics if driven by a sine wave, it is possible to use the non-linear *forward biased* characteristic of Schottky-barrier diodes to achieve frequency multiplication. Such diodes operating in forward bias are sometimes known as varistors. The fundamental difference between varactors and varistors is that varactors use their non-linear reactance to generate harmonics whereas varistors use their non-linear forward resistance. Harmonics then result from distortion of the drive waveform. A consequence of this is that the inherent resistive loss associated with varistors reduces their maximum theoretical efficiency to $1/n^2$ where n is the harmonic order [14]. Set against this, however, is their potential for high harmonic multiplication without special provision for idler circuits.

The harmonics one would expect a varistor to produce are dependent primarily on the shape of the diode's forward current-voltage characteristic. If the characteristic is a square law, then the diode will work best as a doubler, although not as efficiently as a varactor doubler. In the case of the characteristic being an exponential, however, one would expect the diode to produce all harmonics - this can be seen from the Taylor expansion of e^x. The circuit in which one would mount a varistor diode is subject to most of the design considerations for varactor circuits, but with a few modifications. The requirement that the input and output circuits should be properly matched are, of course, still valid. Filtering between input and output circuits has to be carefully considered because the repeated pass-bands of both coaxial and stripline filters can coincide with higher harmonics. Furthermore, it is usually possible to optimise the output circuit impedance at only one frequency, so the coupling of other harmonics will be compromised. Nevertheless, Rothermel et al [4] achieved multiplication factors of up to 8 using a fast mixer diode. The particular diode used by this group

could not sustain more than 3mA forward current so about one volt of reverse bias had to be applied in order to reduce the forward current, but the diode was still operating in varistor mode. The multiplier was shown to operate as a doubler (200 GHz and 230 GHz), and as a tripler (345 GHz) at reported powers of 0.6mW and 150μW respectively, for a pump of 20 mW at 100 GHz. A pyramidal horn with a narrow filter section (cut-off frequency of 750 GHz) enabled approximately 1μW of power at 800 GHz to be detected. These power levels cannot be taken as being absolute for the following reasons. Firstly, output between 200 GHz and 345 GHz was measured using an Anritsu power meter with a sensor head which was only calibrated up to 120 GHz. Experience has shown that Anritsu power meters tend to under-read at frequencies higher than the calibrated pass-band. Secondly, the high (800 GHz) frequency output was measured with a cooled InSb bolometer. Such detectors are widely used at high frequencies because of their good sensitivity, but correct calibration can be very tricky, due in the main part to uncertainty about the optical coupling between the input beam and the InSb itself. Clearly, frequency conversion of such high order would be extremely difficult to acheive with a single varactor diode multiplier block, and single stage frequency conversion to high harmonic numbers using varistors is an attractive proposition. The power levels are in principle sufficient for SIS (superconductor-insulator-superconductor) mixers.

5.7. Quantum -Well Multipliers.

Quantum-well devices have been shown to be capable of extremely fast operation both as detectors and as oscillators. By virtue of their strongly non-linear current-voltage characteristic, these devices have potential as resistive frequency multipliers. Double barrier quantum-well devices exhibit a point-symmetric current-voltage relation which, at zero bias, favours only odd harmonic conversion (Figure 5.10). The existence of polarity-symmetric negative resistance regions is an important feature, for if the device is driven over these regions the $1/n^2$ conversion efficiency may be exceeded, and conversion to higher harmonics can be significant.

Harmonic multiplication using a quantum-well device was first reported by Batelaan and Frerking [15]. The device chip was a direct replacement for the varactor diode chip in an existing 67 - 201 GHz frequency tripler mount. A conversion efficiency of 0.61% was measured, somewhat less than that of the varactor (4%).

However, if we refer back to section 3.4 we see that a high conversion efficiency is dependent on a high f_{cd}/f_{out} ratio, and in this particular case the varactor chip had a higher cut-off frequency than the QW device. Batelaan and Frerking calculated that if the varactor were to operate at a frequency such that its f_{cd}/f_{out} ratio were the same as that of the QW device then the varactor's conversion efficiency would be 0.8%, only slightly greater than the QW device's measured efficiency.

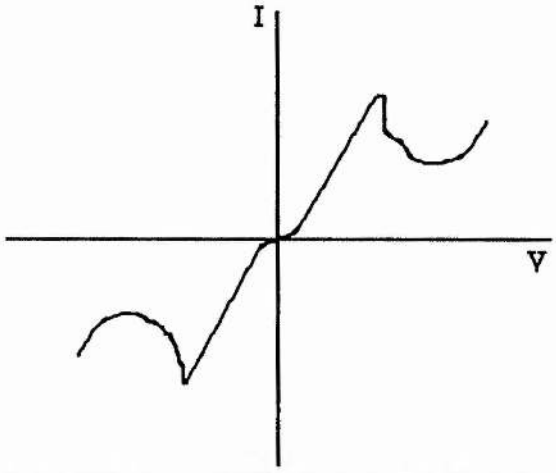

Figure 5.10. Current-voltage curve of symmetric double-barrier quantum well device.

As mentioned above, if the pump signal can drive the QW device over the negative resistance regions, one would expect an increase in conversion efficiency. This effect was reported by Rydberg and Grönqvist [16]. It is also possible to obtain significant amounts of power at the fifth harmonic. Sollner et al [17] measured a conversion efficiency of 0.5% at the fifth harmonic (21.25 GHz) by careful adjustment of the pump power, and proposed that with the proper choice of resonant-tunneling structure and pump amplitude, most of the harmonic output could be confined to a single harmonic frequency. Termination of unwanted harmonics could then be largely unnecessary. In addition, zero-bias operation can greatly simplify circuit design. However, since the I-V characteristic of the QW device is so strongly non-linear in the NDR region, biasing to just below the current peak (for example) would certainly produce harmonic output.

A single current peak in each quadrant of the I-V characteristic can lead to generation of harmonics up to the fifth, providing the sinusoidal pump waveform is of sufficient amplitude to drive the device over both peaks (Figure 5.11). By fabricating a structure which exhibits two or more current peaks in each quadrant, the efficient

generation of yet higher harmonics should be possible. A recent paper by Sen et al. [18] presents such a device, consisting of two QW diodes in parallel connected by a resistance, which exhibits two current peaks in the forward direction. (It is unclear whether this particular device is symmetrical.) Driving over the two peaks with a sinusoidal waveform produced a large fifth harmonic component, albeit at audio frequencies. If such a device is indeed symmetrical and can be driven over both quadrants at zero bias, then output up to the ninth harmonic could be expected (Figure 5.12).

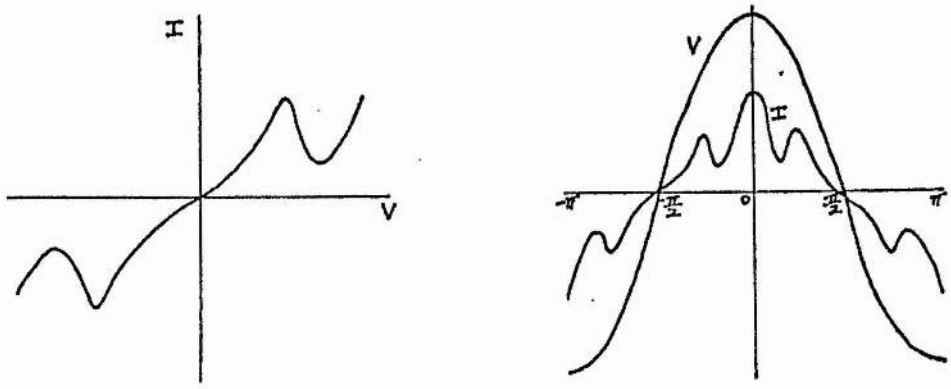

Figure 5.11. Fifth harmonic content in a sinusoidally driven QW device.

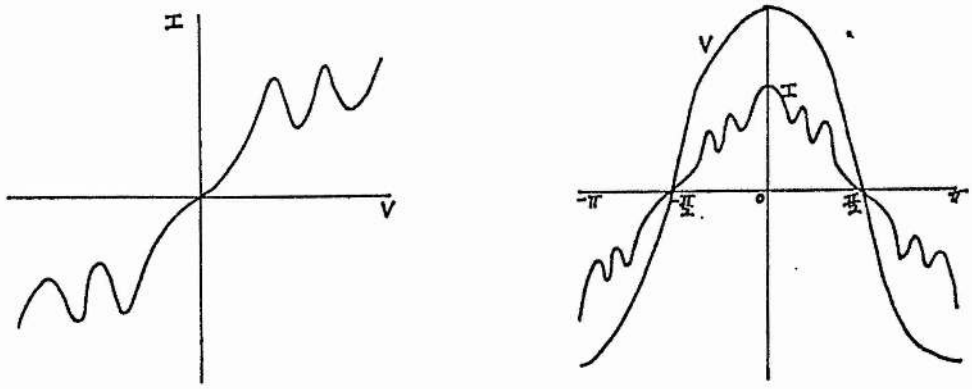

Figure 5.12. Ninth harmonic content in a sinusoidally driven QW device.

The major problems associated in generating high harmonic output at frequencies of several hundred GHz, irrespective of the nature of the non-linear device used, are that conventional waveguide circuits eventually become too small to fabricate successfully, and the resistive losses of small waveguide become prohibitively high. A move away from waveguide towards some form of quasi-optical circuit using free-space propagation, and therefore much lower loss, deserves careful consideration. Of course, a fundamental limitation on the performance of any frequency multiplier must be the cut-off frequency of the non-linear devices themselves. In the case of QW diodes this cut-off frequency now appears to be approaching the terahertz region.

Chapter 5 References.

[1] N.R.Erickson, "A high efficiency frequency tripler for 230 GHz", *Proc. 12th European Microwave Conf.*, p.288, Helsinki, 1982.

[2] J.W.Archer, "An efficient frequency tripler for 200-290 GHz", *IEEE MTT*, vol.32, no.4, p.416, 1984.

[3] J.W.Archer, "A novel quasi-optical frequency multiplier design for millimeter and submillimeter wavelengths", *IEEE MTT*, vol.32, no.4, p.421, 1984.

[4] H.Rothermel, T.G.Phillips and J.Keene, "A solid-state frequency source for radio astronomy in the 100 to 1000 GHz range", *Int. Journal of Infrared and Millimeter Waves,* vol.10, no.1, p.83, 1989.

[5] M.Uenohara and J.W.Gewartowski, "Varactor Applications", Microwave Semiconductor Devices and Their Circuit Applications, ed. H.A.Watson, McGraw-Hill, 1969.

[6] J.M.Manley and H.E.Rowe, "Some general properties of non-linear elements - Part 1. General energy relations", *Proc. IRE*, vol.44, p.904, 1956.

[7] C.B.Burckhardt, "Analysis of varactor frequency multipliers for arbitrary capacitance variation and drive level", *Bell System Technical Journal*, vol.44, p.675, April 1965.

[8] J.W.Archer, "Millimeter wavelength frequency multipliers", *IEEE MTT*, vol.29, no.6, p.552, 1981.

[9] P.Penfield and R.P.Rafuse, "Varactor Applications", M.I.T. Press, Cambridge, MA, 1962.

[10] G.M.Smith,"Transferred electron oscillators at mm-wave frequencies and their characterisation using quasi-optical techniques", PhD Thesis, St.Andrews University, March 1990.

[11] T.Takada and M.Ohmori, "Frequency triplers and quadruplers with GaAs Schottky-barrier diodes at 450 and 600 GHz", *IEEE MTT*, vol.27, no.5, p.519, 1979.

[12] H.Howe, Jr., "Stripline Circuit Design", Microwave Associates, Burlington, MA, 1974.

[13] M.K.Brewer and A.V.Räisänen, "Dual-harmonic noncontacting millimeter waveguide backshorts: theory, design and test", *IEEE MTT*, vol.30, no.5, p.708, 1982.

[14] C.H.Page, "Frequency conversion with positive nonlinear resistors", *J. Res. Nat. Bureau of Standards*, vol.56, no.4, p.179, 1956.

[15] P.D.Batelaan and M.A.Frerking, "Quantum Well Multipliers", *Conference Digest, 12th Int. Conf. Infrared and Millimeter Waves*, ed. R.J.Temkin, IEEE, New York, 1987.

[16] A.Rydberg and H.Grönqvist, "Quantum-well high-efficiency millimeter-wave frequency tripler", *Electronics Letts*, vol.25, no.5, p.348, 1989.

[17] T.C.L.G.Sollner, E.R.Brown, W.D.Goodhue and C.A.Correa, "Harmonic multiplication using resonant tunneling", *J. Appl. Phys.*, 64(8), p.4248, 1988.

[18] S.Sen, F.Capasso, A.Y.Cho and D.Sivco, "Resonant tunneling device with multiple negative differential resistance: Digital and signal processing applications with reduced circuit complexity", *IEEE Trans. Electron Devices*, vol. ED-34, no.10, p.2185, 1987.

6. Waveguide Frequency Doublers.

6.1. Introduction

This section details the design, construction and operation of a crossed waveguide frequency doubler. The output frequency tuning range, power, efficiency and beam pattern are reported. The doubler was operated mainly with a Schottky barrier varactor diode manufactured by Farran Technology of Ballincollig, Cork, Ireland. An attempt was also made to frequency double using a mixer diode in the varistor mode.

6.2. Pump Oscillator Design

The design of the frequency doubler was initially based on the Gunn oscillator / frequency multiplier combination designed by Rothermel et al [1]. In view of the high harmonic multiplication achieved in [1] it was decided that a similar oscillator / multiplier combination should be built, incorporating the following design features.

The Gunn oscillator is of the cap and post resonator type with a 3.0mm diameter variable height coaxial cavity, a standard full-height WG28 rectangular waveguide (cut-off frequency 75GHz) to couple out the power, and a sliding, contacting backshort situated behind the Gunn diode in the waveguide. Machined from aluminium, it is essentially identical to the oscillators designed by Smith [2] at St Andrews University which are in turn based on those designed by Carlstrom [3] with the exception that the coaxial cavity is not placed centrally within the block but is offset towards one side of the oscillator (Figure 6.1). Thus the axis of the coaxial cavity is situated much closer to the outside wall of the block than usual. As a result the top micrometer can not be situated directly above the coaxial choke but is mounted centrally in the top section of the block and drives directly onto an aluminium guide pin which slides smoothly in a PTFE plug through the compression spring. A small bar of aluminium connects the central pin, a second guide pin and the choke sufficiently accurately so that the whole assembly can slide up and down in the block without excessive friction. Bias is supplied to the Gunn diode via an SMA connector on the block, through a small anti-spike RC network and over-voltage protection Zener diode to the aluminium connecting bar. In order to insulate electrically the micrometer from

the bias supply, and to ensure a smooth turning action, a small glass bead is glued into a recess machined in the top of the knurled nut as shown in the diagram.

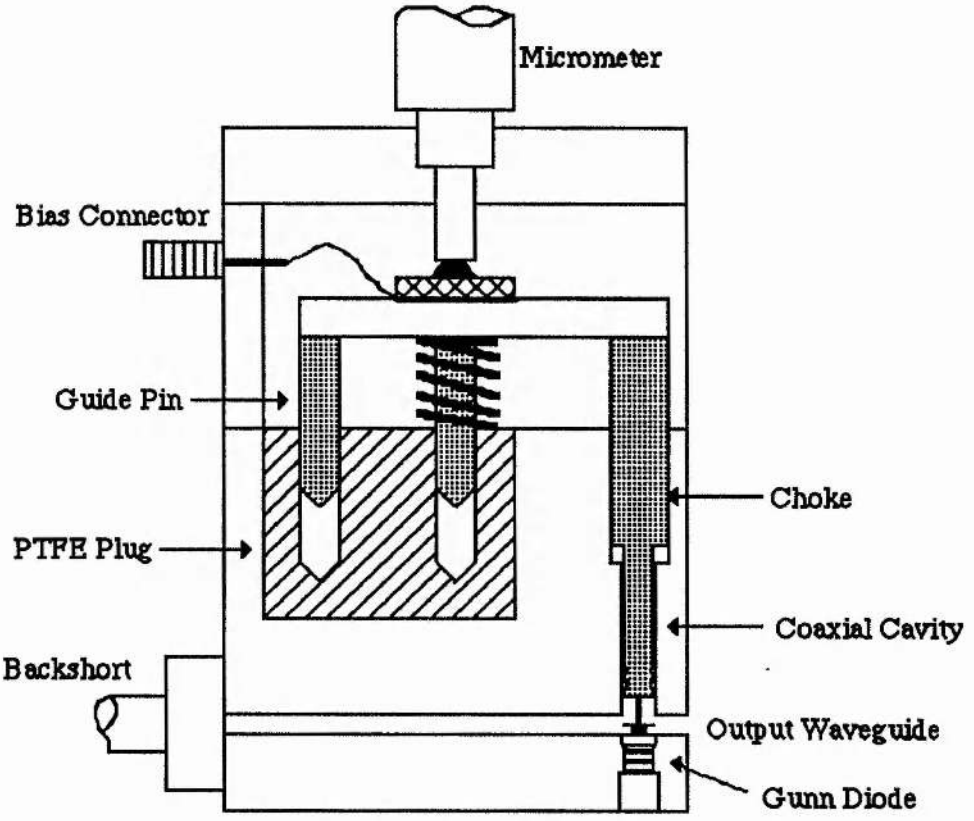

Figure 6.1. Off-centre Gunn Oscillator

The bias is taken from the connecting bar down through the centre of the choke via a spring and the cap and post arrangement to the Gunn diode (Figure 6.2). Contact is maintained by the pressure of the spring, which should be strong enough to give a good contact but not so strong as to risk crushing the diode package, especially at low cavity heights where the spring is near maximum compression. The aluminium choke is anodised to prevent any short-circuit between the bias line and the wall of the coaxial cavity. However, it should be noted that the anodised finish can be scratched quite easily, and care must be taken to machine the coaxial cavity to as smooth a finish as possible.

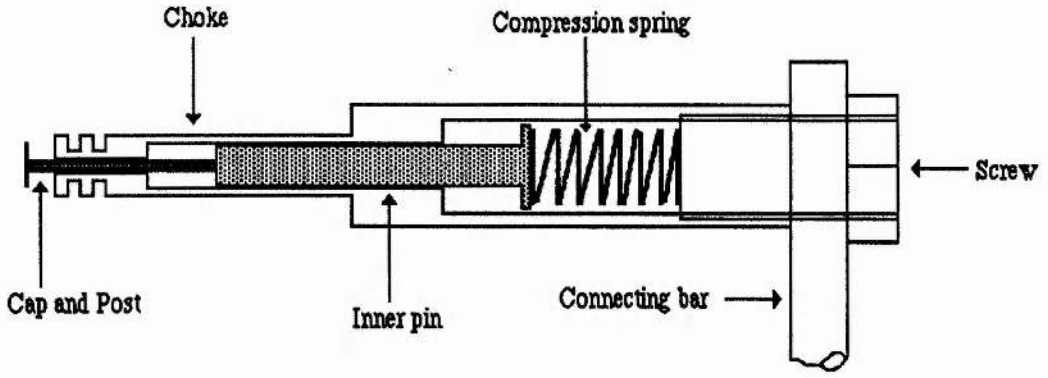

Figure 6.2. Detail of spring-loaded cap and post within the choke.

The filter structure at the lower (diode) end of the choke is a low-pass, five-section low/high impedance design which has been used successfully by Smith [2]. The cut-off frequency is 15GHz, well below the passband edge. The lengths of the various sections had been calculated for both a maximally flat Butterworth filter and a 1dB ripple Chebyshev filter. In practice, it was found that the exact dimensions were not critical, provided that the section lengths were made between $\lambda/8$ and $3\lambda/8$ and avoided half-wave resonance. Similarly, the difference in radius between the low and the high impedance sections should be large so that the reflection coefficient is also large, but should again avoid half-wave resonance. The dimensions of the choke filter are shown in Figure 6.3.

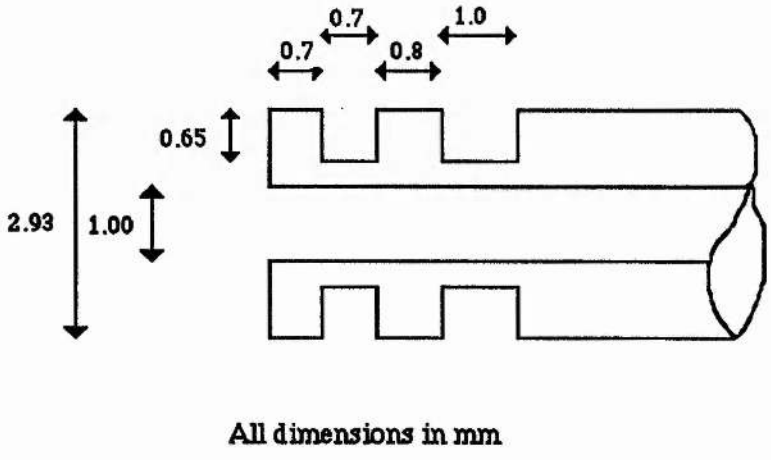

Figure 6.3. Choke filter dimensions.

The cap and post are machined as a single unit from brass or aluminium. The diameter of the post is nominally 1.00mm to give a sliding fit in the centre hole of the choke, and a range of cap diameters can be machined. The caps are usually machined as thin as possible without sacrificing too much mechanical strength - a thickness of about 0.2mm is normal. The overall length of the cap and post is around 10mm. The optimum diameter of cap depends on the particular diode one is using and on the desired output frequency/power, and is determined empirically.

6.3. Doubler Design.

The doubler is similar to the pump oscillator in many respects. The coaxial cavity is identical in position (i.e. it is situated close to the side of the block) and size to the oscillator block. The input waveguide is full-height WG28 with a contacting backshort behind the active device. The output waveguide is machined at right angles to the input guide in the same plane (Figure 6.4) and tapers down linearly from WG28 (2.0x1.0mm) at a point 1.5mm from the centre of the diode, to a 2.5mm long section of WG31(1.1x0.55mm, cut-off frequency 137.5GHz) at the edge of the block. An additional contacting backshort is situated in the WG28 part of the output guide.

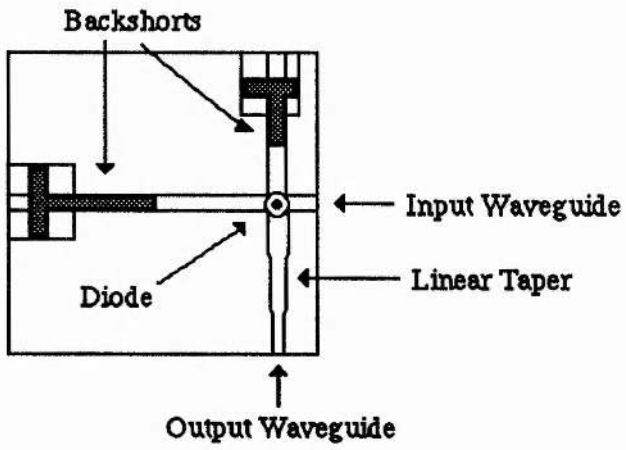

Figure 6.4. Detail of cross-guide section of doubler.

The varactor and varistor diodes were manufactured by Farran Technology and are mounted in pre-contacted miniature pill-packs which facilitate the use of spring-loaded contact techniques similar to those used in the Gunn oscillator. The diode chip with its

honeycomb array of diodes uppermost is mounted on a gold-plated copper rod and is contained in a quartz annulus with a gold lid. The whisker contact is made from the underside of the lid to one of the diodes on the array (Figure 6.5).

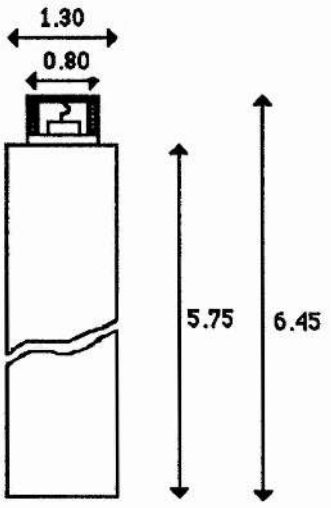

All dimensions in mm.

Figure 6.5. Detail of diode pill pack.

The pill-packaged device is held in a small threaded holder in the bottom section of the doubler block in the same position as the Gunn diode in the oscillator block, and is biased by means of the spring loaded cap and post arrangement. Most of the measurements were made with a 0.8mm diameter post, and the optimum cap sizes were again determined empirically. Electrical protection for the diodes was provided by a 100kΩ bleed resistor connected across the terminals of the SMA connector on the side of the block.

In operation, the oscillator block and the doubler block are bolted together so that the WG28 waveguide windows exactly face each other. Correct alignment is ensured by small dowels mounted on the doubler block which match up with the uppermost two dowel holes of the Hitachi pattern flange on the oscillator block. Once the two blocks are bolted together, the two coaxial cavities are coupled together by a very short length (8mm) of waveguide. Output power is coupled into free space by a feedhorn which consists of a WG31 to circular waveguide transition and a conical section (Figure 6.6).

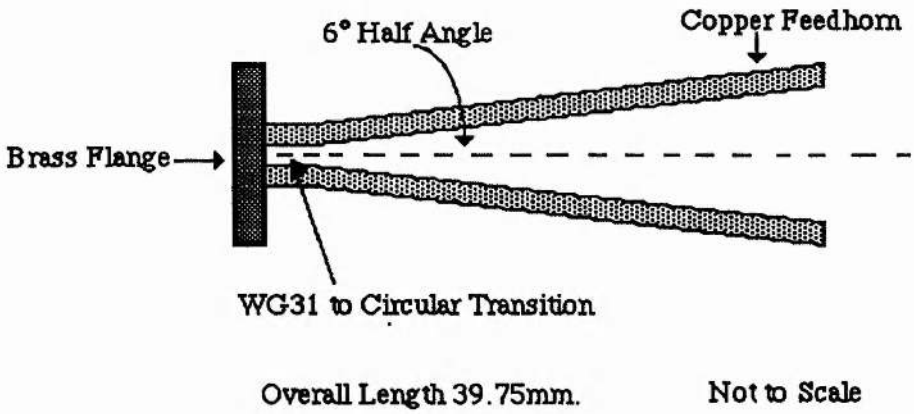

Figure 6.6. Schematic diagram of WG31 feedhorn.

The feedhorn was manufactured first by machining an aluminium mandrel and then by electroforming copper onto the mandrel. The copper bath used was the "No.4 Bright Copper Bath" detailed in The Electroplater's Handbook [4]. Once a sufficient thickness of copper has been deposited on the mandrel it is removed from the electroforming bath and machined down to the desired outer dimensions, (in this case to a wall thickness at the mouth of the horn of about 2.2mm), and the brass flange is fitted. The aluminium mandrel is then etched out in a bath of hydrochloric acid and the feedhorn is cleaned and polished.

At 188GHz the field beam width of the feedhorn was measured to be 14.7° in the H-plane, with a good fundamental Gaussian beam profile. Since a smooth feedhorn such as this does not have a J_0 distribution in the E-plane (vertical plane) but has a 'top-hat' distribution at the mouth of the horn, the field pattern is slightly asymmetrical having a larger beam width in the H-plane than in the E-plane.

6.4. The Varactor Bias Supply.

The bias supply for the varactor diodes (and also the varistor diodes) is shown in Figure 6.7. It is a simple battery-operated supply which enables the centre pin of the SMA connector to be either positive or negative with respect to the outer conductor, i.e. either forward or reverse bias can be applied. A varactor diode requires reverse bias to be applied in order to operate as a multiplier, and the centre-zero ammeter on the bias supply makes it easy to check that no forward current is flowing. Diodes

operating as resistive multipliers, varistors, may however require a small amount of forward bias.

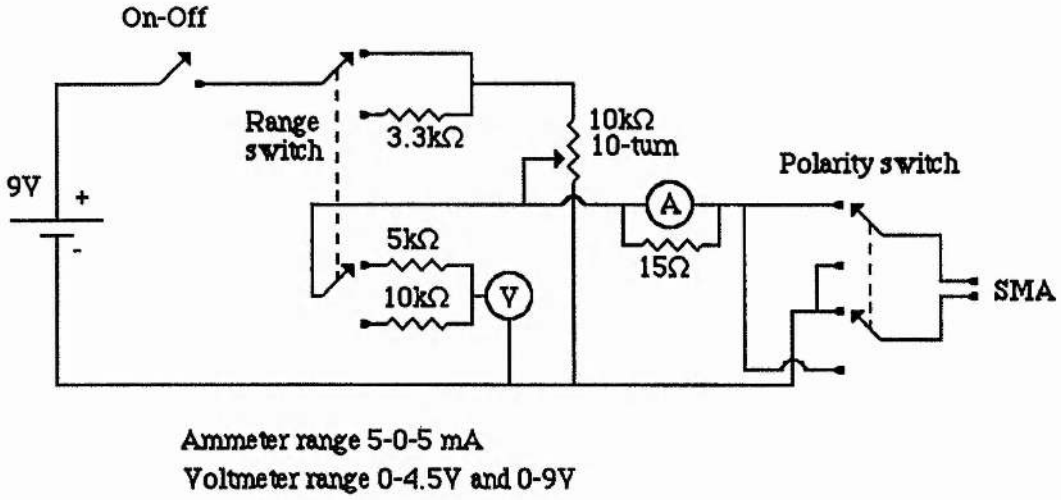

Figure 6.7. Varactor Bias Supply.

6.5. Pump Oscillator Characteristics.

The Gunn oscillator half of the oscillator/multiplier combination can of course operate as a "stand-alone" oscillator and was set up to provide reasonable power over a sufficiently wide tuning range. Frequency measurements were made using a Martin-Puplett polarising interferometer and Golay detector, and the power measurements were taken using an Anritsu ML83A power meter with a WG27 thermistor power head. A Flann WG28 - WG27 transition was mounted between the oscillator block and the power head in order to match the two different waveguide sizes and reduce the VSWR.

Two different Gunn diodes were chosen, one a GaAs device and the other an InP device. Both devices were made by Varian and both operated in the second harmonic mode. Second-harmonic Gunn oscillators are relatively load-insensitive when compared with fundamental oscillators and consequently are better suited to driving reactive loads such as varactors. The tuning characteristics and power-frequency curves of both oscillators are shown in Figure 6.8.

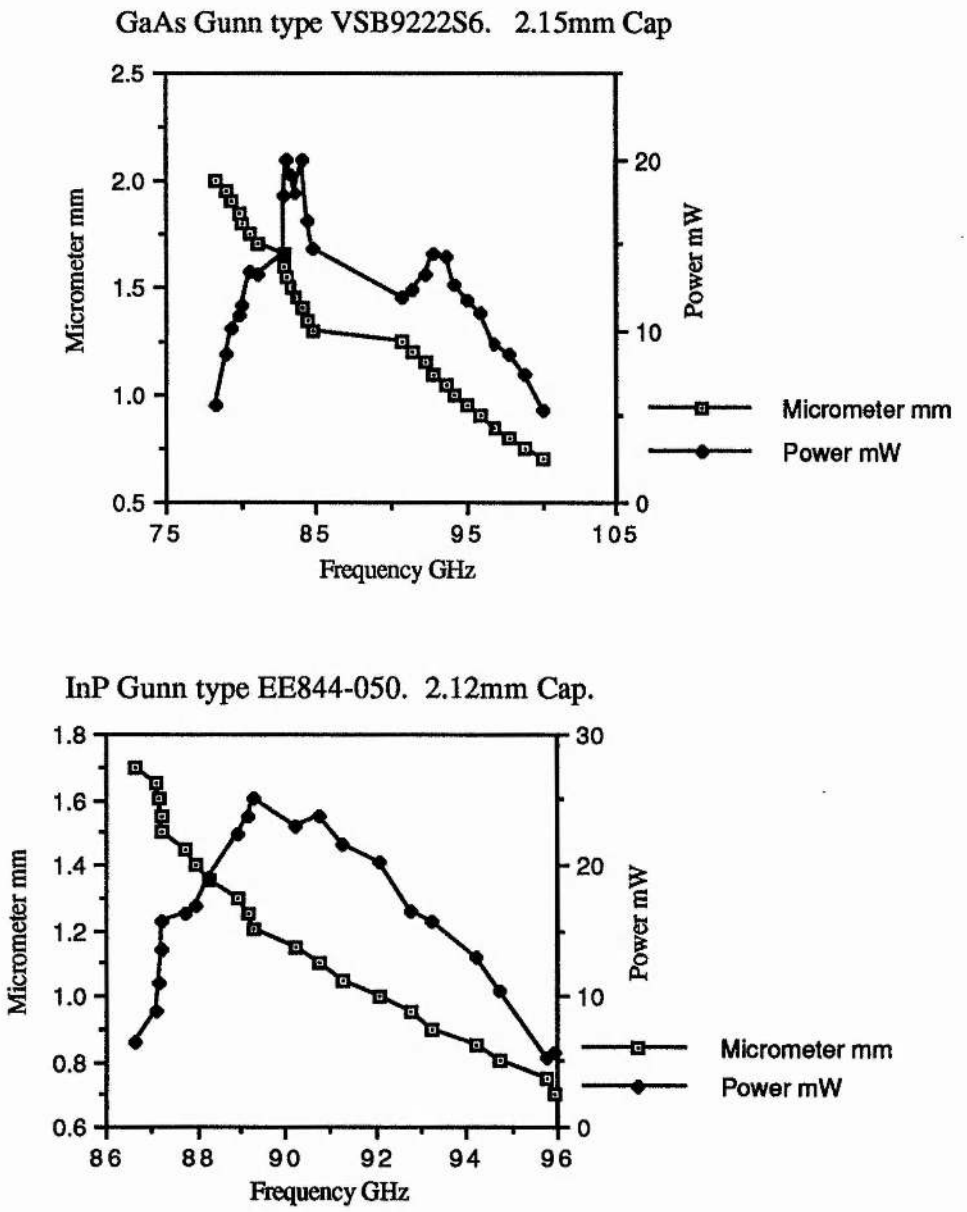

Figure 6.8. Pump oscillator characteristics.

As can be seen from Figure 6.8, the InP device gave a more even spread of power over the band than the GaAs device and therefore was used for the majority of the subsequent measurements.

6.6. Varactor Doubler Measurements.

Most of the measurements were made with a pill packaged Schottky varactor diode manufactured by Farran Technology. Designated VD010/014-01, the diode has the following DC characteristics:

Series resistance R_s	9.7Ω
Zero-bias capacitance C_0	22.4fF
Ideality factor η	1.11
Reverse breakdown voltage V_{BB}	15.8V @ 1μA
Cut-off frequency $F_c=1/2\pi R_s C_0$	800GHz
Package capacitance	50fF
Anode diameter	5.7μm
Anode spacing (centre to centre)	10μm
Recommended output frequency	<170GHz

Under forward bias the IV characteristic of the Schottky barrier diode may be expressed as:

$$I=I_0\exp[q(V-IR_s)/\eta kT)] \qquad (6.1)$$

R_s can be estimated by taking four IV data pairs at 1μA, 10μA, 1mA and 10mA, and using the expression

$$R_s=100[(V_4-V_3)-(V_2-V_1)] \quad \text{ohms} \qquad (6.2)\ [5]$$

The diode is configured by the manufacturer so that the voltage - capacitance variation is very close to the $V\propto C^{-2}$ characteristic of the ideal abrupt-junction varactor.

With the GaAs Gunn diode as the pump source, the optimum cap size for the multiplier was found empirically to be 1.35mm on a 0.8mm post. The process of trial and error by which the best cap size is found is similar to that followed when optimising the performance of a Gunn oscillator, and involves the precise machining of several different sizes of brass caps, and mounting each one in turn in the coaxial cavity. The optimum cap size is that which gives the best power over as wide a range

of frequency as possible. The tuning range is, of course, wholly dependent on the pump oscillator.

Figure 6.9 is a plot of the position of the micrometer (and hence the cavity height) of the multilplier block against the output frequency. Several points can be noted from this graph. Firstly, at each new frequency the position of the micrometer and the positions of the backshorts were adjusted to give the largest possible signal through the Martin-Puplett interferometer, and it was noticed that the position of the micrometer was not particularly critical in the majority of readings taken. In addition, one could usually find two positions of the micrometer, i.e. two cavity heights where the cavity was resonant at the pump frequency (although the output signal levels often differed). This corresponds to fitting an extra half wavelength at the pump frequency in the cavity. Hence the "regions" of cavity height shown in Figure 6.9.

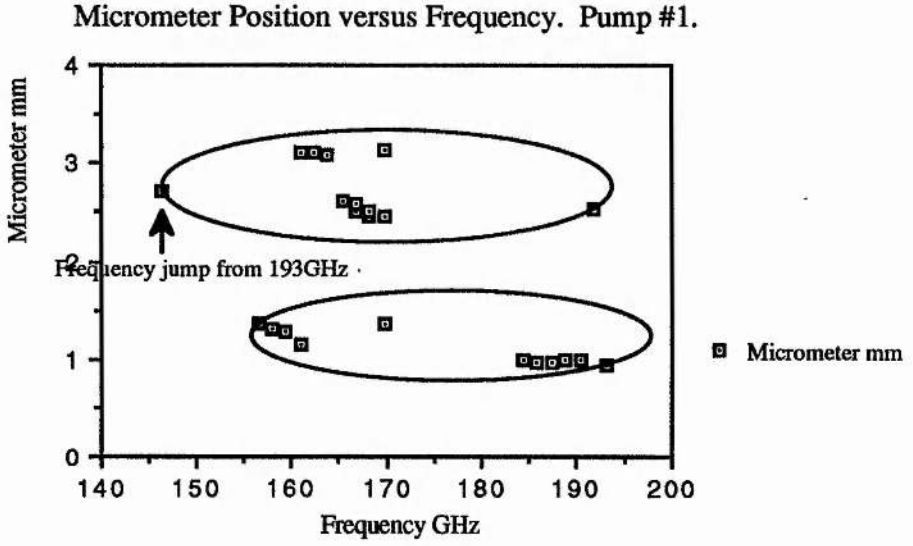

Figure 6.9. Doubler cap size 1.35mm, 0.8mm post. GaAs pump oscillator.

The point marked "frequency jump from 193GHz" is at 146GHz and occurred at the upper limit of the pump oscillator's range. Either the pump oscillator jumped mode at this point to 73GHz (just below cut-off for WG28 waveguide) or the varactor was exhibiting some anharmonic effect, i.e. multiplying by a factor of 3/2. Since the varactor has a voltage-capacitance relationship close to the ideal $V \propto 1/C^2$, and the reverse bias at this point could be varied considerably without having an effect on the output signal (Figure 6.12), it seemed unlikely that anharmonic multiplication was taking place. Much more likely was that the pump oscillator had jumped mode to

73GHz, a frequency normally below cut-off for WG28 (75GHz) but possible if the waveguide was very slightly oversize. In fact the large dimension of the waveguide was found to be approximately 2.05mm, giving a cut-off frequency of 73.17GHz.

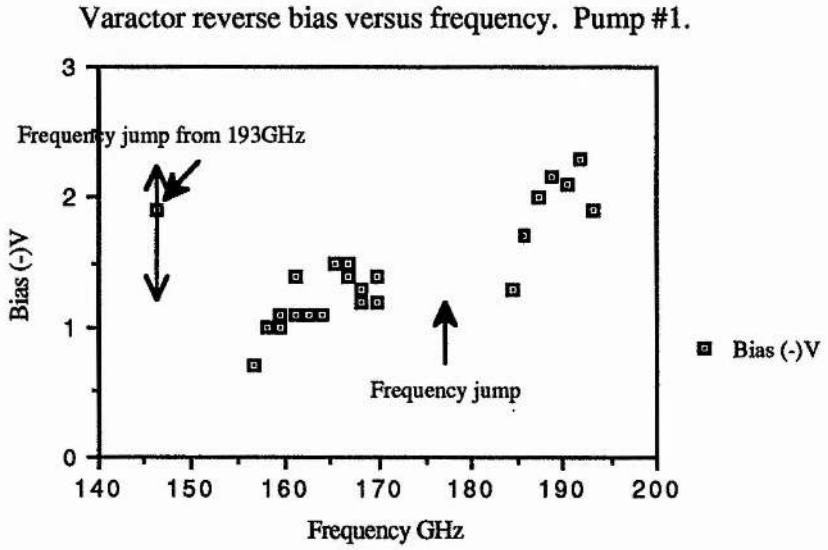

Figure 6.10. Doubler cap size 1.35mm, 0.8mm post. GaAs pump oscillator.

Normally, the reverse bias applied to the varactor which gives the best power is that which is just sufficient to prevent any forward current to flow, and may be regarded as an indication of how much power is being coupled to the diode. Figure 6.12 also shows clearly the output frequency jump due to the frequency jump of the GaAs pump oscillator.

The power levels obtained from the doubler were noted as being low, judged by the signal level received by the interferometer, an initial estimate being a few tens of microwatts. As a calibrated power meter did not exist at St Andrews at the time, the oscillator/multiplier combination was taken to the National Physical Laboratory in Teddington, where several power measurement systems are available. The free space power meter at the NPL measures the absolute power in free space beams to levels of a few microwatts. The chopped input radiation enters the meter through a Brewster angle window, is absorbed by a thin metallic film, and is detected photo-acoustically. The absolute calibration of the meter is acheived by ohmic heating of the film with the same modulation envelope as the radiation. This type of meter will give an absolute power measurement over a very broad band (60-1000GHz) with an accuracy of 10%, and power levels of the order of a few tens of microwatts would be easily detected.

Unfortunately, the NPL meter had suffered damage to the metallic film and consequently was much less sensitive than specified. As a result no signal at all could be detected.

Measurement with a cooled InSb bolometer gave 35μW at 196GHz, a figure which is likely to be of the correct order of magnitude but which cannot be taken as being absolute since the bolometer had been calibrated at 100GHz, and the matching of the power into the InSb was unknown - a common problem with such detectors. Consequently, to a first approximation the absolute power levels acheived with the doubler may be regarded as a few tens of microwatts, although relative power levels can be estimated from the signal level detected by the Golay detector on the interferometer.

The following measurements were all taken with the InP diode in the pump oscillator. As well as giving a more even spread of power over the band, the oscillator was also more powerful (Figure 6.8).

With the multiplier set up with the 0.8mm post and 1.35mm cap, the tuning characteristic is shown in Figure 6.11. Comparing with the previous plot of micrometer position versus frequency, one can see that just one of the two possible cavity heights was chosen at each frequency (because the power output was better) and, allowing for scatter, the micrometer mimics the position of the pump oscillator's micrometer as the frequency is tuned. Over the range of output frequency, the cavity of the multiplier changes by approximately 0.5mm, while that of the pump changes by 1.0mm since the InP is a second harmonic oscillator.

A plot of the varactor reverse bias versus the output frequency (Figure 6.12) shows a distinct dip in the bias just above 180GHz which corresponded to a dip in the power coupling to the varactor and also to a dip in the output power. When one refers to the power/frequency characteristic of the pump oscillator (Figure 6.8) there is no such dip in the power. The power dip must therefore either be due to a resonance in the multiplier which couples only weakly to the varactor diode, or to a reflection of power back from the varactor and circuit.

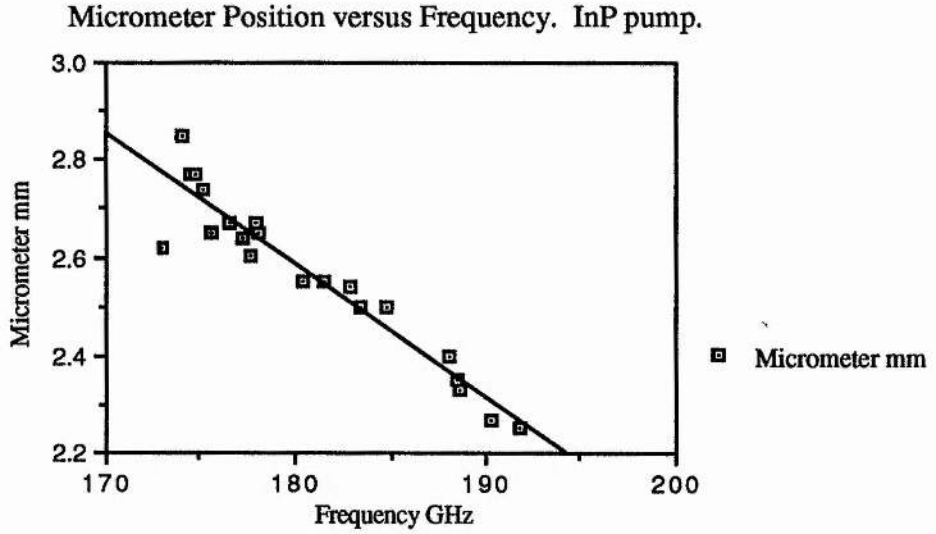

Figure 6.11. Doubler cap size 1.35mm, 0.8mm post. InP pump oscillator.

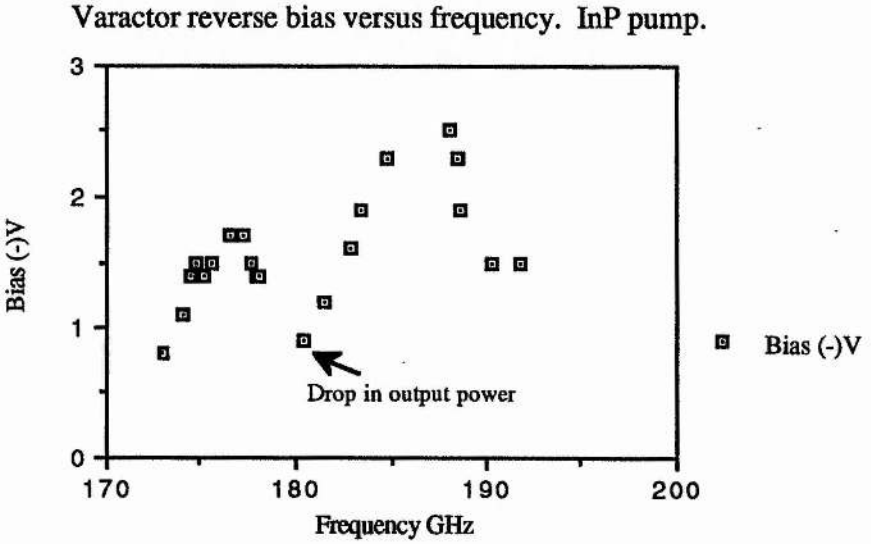

Figure 6.12. Doubler cap size 1.35mm, 0.8mm post. InP pump oscillator.

The next measurements were made with the 1.35mm cap replaced by a 1.45mm cap. The post size remained at 0.8mm diameter. Figure 6.13 shows the tuning characteristic to be fairly similar to that obtained with the 1.35mm cap with the exception of the last two points which were measured at a lower cavity height.

Interestingly, this jump in cavity heights is close to $\lambda_p/4$ where λ_p is the pump wavelength, and not $\lambda_p/2$ as might be expected.

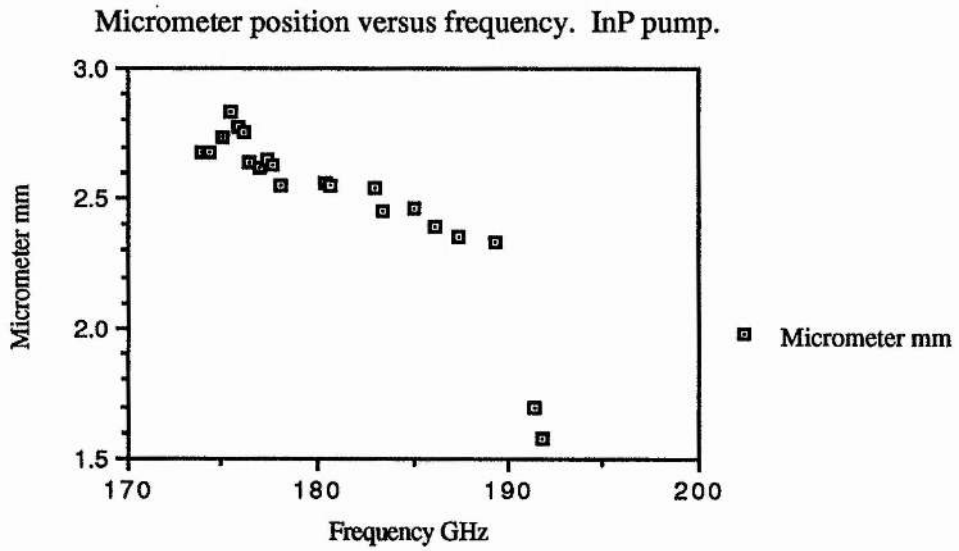

Figure 6.13. Doubler cap size 1.45mm, 0.8mm post. InP pump oscillator.

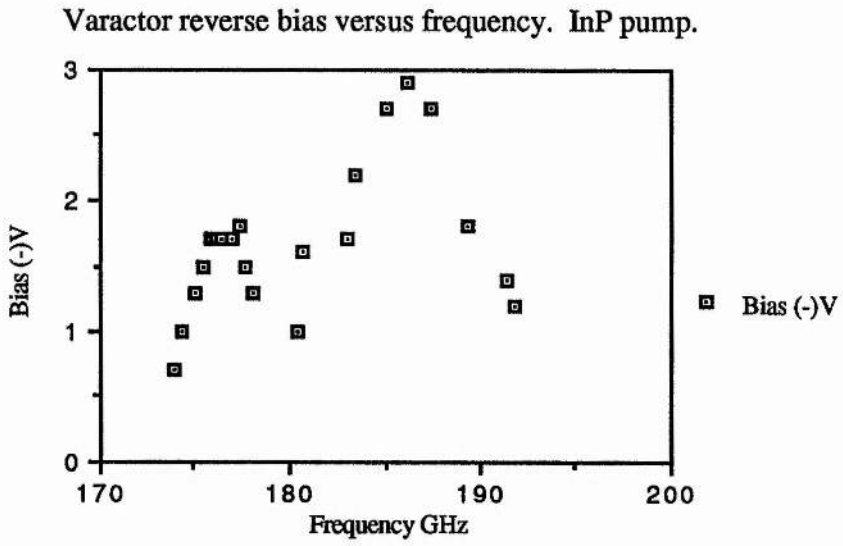

Figure 6.14. Doubler cap size 1.45mm, 0.8mm post. InP pump oscillator.

The plot of the varactor reverse bias shows clearly the dip in power coupled to the diode which again corresponded to a dip in the output power, and also shows a peak

in the power coupled to the diode. Neither feature can be attributed to variations in the pump power of the Gunn oscillator. A further increase in cap size gave similar results, although the power output was a little lower than that obtained with the 1.45mm cap (Figures 6.15 and 6.16).

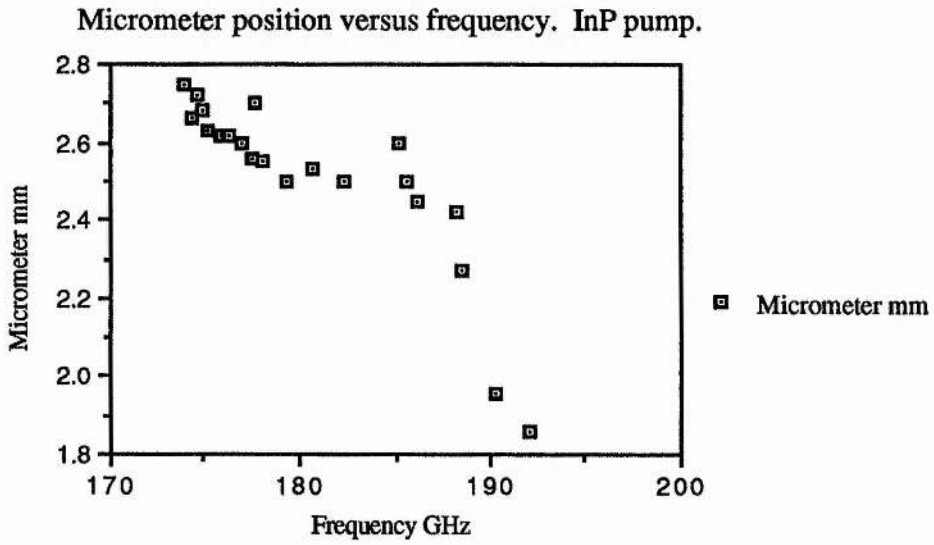

Figure 6.15. Doubler cap size 1.50mm, 0.8mm post. InP pump oscillator.

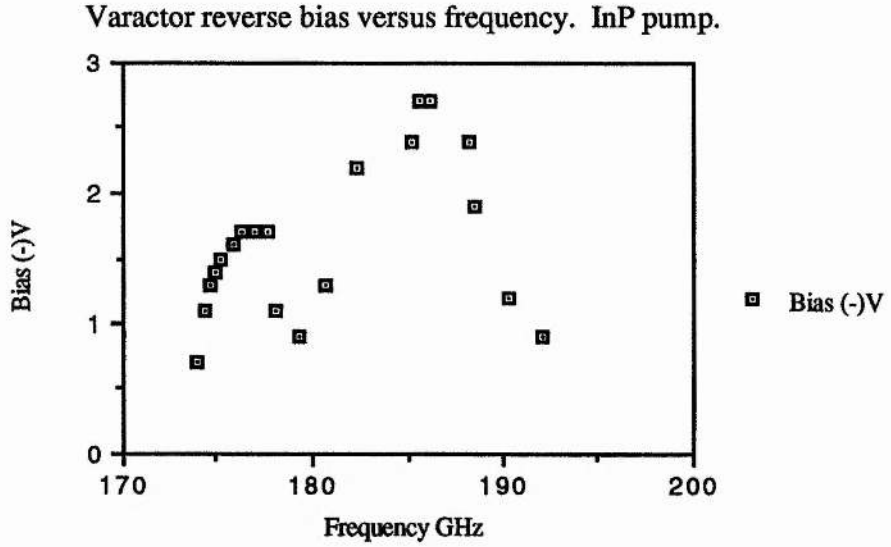

Figure 6.16. Doubler cap size 1.50mm, 0.8mm post. InP pump oscillator.

The varactor was then replaced by a varactor with a lower series resistance of 8.46Ω and a lower zero-bias capacitance of 12.5fF, giving a higher cut-off frequency

of 1500GHz and theoretically better efficiency. The recommended output frequency range for this diode, designated VD011/014-01, is 170-260GHz. The diode was packaged in the same way as the VD010 diode, with a package capacitance of 50fF. The precise effect that the package capacitance has on the performance of the doubler is difficult to quantify and depends on the inductance of the whisker, the inductance of the coaxial post in the waveguide, the capacitance due to the cap, and the Q of the cavity. Using a 0.8mm diameter post with a 1.45mm diameter cap gave a slightly higher power output than the previous diode with the same cap and post (Figures 6.17, 6.18). The graphs show similar features to those observed previously, particularly the dip and peak in the bias plot. The dip again corresponded to a dip in the output power whilst the peak corresponded to an increase in the output power, although one must bear in mind that an increase in the necessary reverse bias is only a measure of the power coupled into the diode and not necessarily a measure of the output power at the harmonic.

Micrometer position v. frequency. VD011 varactor, InP pump.

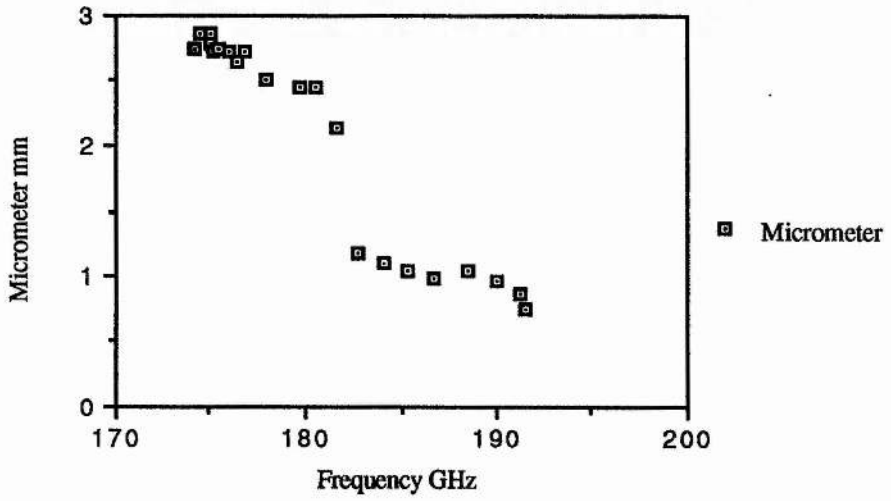

Figure 6.17. Doubler cap size 1.45mm, 0.8mm post. InP pump oscillator

Varactor reverse bias v. frequency. VD011 varactor, InP pump.

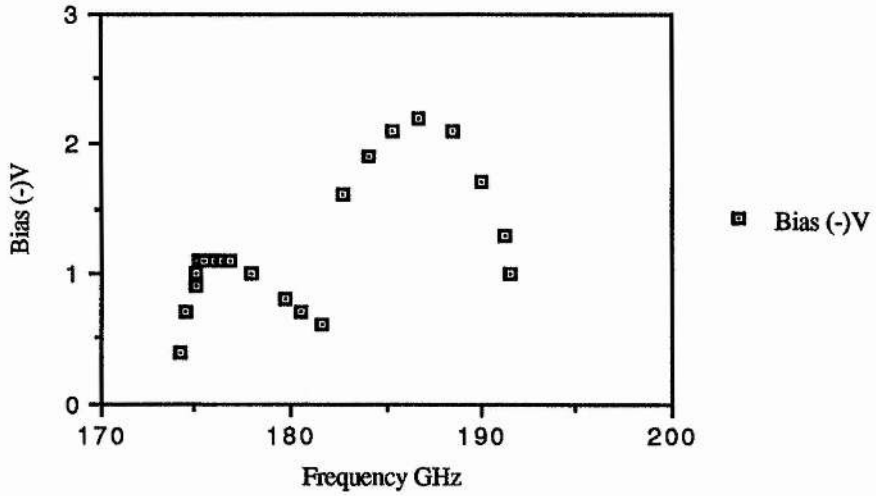

Figure 6.18. Doubler cap size 1.45mm, 0.8mm post. InP pump oscillator.

6.7. Varistor Doubler Measurements.

The varactor diode used in the previous measurements was now exchanged for a fast detector/mixer diode which would rely on its non-linear forward IV characteristic to frequency double. The diode was a GaAs Schottky barrier diode designated SD012-014-01 manufactured by Farran Technology and mounted in an identical package to the varactor diodes. Its DC characteristics are as follows:

Series resistance R_S 8.75Ω at 10mA
Zero-bias junction capacitance C_0 7fF
Ideality factor η 1.14
Reverse breakdown voltage V_{BB} 5V min/8V typ. at 10μA
Cut-off frequency $F_c=1/2\pi R_S C_0$ 2800GHz
Package capacitance 50fF

The pump oscillator was also reconfigured to provide slightly more power (Figure 6.19).

Reconfigured pump oscillator. InP diode type EE844-050

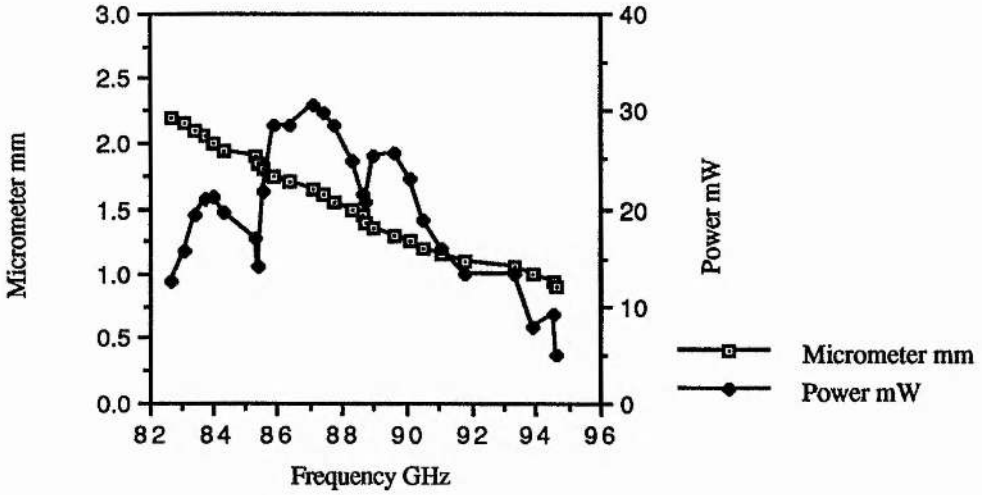

Figure 6.19. Reconfigured pump oscillator characteristic.

With no RF applied, the diode was biased to the point where forward current just starts to flow, at about 0.75V. With the Gunn oscillator switched on, the diode successfully frequency doubled, with the power ouput similar to that obtained with the varactor diodes (Figures 6.20, 6.21).

Micrometer position v. frequency. SD012 mixer/detector diode, InP pump.

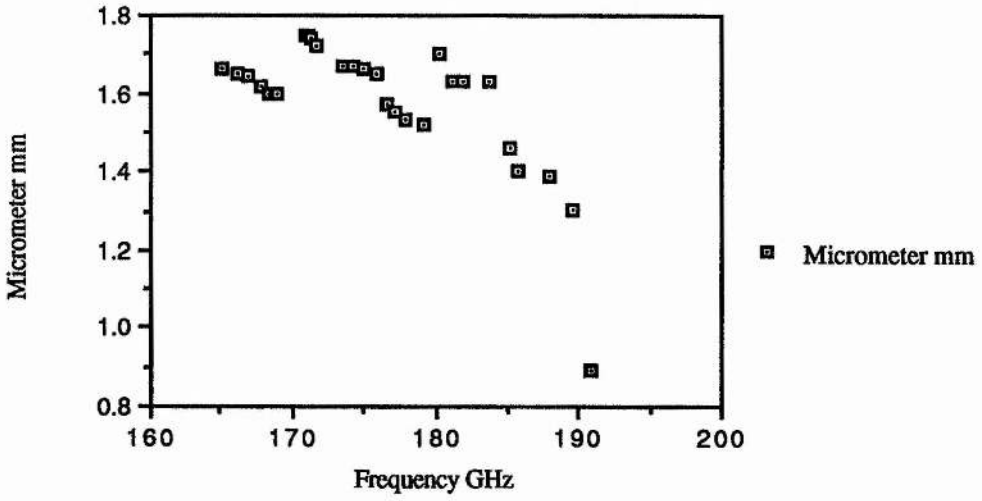

Figure 6.20. Doubler cap size 1.45mm, 0.8mm post. Mixer/detector diode operating as varistor.

Forward current v. frequency. SD012 mixer/detector diode, InP pump.

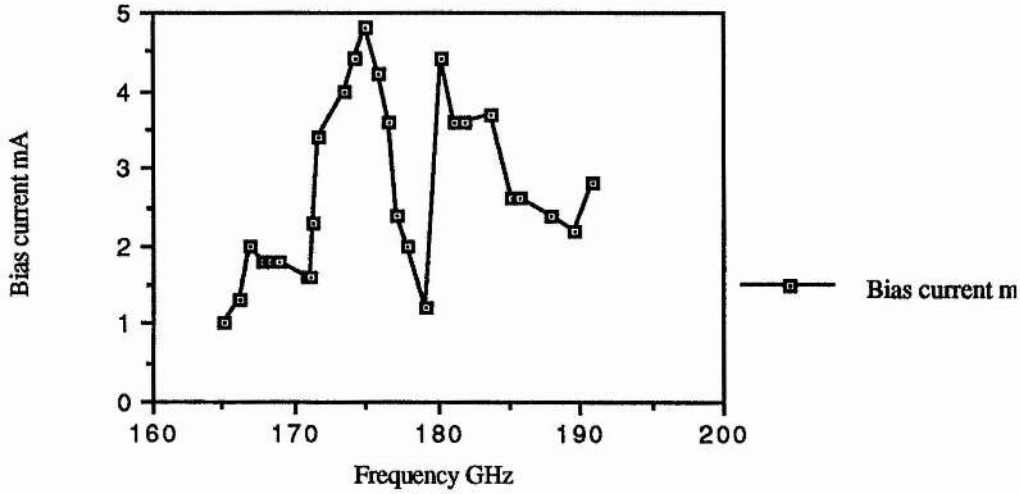

Figure 6.21. Doubler cap size 1.45mm, 0.8mm cap. Mixer/detector diode operating as varistor.

As the RF is applied to the diode, the current through the diode increases and the bias voltage decreases along the load-line of the bias supply. The bias supply was identical to that used to bias the varactor diodes with the exception that the voltmeter had been exchanged for a centre-zero voltmeter. To illustrate the way in which the DC IV characteristic changes as RF is applied, consider Figure 6.22.

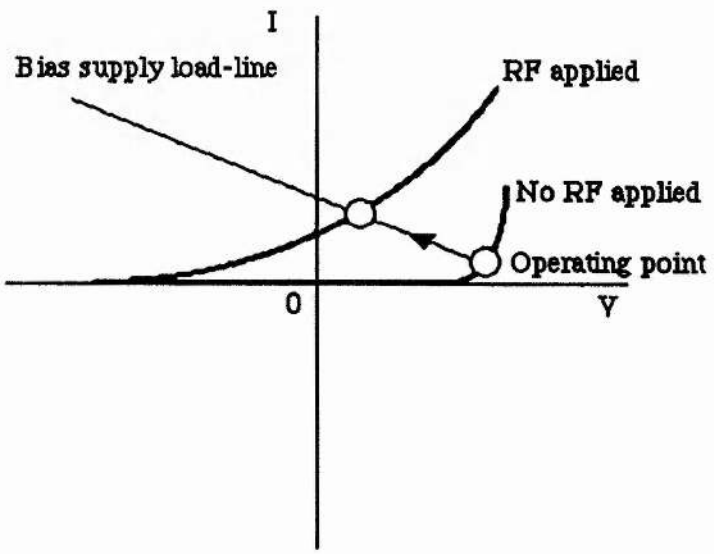

Figure 6.22. Change in DC characteristic of diode as RF is applied.

With no RF applied to the diode, the IV curve follows the x-axis, i.e. 'no current' (that is, very little) flows through the diode until the bias reaches about 0.75V at which point the diode starts to conduct. If we assume that we are now at the operating point illustrated in the diagram, we now apply RF to the diode. The diode now draws current on each alternate half cycle from the bias supply, and the operating point moves up and to the left as shown in the diagram, along the load-line of the bias supply. If the bias supply was an ideal constant-voltage source (zero output impedance) the load-line would be vertical, that is the bias supply would maintain the same bias voltage and simply supply more current. On the other hand, if the bias supply had an infinite output impedance - a constant-current supply - the load-line would be horizontal. In this case the bias supply is neither constant-voltage nor constant-current, but somewhere in between, with a load-line gradient of about -1.5kΩ.

When one applies RF, the DC characteristic changes shape as well as shifting the operating points. The distinctive J shape of the IV curve lifts and flattens out, becoming more like a series resistance as the level of RF is increased, due to the averaging effect of the external circuitry on the diode's rectification. As shown in Figure 6.22, it is also possible to move the operating point to a region in which the measured bias voltage is negative. To show how this can happen, consider Figure 6.23.

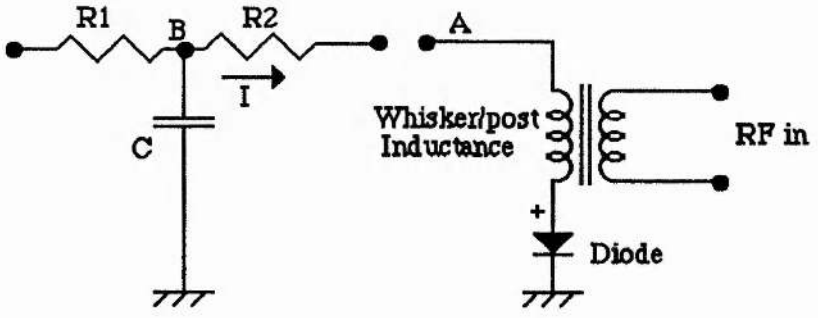

Figure 6.23. Schematic of diode and external circuit.

The coupling of the RF to the diode via the whisker/post inductance may be represented as shown in the diagram. Capacitances associated with the diode package

and the cap are omitted for simplicity. During those half cycles which make the anode of the diode positive, the diode will conduct. In order to draw current down through the diode, the potential at point A must fall with respect to B, drawing current through resistor R2, where R2 is the resistance due to the diode contact. During those half cycles where the anode is negative, no current is drawn. Averaged over time by the inherent low-pass characteristics of the bias supply, supply leads and other circuitry, a 'DC' current component due to the RF rectification is present, its magnitude dependent on the RF level. The voltage drop across resistor R2 is determined by the current drawn through it by the diode (by Ohm's Law) and consequently the voltage seen at B (that is indicated by the meter on the bias supply) may become negative as it follows the potential at A.

One of the parameters which requires to be optimised to maximise the signal at the second harmonic, is the operating point. Generally, for small-signal applications where the voltage swing across the diode is very small, the point on the DC characteristic with maximum non-linearity would be chosen. For the Farran diode, this point is at about 0.75V. When one applies RF to the diode, the current one measures is now a sum of the current due to the DC characteristic of the diode itself and the current due to rectification of the RF. In addition, the operating point will have moved along the load-line of the bias supply by an amount dependent on the level of RF being coupled to the diode in the cavity, which in turn depends on the cavity Q, and normally has some frequency structure. The bias supply therefore has to be adjusted until the second harmonic signal reaches a maximum value at each frequency.

6.8. Doubler Efficiency.

From the estimated power of the doubled frequency and the measured power of the input frequency we can to a first approximation estimate the efficiency of the doubler to be around 0.1%, whether using a varactor or a varistor diode. This compares with an efficiency of between 5 and 12% quoted by the diode manufacturer Farran for the waveguide doublers which they market for the output frequency range 170 - 200GHz, which use whisker-contacted chips on pins rather than the pill-packaged devices.

Several reasons exist for the comparatively low efficiencies which have been noted here. Firstly, the simple design of the doubler block, although enabling the pump

power to be coupled reasonably well to the diode, also allows the second harmonic to propagate back down the waveguide towards the pump oscillator. Some reflection of the pump power from the diode will also occur. Isolation of the output signal from the input signal is required, by means of a split block and low-pass coupling filter between the input and the output. The filter should allow the input frequency to pass to the diode but should reject the doubled frequency. Secondly, WG28 waveguide will become overmoded at the doubled frequency, allowing power to be coupled into modes other than the TE_{10} mode. Therefore, the output waveguide should be smaller in order to remain single mode over the output frequency band. Thirdly, the 'shared cavity' design makes it difficult to match the impedances at the input and output frequencies simultaneously, with the same circuit. Finally, performance has been traded for ease of use in the choice of the packaged devices rather than whisker contacted chips.

Chapter 6 References.

[1] H.Rothermel, T.G.Phillips and J.Keene, "A solid-state frequency source for radio astronomy in the 100 to 1000 GHz range", Int. Journal of Infrared and Millimeter Waves, nol.10, no.1, p.83, 1989.

[2] G.M.Smith, "Transferred electron oscillators at mm-wave frequencies and their characterisation using quasi-optical techniques", PhD Thesis, St.Andrews University, March 1990.

[3] J.E.Carlstrom, R.L.Plambeck and D.D.Thornton,"A continuously tunable 65-115 GHz Gunn oscillator", *IEEE MTT*, vol. MTT-33, no.7, p.610, 1985.

[4] C.W.Ammen, "The Electroplater's Handbook", Tab Books Inc., Blue Ridge Summit, PA, 1986.

[5] Application Note 87/1-AN11, Farran Technology Ltd, Ballincollig, Cork, Ireland.

7. QW Devices as Detectors.

7.1. Introduction.

The first resonant-tunneling double-barrier diodes supplied to St.Andrews University by Nottingham University as part of the NUMBERS project were mounted in N34 packages (similar to the package used for W-band Gunn diodes), and as such were suitable for mounting in coaxial cavity oscillator blocks. The blocks were identical to the Gunn oscillator blocks detailed in previous chapters.

The devices under investigation were taken from wafers of three different layer profiles, and diced into chips of 200μm, 100μm and 20μm diameter, with a variety of bond wire configurations. While none of the devices oscillated at millimetre wave frequencies, several could detect millimetre wave radiation.

7.2. Layer Strucures.

The three layer profiles of the wafers from which the devices were taken were designated NU195, NU298 and NU234. They are shown schematically in Figures 7.1, 7.2 and 7.3. NU195 has a symmetric structure with fairly thick barriers, and NU298 is also symmetric with very thin, but higher, barriers. NU234 is a superlattice-barrier-superlattice structure. It too has a symmetric layer profile.

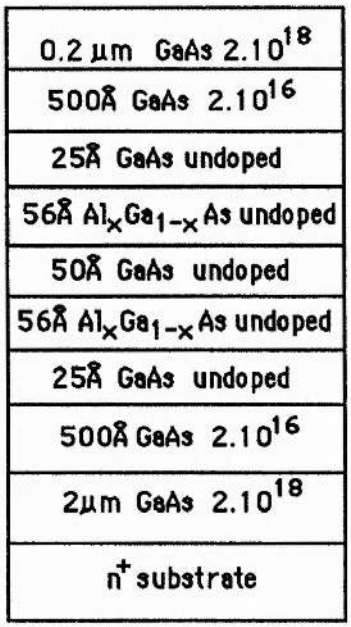

Figure 7.1. NU195 layer structure. x=0.4

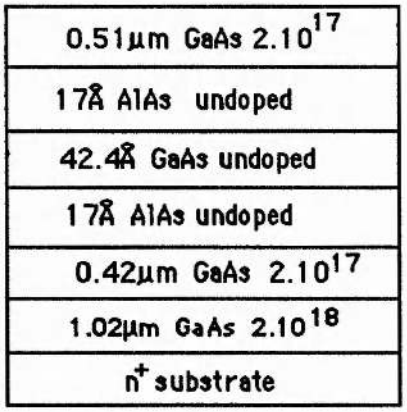

Figure 7.2. NU298 layer structure.

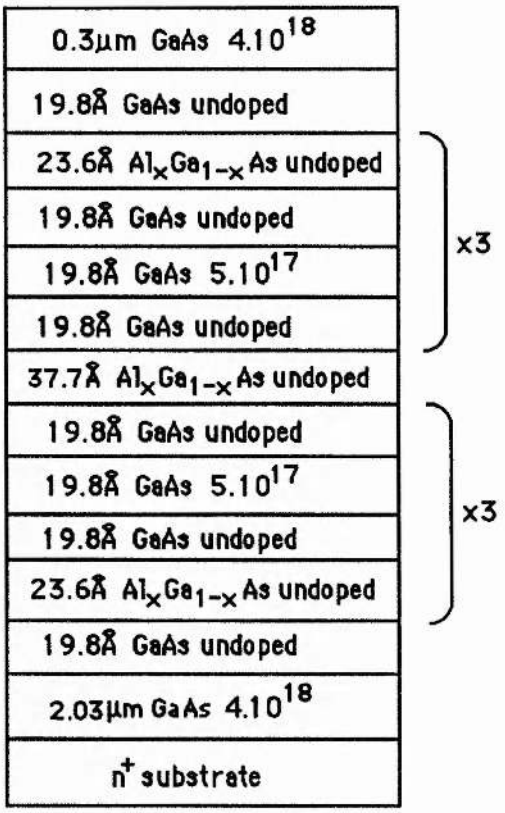

Figure 7.3. NU234 layer structure. x=0.4

7.3. Asymmetric IV Characteristics.

Despite the nominally symmetric layer profiles of devices from all three wafers, devices from NU195 and NU234 showed distinct asymmetry in their IV curves (Figures 7.4 to 7.6). There are several possible causes for this asymmetry. Discounting the possibility that the asymmetry is due to non-ohmic contacts [1], the asymmetry must be due to the layer structure itself.

Broadly speaking, the width and the height of the barriers determines the peak current on resonance; and the level of the quasi-stationary state within the well determines the peak voltage. However, the position of the peak voltage is also strongly dependent on the Fermi energy outwith the barrier/well region. Assuming that in the case of the NU195 layer structure the asymmetry in the IV is not due to asymmetry in the barriers [2], one concludes that the asymmetry is due to differences

in the layers either side of the barriers. It is thought that this is due to the finite time taken to increase or decrease the level of doping in the layers.

Consider the NU195 layer profile. The layers are grown from the substrate up, so the 2μm GaAs doped to a level of $2x10^{18}$ cm^{-3} is grown first. The temperature of the silicon cell is then ramped down to lower the doping level to $2x10^{16}$ cm^{-3}, a process which will take a finite time and a finite thickness of growth to complete, typically over 300-500Å. Once the barrier-well-barrier structure and the undoped 'clouding' layers have grown, Si is introduced again to grow the 500Å $2x10^{16}$ cm^{-3} layer, and then the temperature of the Si cell is ramped up to increase the doping to $2x10^{18}$ cm^{-3}. Once again, this increase in the doping level takes typically 300-500Å. The net effect, therefore, is that on the substrate side there is a thinner lower-doped region than implied by the nominal layer profile; and on the top contact side, there is a thicker lower doped region.

Other mechanisms which may have a degrading effect on layer growth are diffusion of silicon from the substrate into the first barrier, and poor interface quality. Interface quality may be affected by the fact that AlGaAs tends to grow with a better interface on GaAs than GaAs does on AlGaAs. In some cases, it is also possible for damage to occur to the topmost barrier during the process of ultrasonic bonding of the contact wire to the top of the mesa.

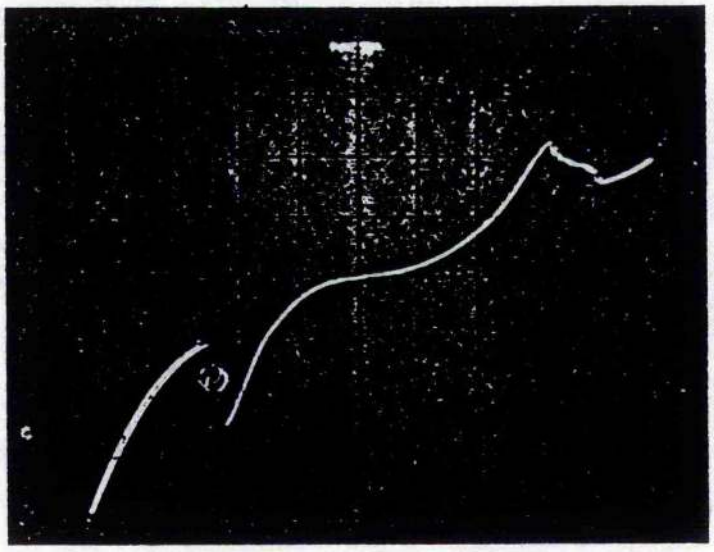

Figure 7.4. Asymmetric IV curve of NU195, 200μm diameter device, Maltese cross contact. Scale 0.2V/div horiz., 20mA/div vert.

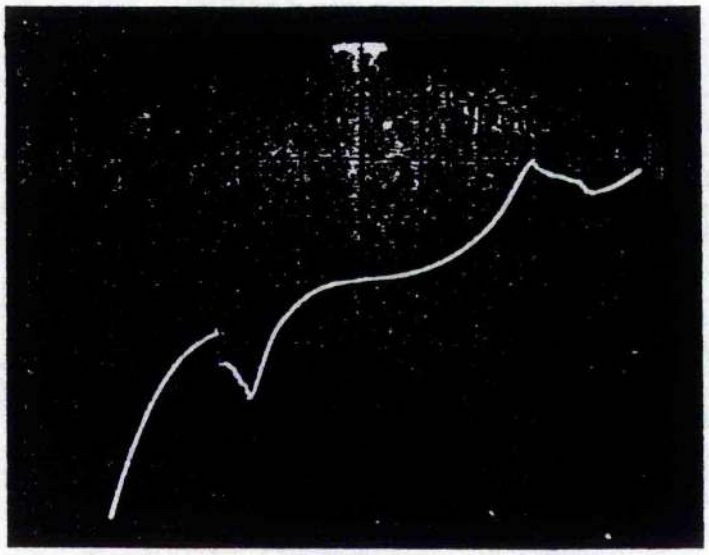

Figure 7.5. Asymmetric IV curve of NU195, 100μm diameter device, Maltese cross contact. Scale 0.2V/div horiz., 5mA/div vert.

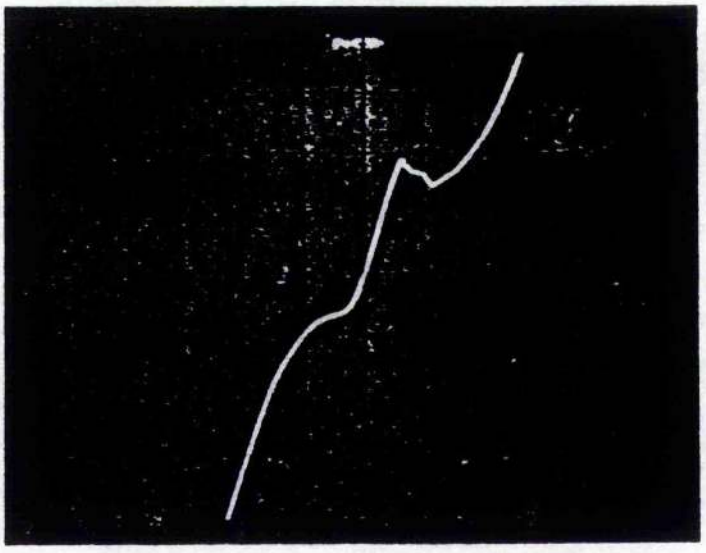

Figure 7.6 Asymmetric IV curve of NU234, 100μm diameter device, Maltese cross contact. Scale 0.2V/div horiz., 10mA/div vert.

7.4. Large Diameter Devices.

Four of the devices, three of which were taken from layer NU195 and one from NU234, were very large diameter devices. One of the NU195 devices was 200μm in diameter; the other devices were 100μm in diameter (see Figures 7.4-7.6 above). Such large diameter devices are bound to have very large capacitances which lower their maximum oscillation frequency. Since QW devices which are designed for high-frequency operation are typically only a few microns in diameter, it was not surprising that none of them could be induced to oscillate at W-band. The devices were also tested for ability to detect millimetre wave radiation. The three devices whose IV characteristics are shown above showed no response to radiation.

The fourth device, a 100μm device from NU195 mounted in a package without a lid, was able to detect radiation at 86GHz. The input power level was around 50mW. With no radiation coupled into the device, the forward IV characteristic was measured (Figure 7.7).

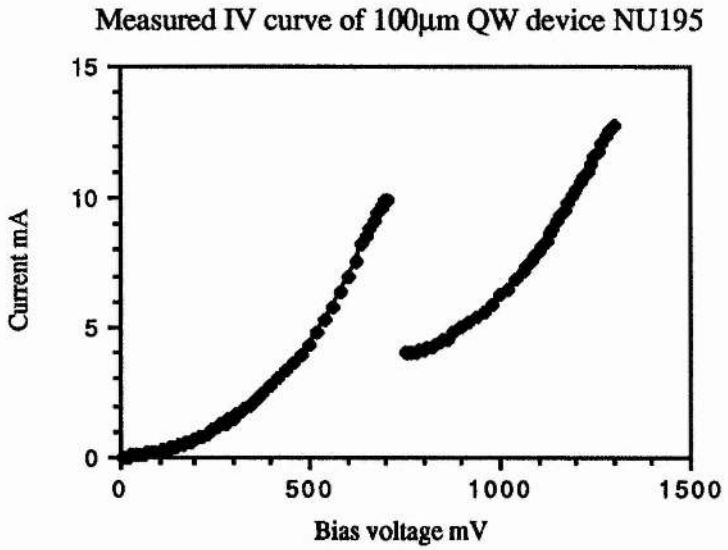

Figure 7.7. NU195 forward bias IV characteristic.

Modulated power at 86GHz was then coupled into the device and the output detected by phase sensitive detection (Figure 7.8).

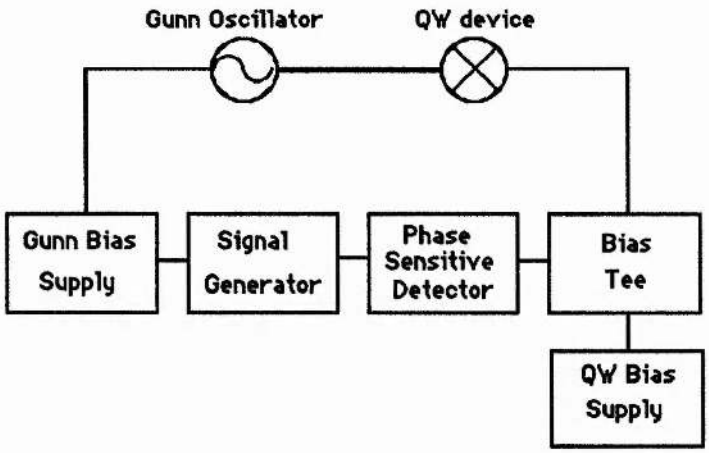

Figure 7.8. Millimetre wave detection by device NU195.

At zero DC bias, a small output signal, which depended on the incident power level, was detected. This suggests asymmetry about the origin in the IV characteristic of the device, confirmed by IV curves of other devices from the same wafer. The DC bias to the QW device was varied from zero through the negative resistance region and the output of the PSD recorded (Figure 7.9).

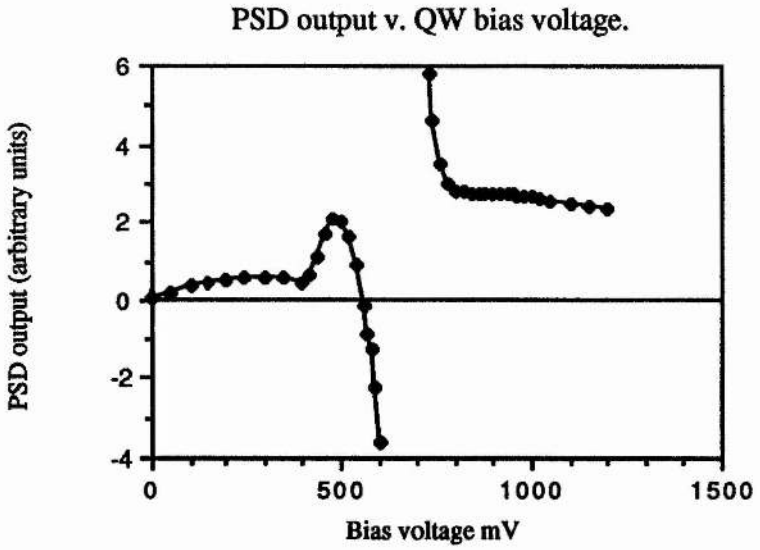

Figure 7.9. Variation of PSD output with QW bias.

The curve shown in Figure 7.9 is a measure of the average change in current caused by the RF voltage swing across the device. When RF is coupled into a non-linear device, the average value of the current at the bias point changes, a familiar effect in devices such as square-law detector diodes. The amount by which the current changes depends on the extent of the RF voltage swing about the bias point and on the degree of non-linearity of the IV characteristic. The sign of the change in current depends on the sign of the second differential of the IV curve about the bias point. The overall effect with a device which exhibits NDR, therefore, is a tendency for the IV curve to flatten out when RF is applied, and the magnitude of the PSD output in Figure 7.9 is a measure of the degree of flattening of the curve.

It is worth noting that the gradient of the NDR region was steep enough to cause problems when attempting to bias into the NDR region since the output resistance of the bias supply must be less than the gradient of the NDR region - in this case, just a few ohms. It is an important device parameter that the negative resistance region is shallow enough to allow a non-ideal (i.e. real) voltage source to bias into this region. This requirement is especially important for devices being used as oscillators.

7.5. Smaller Diameter Devices.

A number of 20μm diameter devices were made available, also mounted in N34 packages, from the NU298 wafer. Their IV characteristics were nominally symmetric about zero volts, as shown in Figures 7.10-7.13. Four devices were investigated, one of which had a Maltese cross contact, one with a 10μm wire V-bond, one with a 10μm wire I-bond, and one with a 25μm wire V-bond. All four devices showed a change in the shape of their IV curves when RF power was coupled into them.

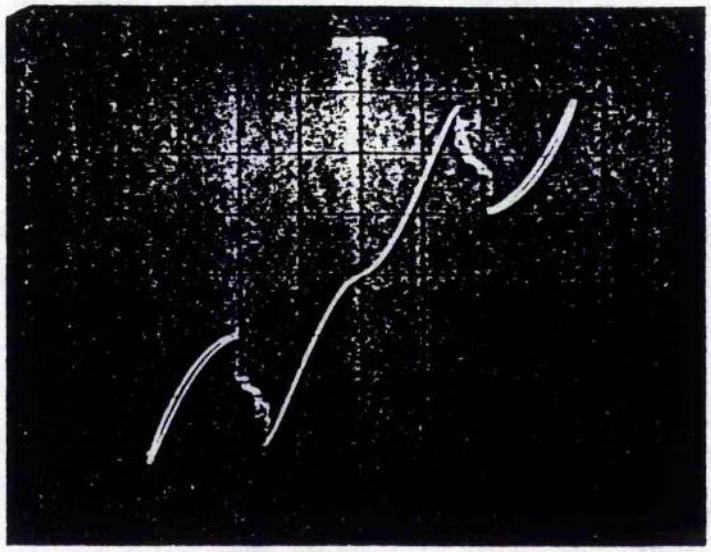

Figure 7.10. IV curve of NU298, 20μm diameter device, Maltese cross contact. Scale 0.5V/div horiz., 20mA/div. vert.

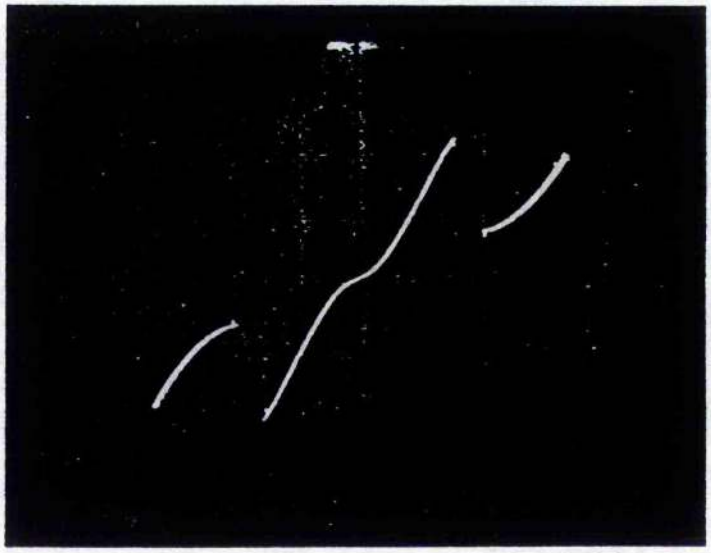

Figure 7.11. IV curve of NU298, 20μm diameter device, 10μm wire V-bond contact. Scale 0.5V/div horiz., 20mA/div vert.

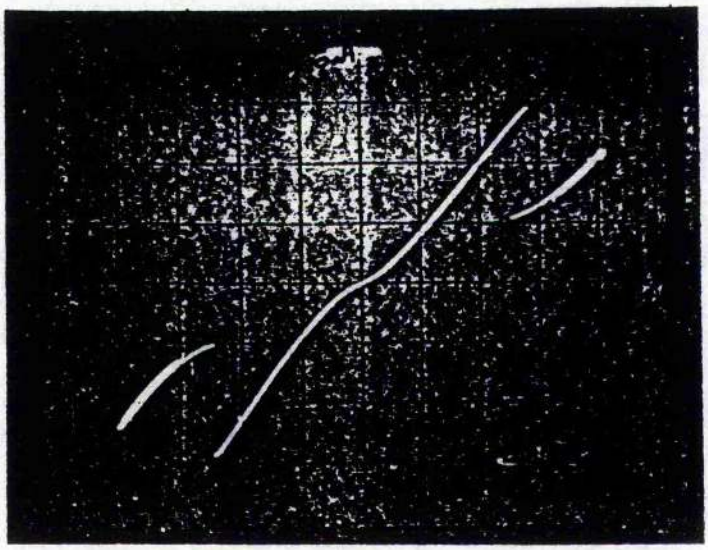

Figure 7.12. IV curve of NU298, 20μm diameter device, 10μm wire I-bond contact. Scale 0.5V/div horiz., 20mA/div vert.

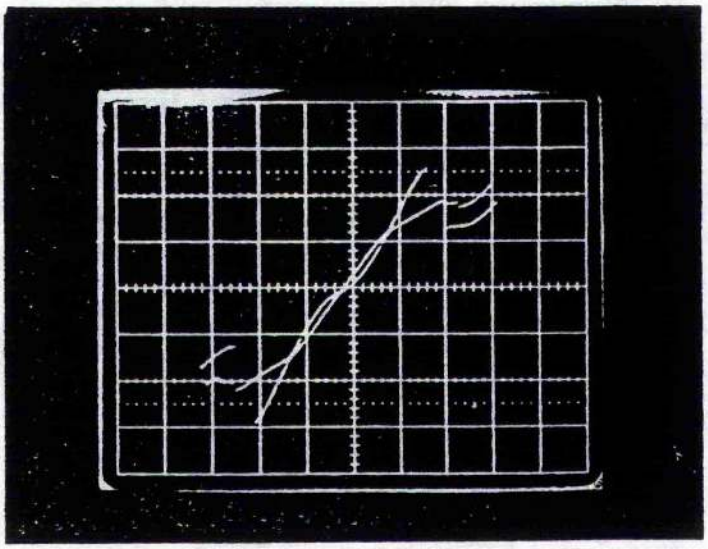

Figure 7.13. IV curve of NU298, 20μm diameter device, 25μm wire V-bond contact. Also showing effect of applied RF power. Scale 0.5V/div horiz., 10mA/div vert.

As discussed above, the effect of coupling RF power into a non-linear device is a tendency for the non-linearities of the IV curve to "straighten-out". This effect was observed in all four 20μm diameter devices, and was largest at regions of greatest non-linearity, i.e. the negative resistance regions.

With a maximum available pump power of around 10mW at 85GHz, the length of the coaxial cavity and the position of the backshort were adjusted to produce the maximum response. The response of the device with the 25μm wire V-bond contact has already been shown in Figure 7.13. Figures 7.14-7.16 show the responses of the three remaining diodes. Note that both the Maltese cross contact device and the 10μm wire V-bond contact device show degraded peak to valley ratios, due to overvoltage damage. While the position of the peaks have remained the same in terms of voltage for both devices, the values of the peak currents in both cases are slightly higher. The increased current density, together with the increased scattering in the well, suggests possible degradation of the barrier interfaces, possibly through diffusion of silicon from the doped layers either side of the barriers [1]. However, it was not possible to verify this.

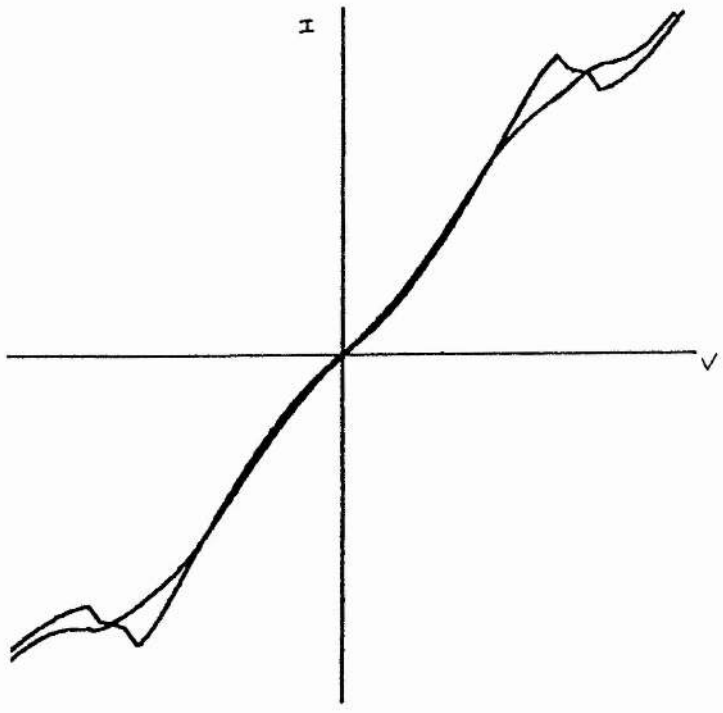

Figure 7.14. IV curve of NU298, 20μm diameter device, Maltese cross contact. Showing effect of applied RF power. V_{peak}~±0.8V, I_{peak}~±60mA

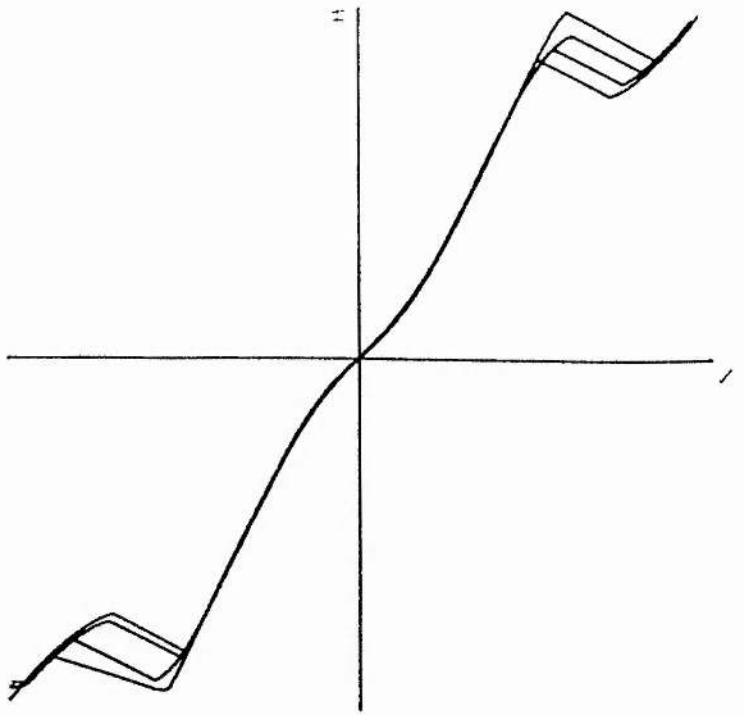

Figure 7.15. IV curve of NU2948, 20μm diameter device, 10μm wire V-bond contact. Showing effect of applied power. V_{peak}~±0.75V, I_{peak}~±60mA

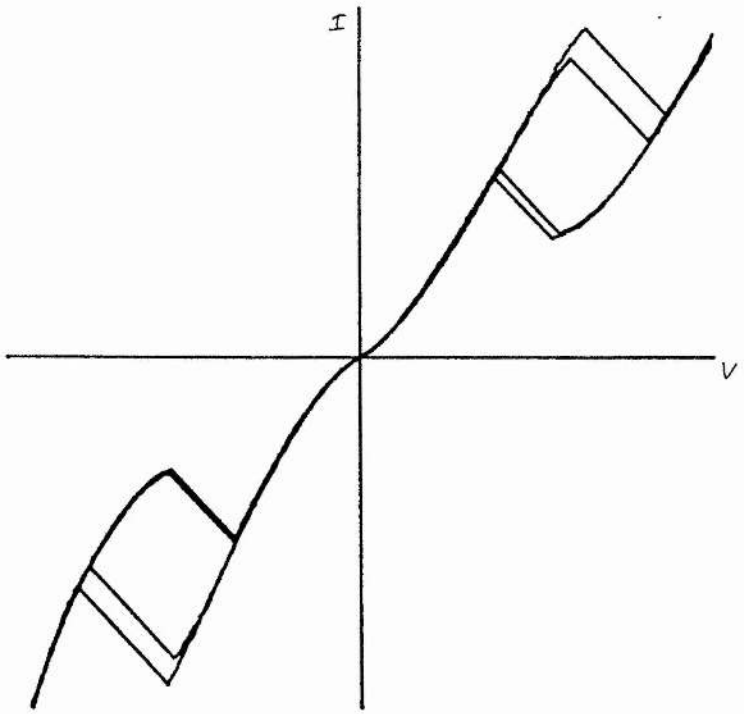

Figure 7.16. IV curve of NU298, 20μm diameter device, 10μm wire I-bond contact. Showing effect of applied power. V_{peak}~±1.35V, I_{peak}~±50mA.

7.6. Sensitivity.

For a given bias point on the IV curve of the QW devices, the amount by which the external current and voltage change when radiation is coupled into the device is a measure of the sensitivity of the device/circuit combination. The current and voltage - the operating point - will move along the load line of the particular bias circuit in use at the time. The load line is visible in Figures 7.15 and 7.16. In the case where the bias circuit has a very low output impedance, such as an ideal voltage source, only the current will change when RF is applied. At the other extreme, a bias circuit with a very high output impedance (a current source), will allow only a change in voltage. In reality, the output impedances of practical bias circuits lie somewhere in between these two extremes.

Since the bias supplies were used in these measurements in a swept mode, we can choose a point on the IV curve and express the detector sensitivity as a change in current for a given voltage at that point, and as a change in voltage for a given current at that point. The greatest current/voltage change in these devices occurs when they are biased close to the negative resistance region. Hence we may estimate the maximum current and voltage changes for the QW devices, as follows:

25μm wire V-bond device:	At -1.0V, $\Delta I \approx 10$mA.	At -15mA, $\Delta V \approx 0.8$V
Maltese cross device:	At +0.8V, $\Delta I \approx 8$mA.	At +60mA, $\Delta V \approx 0.25$V
10μm wire V-bond device:	At +0.75V, $\Delta I \approx 4.5$mA.	At +60mA, $\Delta V \approx 0.07$V
10μm wire I-bond device:	At +1.3V, $\Delta I \approx 2$mA.	At +46mA, $\Delta V \approx 0.1$V

for a maximum input power of 10mW at 85GHz.

7.7. Conclusion.

Clearly, for the particular circuit parameters, the 25μm wire V-bond device showed the greatest sensitvity, roughly 0.08V/mW if measured with a high impedance bias circuit. This is at least an order of magnitude less sensitive than commercially available room-temperature Schottky diodes. However, it should be borne in mind

that at 20μm in diameter these devices are still very much larger than conventional detector diodes for W-band and beyond, and will therefore have a much higher capacitance than is desirable.

It has already been established that the tunneling process is inherently very fast, with detection up to 2.5THz being demonstrated [3]. It is possible, therefore, given devices of about 1 or 2μm in diameter, with a low-parasitic contact such as a whisker, that quantum well devices may be a suitable alternative to Schottky devices as detectors in the millimetre and submillimetre regions.

Chapter 7 References

[1] D.P.Steenson, Private Communication

[2] Th.G.van de Roer, H.C.Heyker, L.M.F.Kaufmann, J.J.M.Kwaspen, M.Schemmann, H.P.Joosten, D.Lenstra, H.Noteborn, M.Henini and O.H.Hughes, "Double-barrier resonant tunneling diodes: theory and experiment", *Inst. Phys. Conf. Ser. No 106: Chapter 11*, pp.831-836, 1990. Paper presented at Int. Symp. GaAs and Related Compounds, Karuizawa, Japan, 1989.

[3] T.C.L.G.Sollner, W.D.Goodhue, P.E.Tannenwald, C.D.Parker, and D.D.Peck, "Resonant tunneling through quantum wells at frequencies up to 2.5THz", *Appl. Phys. Lett.*, vol.43, no.6, p.588, 1983.

8. QW Oscillators.

8.1. Introduction

The second generation of double-barrier diodes produced by Nottingham University for investigation at millimetre-wave frequencies differed from the diodes detailed in the previous chapter in several important respects: they were etched into smaller mesas (10μm and 5μm); they were whisker-contactable; and they had a greater ΔV in the negative resistance region, making it easier to bias into this region. A number of devices from wafer NU366 were measured, showing oscillations in the range 65GHz to 96GHz.

8.2 Device Layer Structure

The layer structure of wafer NU366 is shown in Figure 8.1. It has thin, symmetric barriers and an asymmetric layer profile outwith the barrier/well region. This gives rise to a pronounced aymmetry in the IV curve (Figure 8.2).

0.4μm GaAs 2.10^{18} cm^{-3}
17Å GaAs undoped
17Å AlAs undoped
42Å GaAs undoped
17Å AlAs undoped
17Å GaAs undoped
0.15μm GaAs 5.10^{16} cm^{-3}
2μm GaAs 2.10^{18} cm^{-3}
n^+ substrate

Figure 8.1. NU366 Layer profile.

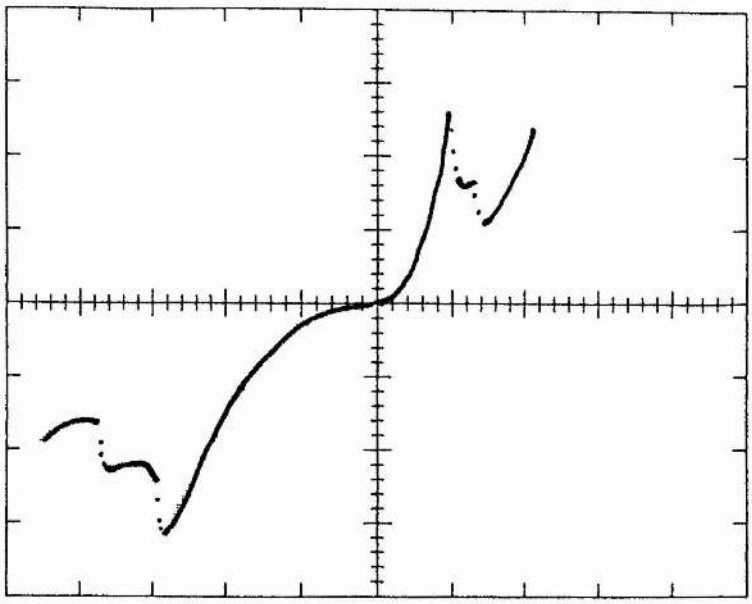

Figure 8.2. IV curve of 5μm NU366 device. Scale 1V/div horiz., 1mA/div vert.

8.3. Diode Circuit.

The diodes were in the form of honeycomb chips roughly 350μm square, suitable for whisker contacting (Figure 8.3). Two similar circuits were used in the measurements. The first was a modified Flann wafer crystal mount [1], essentially a short (5mm) section of WG27 waveguide. The diode chips were bonded with metal-loaded epoxy onto the end of a small brass pin, and contact was achieved with a 700-800μm long whisker made of 25μm diameter phosphor bronze wire, bent into a ? shape and etched to a point. The whisker pin was at the potential of the centre conductor of the nanohex connector, and the device pin was at the potential of the body of the waveguide (Figure 8.4). This particular arrangement enabled diodes to be exchanged fairly easily. The drawback of this particular circuit was that the whisker could easily suffer damage to its tip after only a few contacts, and was time-consuming to replace.

An alternative mount was constructed which reversed the positions of the whisker and diode pins. This enabled the whisker to be rapidly changed if the whisker tip suffered damage. The whisker pin was now at the potential of the waveguide body, and the diode pin was at the potential of the centre conductor of the coaxial connector, i.e. the polarity was the reverse of the Flann mount. In addition, the waveguide was

circular, 2.30mm in diameter, giving a cut-off frequency of 76.4GHz for the TE_{11} mode.

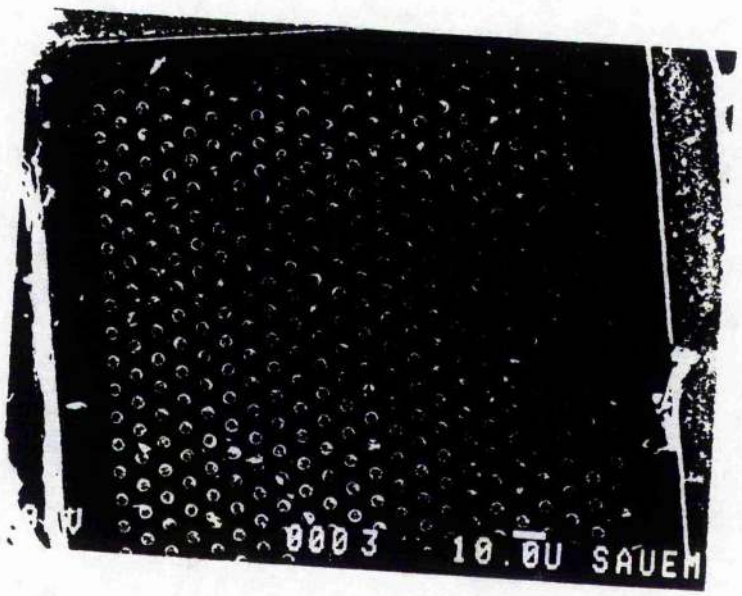

Figure 8.3. Honeycomb array of NU366 5μm diameter devices.

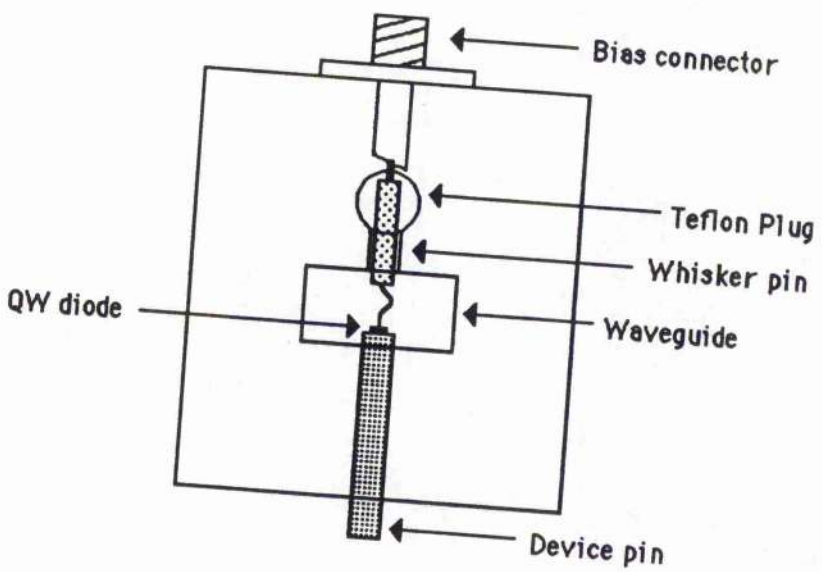

Figure 8.4. QW wafer mount.

8.4. W-band Oscillation.

With the diode mount bolted between a 94GHz feedhorn and a circular backshort, the free-running frequency of oscillation of the devices was measured with a Martin-Puplett Interferometer. The first device to be mounted in the Flann waveguide was a 5μm device, originally (and incorrectly) labelled as a 15μm device. When biased to -3.55V, 5mA, corresponding to the feature lying half way between the peak and the valley in the negative part of the IV curve, the device oscillated at 65GHz and 87GHz simultaneously, as shown in Figure 8.5. No oscillations could be detected if the device was biased either to the peak or the valley of the negative resistance region. Later devices were also biased into the positive part of the IV curve.

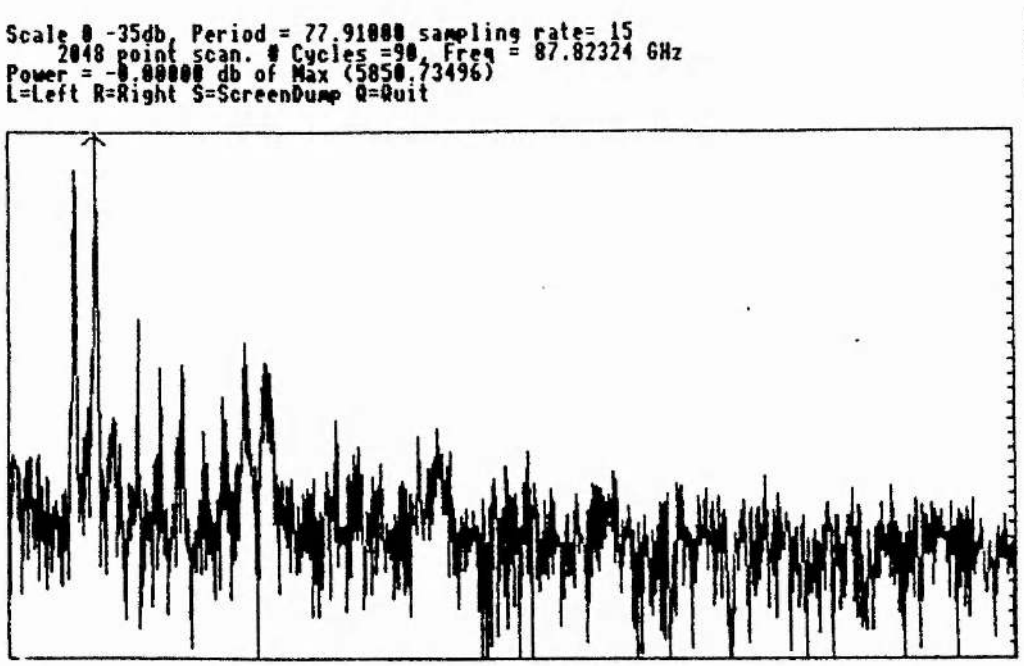

Figure 8.5. Output from 5μm NU366 device #1. Horiz. scale 0-1000GHz.

The relative amplitudes of the 65GHz and 87GHz components depended on circuit conditions, primarily bias voltage but also on backshort position. For example, by maintaining the bias at -3.55V and moving only the backshort, the 65GHz component could be made to dominate (Figure 8.6). Note also that here there is a large component at 130GHz. It is quite likely that this second harmonic is real, because of its large amplitude. However, imperfect coupling to the Golay detector in the MPI system can often result in reflections which cause multiple passes through the interferometer and modulation of the source, resulting in spurious harmonics, especially at the second and third harmonic. Also, the high noise floor is thought to be

an artefact of the data acquistion software of the MPI.

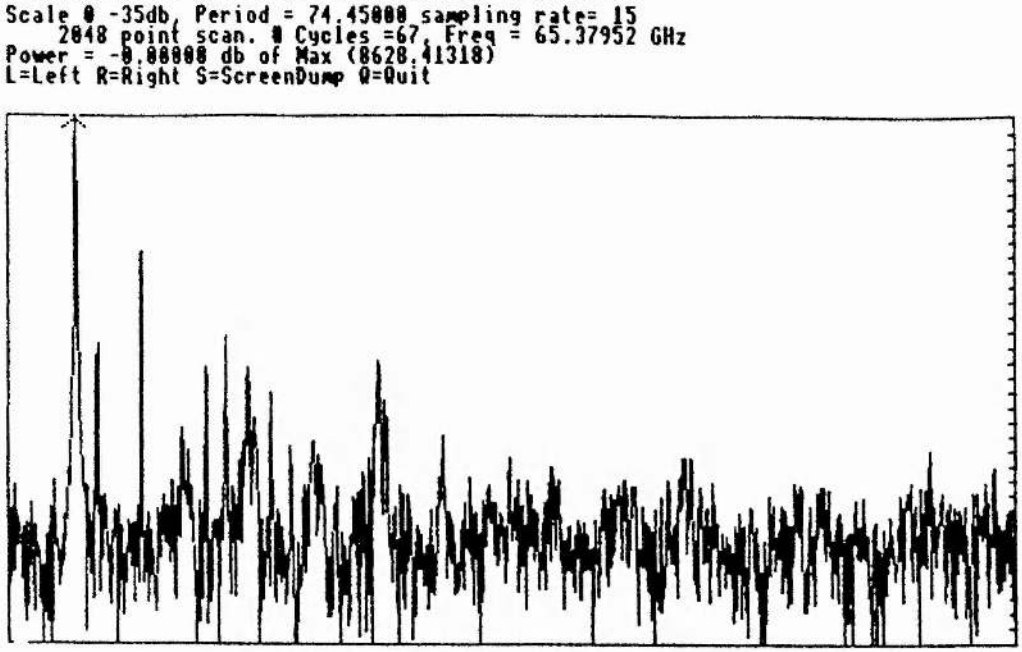

Figure 8.6. Output from 5µm NU366 device #1, showing dominant 65GHz component. Horiz. scale 0-1000GHz.

In general, for a given backshort position, low values of bias voltage (around 3.44V - 3.60V) allowed the low frequency component to dominate, while higher values of bias voltage (around 3.70V) allowed the 87GHz component to dominate (Figure 8.7).

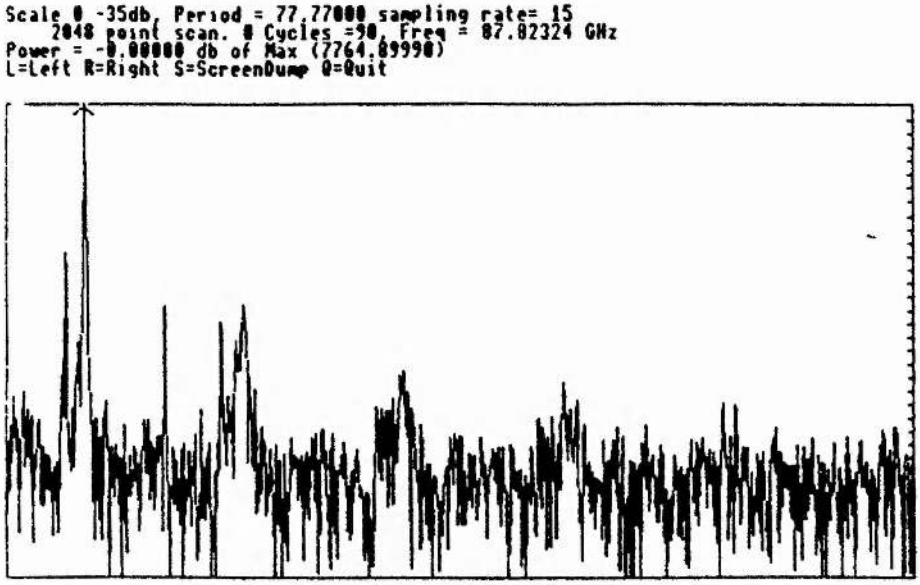

Figure 8.7. Output from 5µm NU366 device #1 showing dominant 87GHz component. Horiz. scale 0-1000GHz.

Two other devices mounted in the wafer with the circular waveguide were investigated. The first was a 10μm device, biased to -4.0V, 14mA on the whisker (with respect to the diode) which oscillated at 87.8GHz (Figure 8.8). The output once again shows a significant harmonic content, the origins of which are not certain.

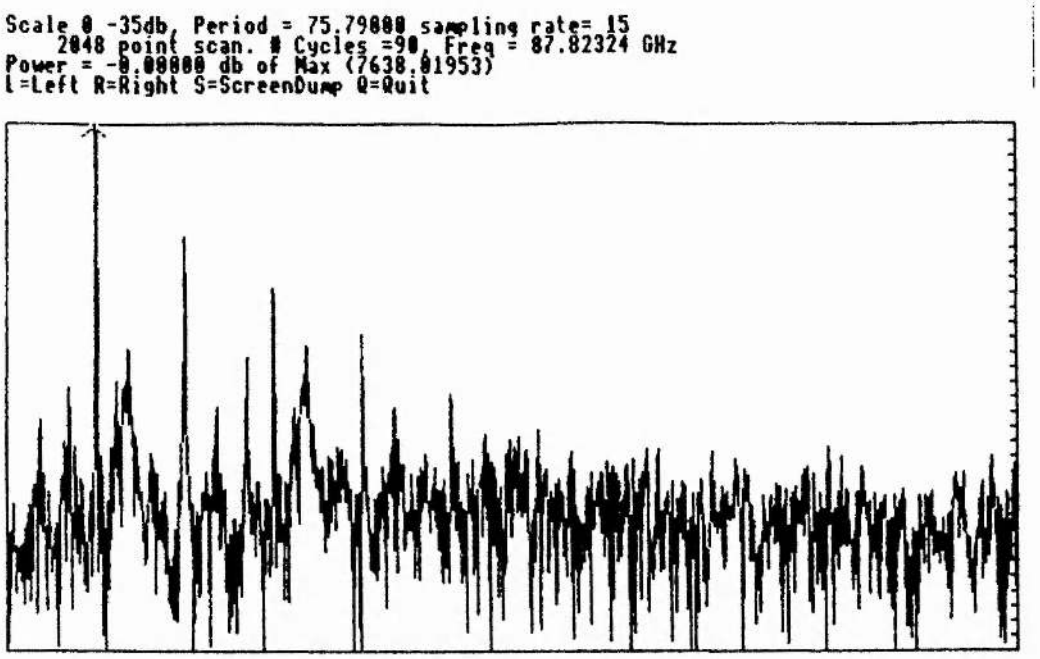

Figure 8.8. Output from 10μm NU366 device. Horiz.scale 0-1000GHz.

The second was another 5μm device which oscillated at 80GHz when biased into the positive part of the IV curve (+1.2V) and oscillated with slightly higher power at 81GHz when biased into the negative part of the IV curve (-3.6V) (Figures 8.9, 8.10). Subsequent re-whiskering of the device after moving its position in the waveguide gave output at 78GHz, 93GHz and 96GHz in turn (Figures 8.11-8.13).

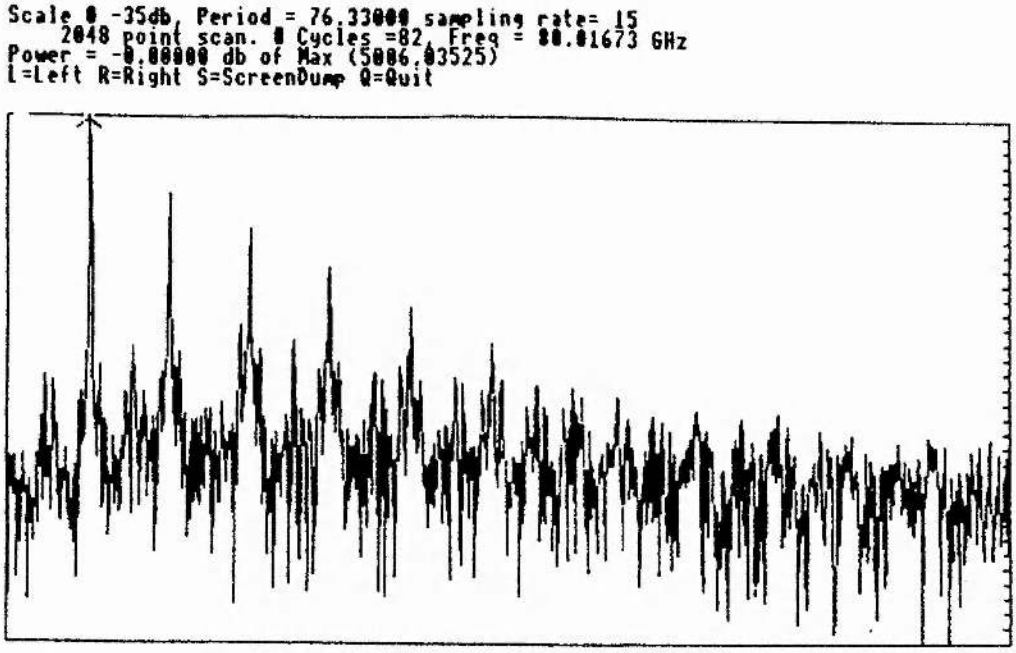

Figure 8.9. 80GHz output from 5µm NU366 device #2, biased to +1.2V on whisker. Horiz. scale 0-1000GHz.

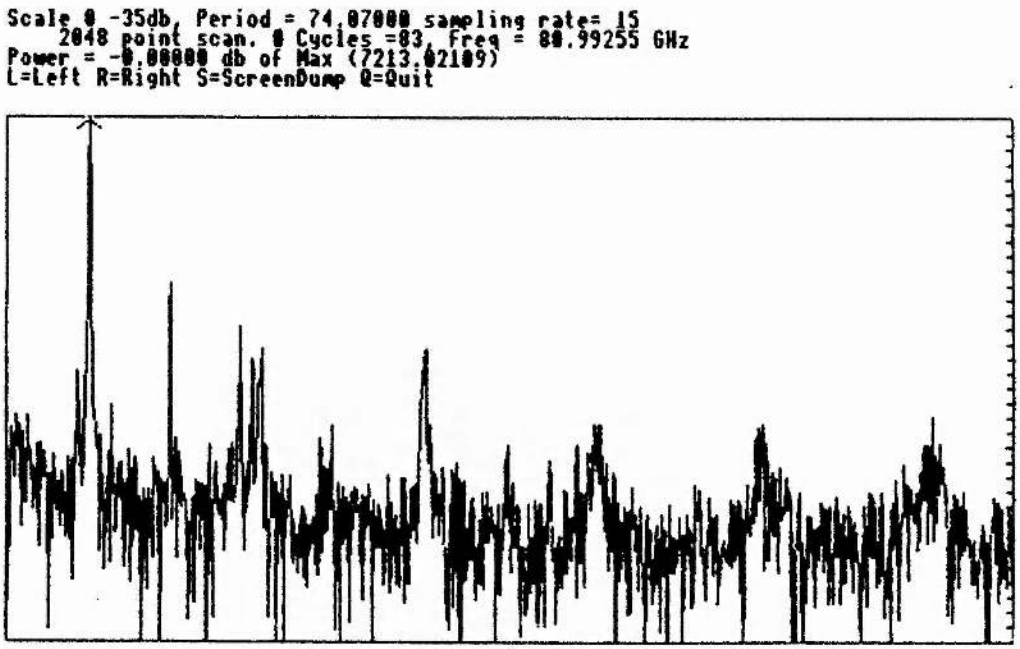

Figure 8.10. 81GHz output from 5µm NU366 device #2, biased to -3.6V on whisker. Horiz. scale 0-1000GHz.

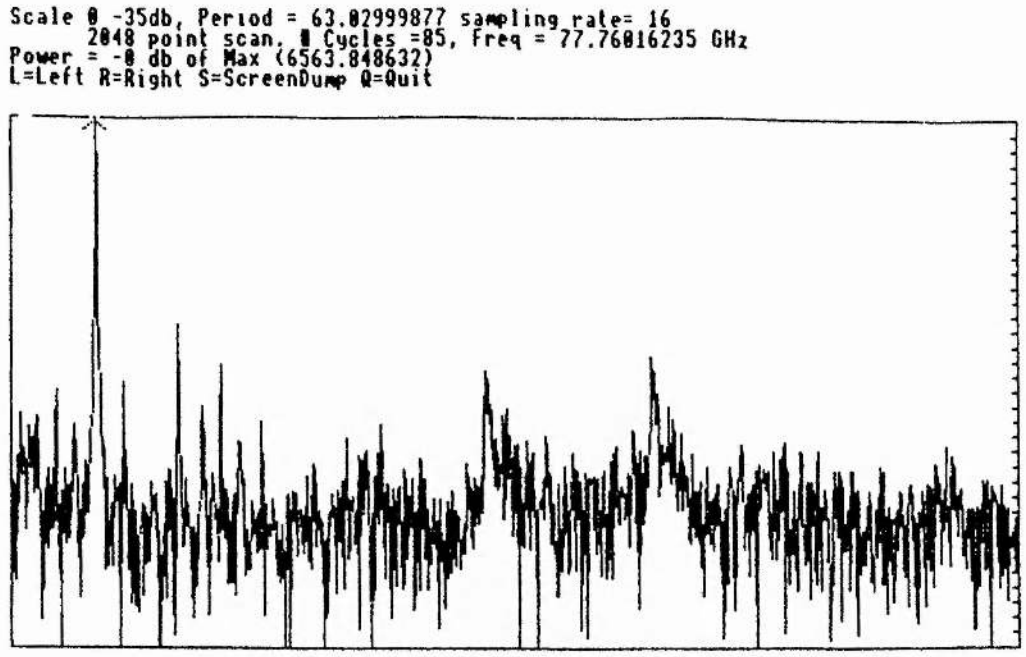

Figure 8.11. 77.8GHz output from 5μm NU366 device #2, biased to -3.6V on whisker. Horiz. scale 0-1000GHz.

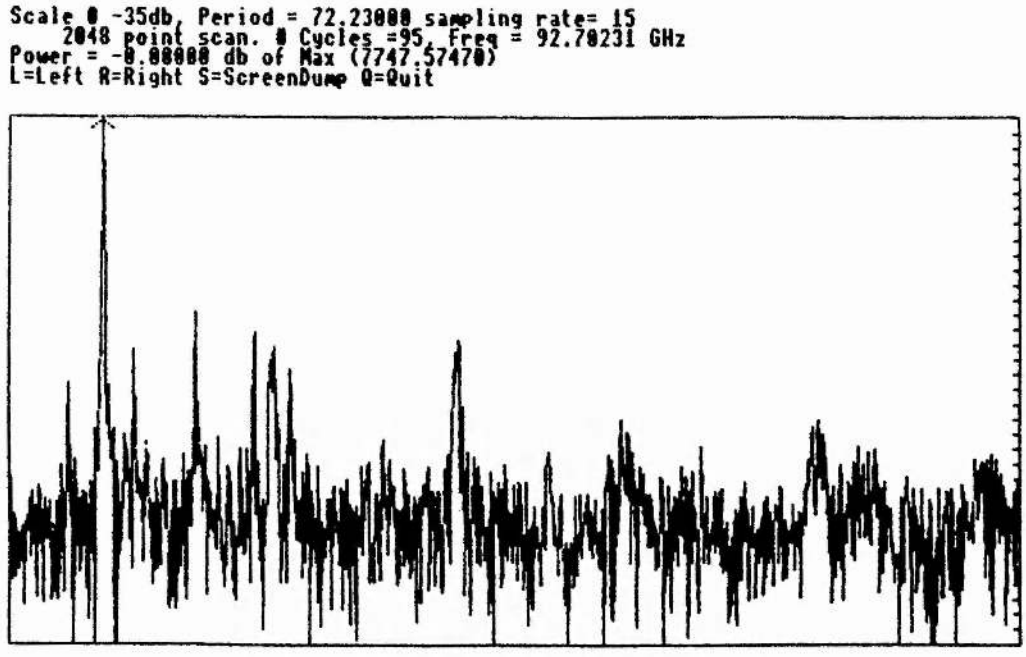

Figure 8.12. 92.7GHz output from 5μm NU366 device #2, biased to -3.6V on whisker. Horiz. scale 0-1000GHz.

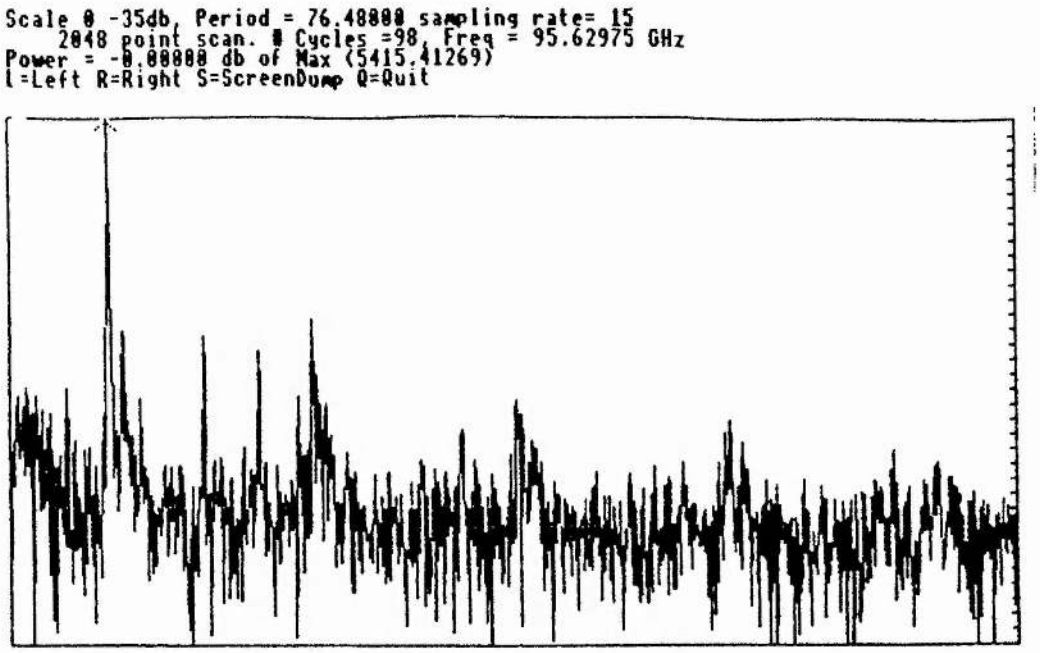

Figure 8.13. 95.6GHz output from 5μm NU366 device #2, biased to -3.6V on whisker. Horiz. scale 0-1000GHz.

8.5. Conclusion

The results presented in this chapter were the the first demonstration that the Quantum Well devices grown at Nottingham University could oscillate at millimetre-wave frequencies. The power output, estimated (and later measured) to be in the region of a few microwatts, is comparable to that obtained by Brown et al [2] at 102-112GHz of 5μW, with a similar barrier/well layer profile to NU366. The devices due to Brown et al were 4μm in diameter, and went on to produce fundamental oscillations at 200GHz, at a power level of 0.2μW. Modified devices from the same workers produced the same amount of power at 420GHz, the highest reported oscillation frequency for the GaAs/AlAs material [3].

At "low" frequencies around W-band, QW oscillators are competing directly with Gunn and IMPATT diodes, which are capable of far higher output powers. However,

at higher frequencies where Gunn and IMPATT diodes cease to operate, the resonant tunneling diodes may prove to be viable alternative millimetre and submillimetre wave sources.

Chapter 8 References.

[1] Flann Microwave Instruments Ltd, Dunmere Road, Bodmin, Cornwall.

[2] E.R.Brown, W.D.Goodhue, and T.C.L.G.Sollner,"Fundamental oscillations up to 200GHz in resonant tunneling diodes and new estimates of their maximum oscillation frequency from stationary-state tunneling theory", *J. Appl. Phys.*, vol. 64, no.3, p.1519, 1988.

[3] E.R.Brown, T.C.L.G.Sollner, C.D.Parker, W.D.Goodhue, and C.L.Chen, "Oscillations up to 420GHz in GaAs/AlAs resonant tunneling diodes", *Appl. Phys. Lett.*, vol. 55, no.17, p.1777, 1989.

9. QW Multipliers.

9.1. Introduction.

Quantum well double-barrier diodes have strongly non-linear current-voltage characteristics, which make them suitable devices for resistive frequency multiplication [1]. If the device IV curve is point symmetric about zero volts, then at zero bias only odd-harmonic frequency conversion will occur. If in addition the device is driven over the negative resistance regions, two effects may be observed. Firstly, the theoretical $1/n^2$ maximum conversion efficiency for resistive multipliers, where n is the harmonic number, may be exceeded [2]; secondly, it is possible to obtain significant power at the 5th harmonic [3]. Both of these effects will depend to a very large extent on the circuit conditions presented to the device.

Two devices were successfully whisker-contacted and exhibited zero-bias tripling at 255GHz when pumped at around 85GHz. It is believed that this represents the highest frequency involving QW devices from the Nottingham University NUMBERS project.

9.2. Device Layer Structure.

In order to operate as zero-bias triplers, QW devices need to have IV characteristics which are symmetric about zero volts. Honeycomb chips of 5μm devices from wafers NU298 (Figure 9.1) and NU367, the symmetrical version of NU366 (Figure 9.2) were measured. Figures 9.3 and 9.4 show their IV characteristics.

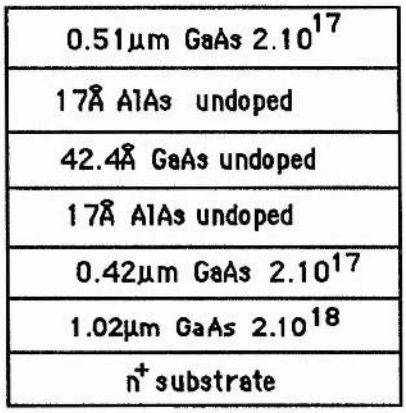

Figure 9.1. NU298 layer structure.

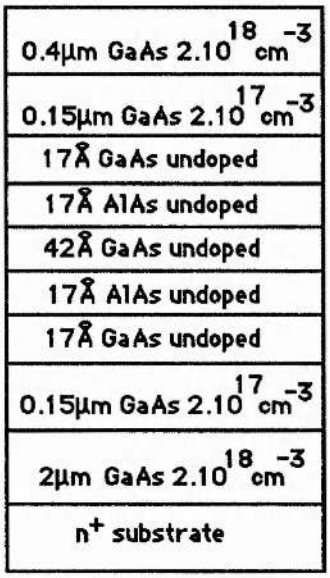

Figure 9.2. NU367 layer structure.

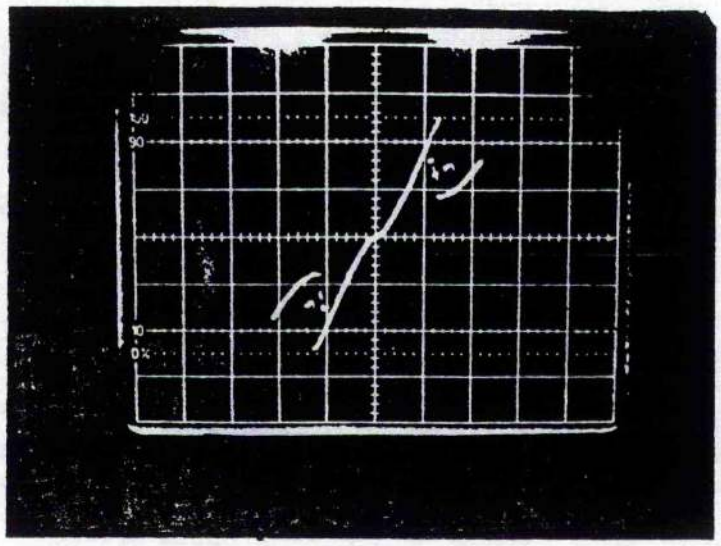

Figure 9.3. IV curve of 5µm NU298 device. Scale1V/div horiz., 2mA/div vert.

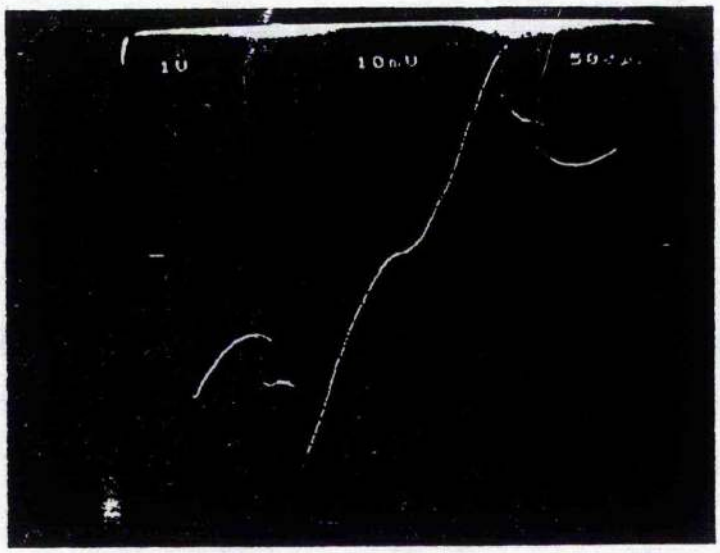

Figure 9.4. IV curve of 5µm NU367 device. Scale 1V/div horiz., 1mA/div. vert. Vpeak=2V, Ipeak=4mA

9.3. Multiplier Circuit Design.

The design of the waveguide doubler was based on the design of the off-centre doubler detailed in Chapter 6. The device chips were bonded to the end of long aluminium device pins, and held firmly by the device pin screw (Figure 9.5). The device pin screw was threaded into the top of the multiplier block which precisely located the device pin through the middle of the coaxial choke. A small grub screw ensured that the device pin was held rigidly with respect to the block. This arrangement enabled the coaxial choke to be moved up and down in the coaxial cavity without disturbing the position of the device, although the vertical movement was limited to about 2mm and depended on good surface finishes for smooth operation.

With the diode chip suitably positioned in the full height WG28 input waveguide, the whisker pin could be brought up to contact the device. Since the device pin was at the potential of the multiplier block, the whisker pin required to be electrically isolated from the block. This was achieved by mounting the 5mm long, 0.9mm diameter whisker pins in a perspex sleeve, into which was threaded a small brass screw. A generous quantity of conductive paint ensured electrical contact between the screw and the whisker pin. A small bias tag attached to the top of the brass screw was connected to the centre conductor of the SMA bias connector via a short length of insulated wire and a 100kΩ bleed resistor. Finally, a small glass bead was fixed to the head of the brass screw to insulate it from the micrometer which was used to push the whisker pin into contact with the device. This micrometer was removable once contact had been made, and is not shown in Figure 9.5.

As before (Chapter 6), the output waveguide was in the same plane as, and at right-angles to, the input waveguide. The output guide tapers linearly from WG28 (2.0x1.0mm) to WG31 (1.1x0.55mm) near the edge of the block (Figure 9.6). Both waveguides had sliding contacting backshorts behind the device. The WG31 feedhorn detailed in Chapter 6 coupled power out of the block and into the Martin-Puplett Interferometer.

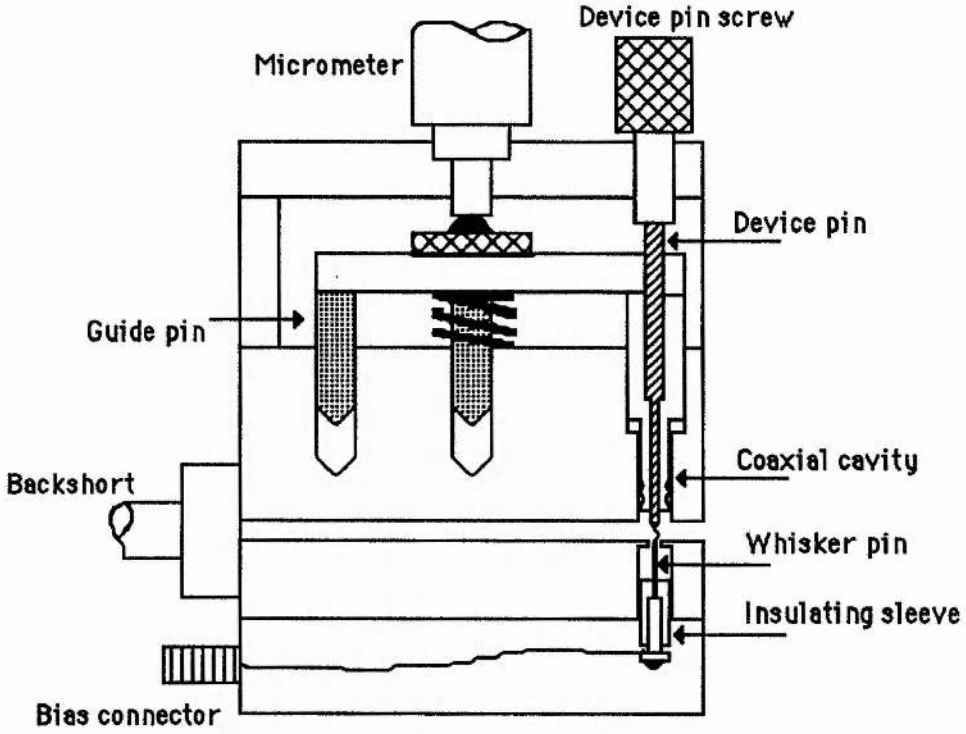

Figure 9.5. Whisker-contacting multplier block.

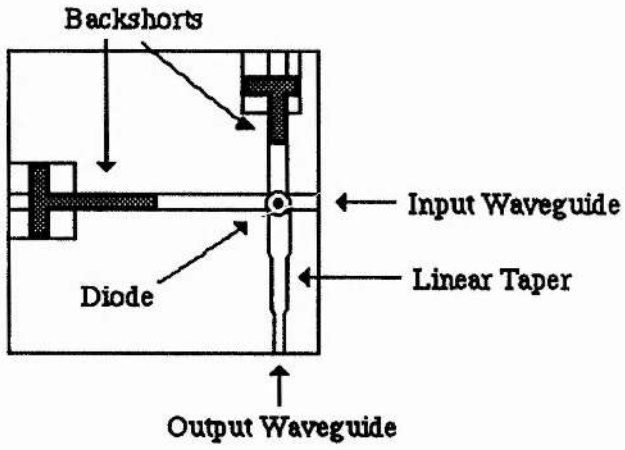

Figure 9.6. Detail of cross-guide section of multiplier block.

9.4. Frequency Multiplication.

The first successfully contacted device, NU298, was pumped with around 20mW of power at about 84.5GHz. After careful adjustment of the multiplier coaxial cavity and its backshorts, tripled output at 253.4GHz was observed (Figure 9.7). This was achieved with the bias supply connected, set to zero volts. The ouput power level was extremely low, estimated to be well below a microwatt, and possibly only a few tens of nanowatts.

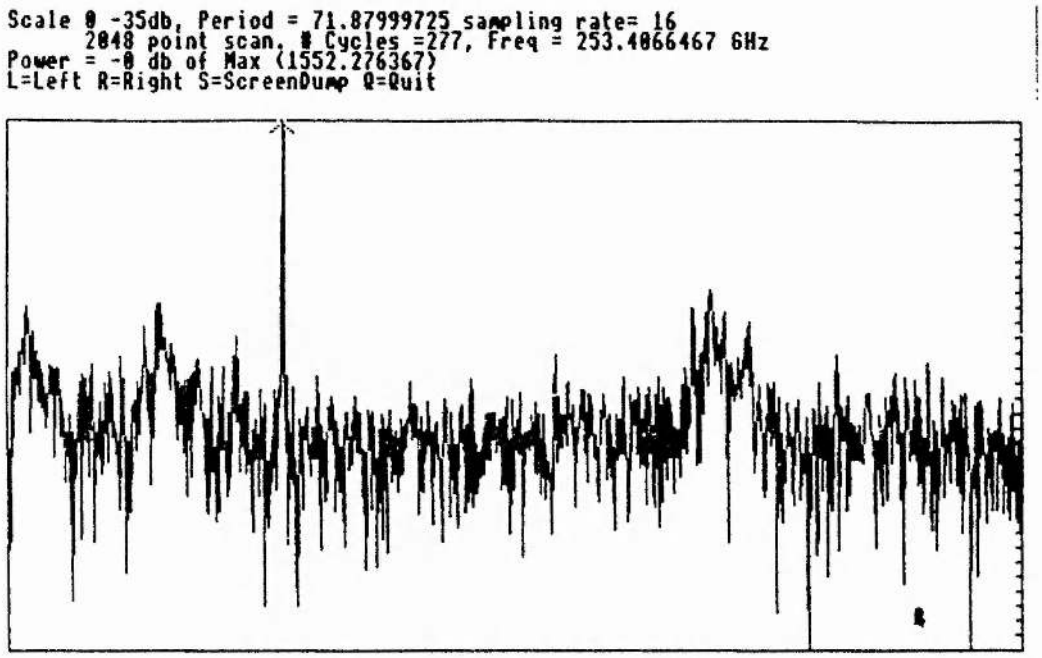

Figure 9.7. Zero-bias tripling from NU298. Horiz. scale 0-1000GHz.

If either forward or reverse bias was applied to the device, the output showed significant amounts of power at the second harmonic as the operating point was moved away from the zero bias point (Figures 9.8, 9.9). This shows that the amount of RF power coupled into the device was not large, certainly not large enough to extend across the negative resistance regions.

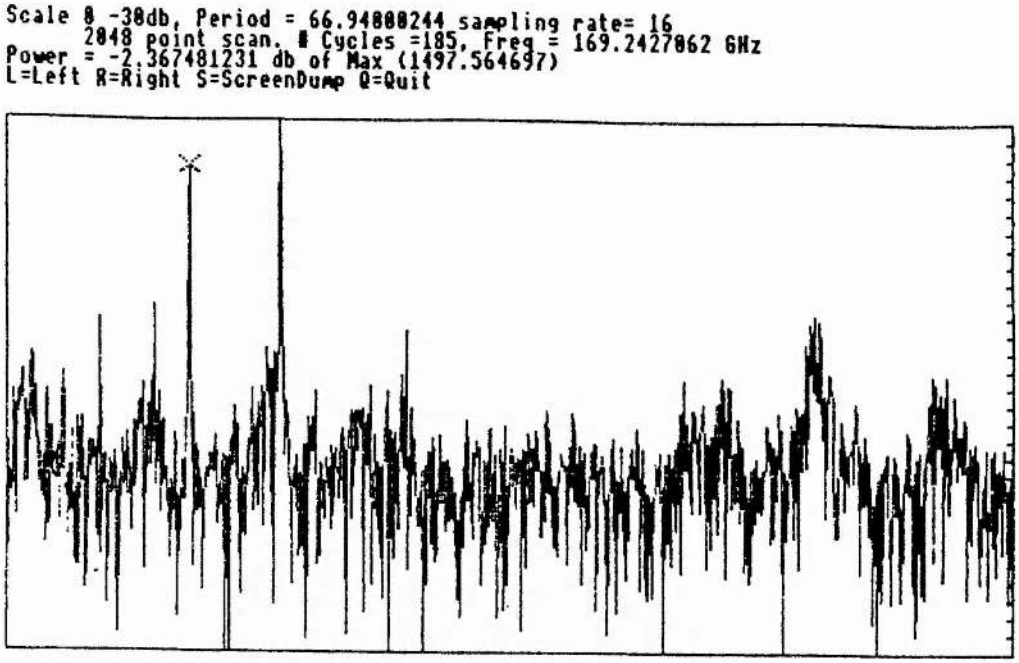

Figure 9.8. NU298, 0.2V reverse bias. Horiz. scale 0-1000GHz.

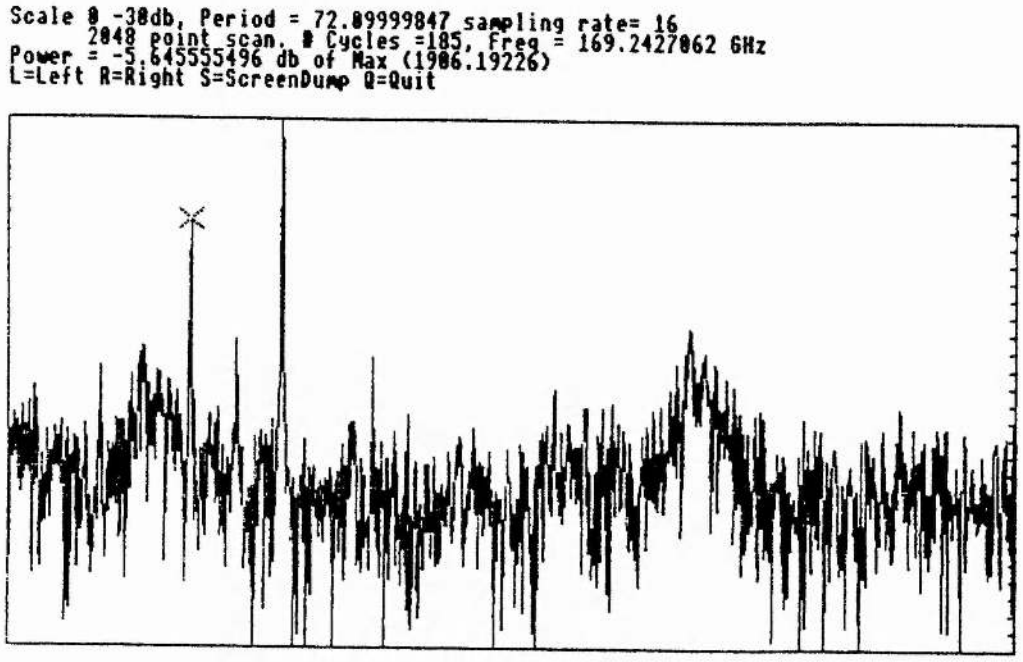

Figure 9.9. NU298, 0.2V forward bias. Horiz. scale 0-1000GHz.

By increasing the bias further, for example to 0.4V reverse bias, the second harmonic component could be made to dominate the third harmonic (Figure 9.10), and eventually the third harmonic would completely disappear, at around 1.0V reverse (or forward) bias (Figure 9.11).

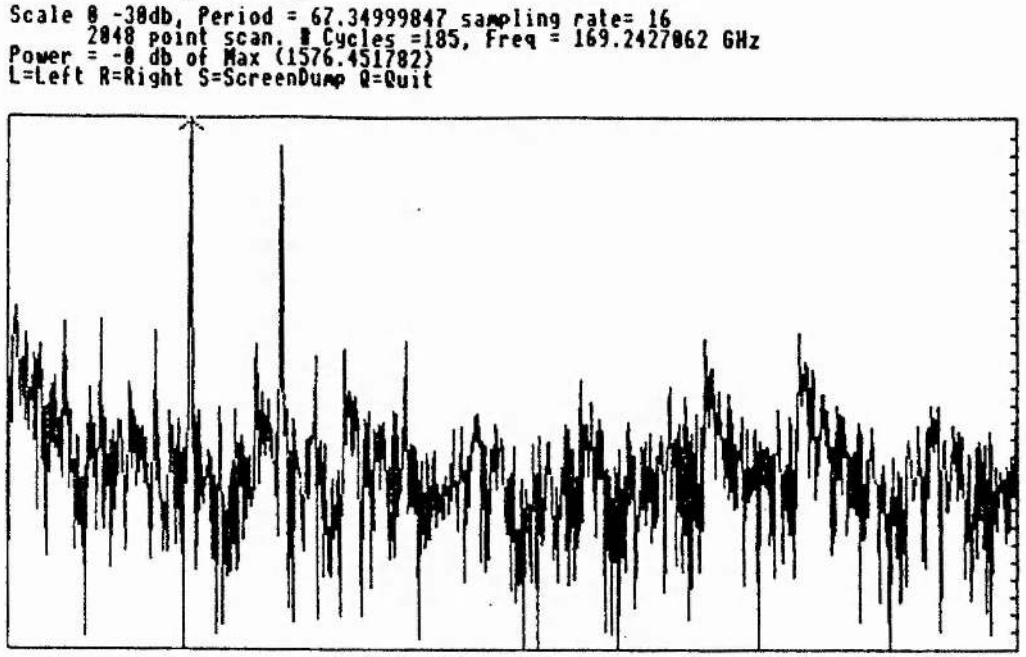

Figure 9.10. 2nd harmonic component dominating at 0.4V reverse bias. Horiz. scale 0-1000GHz.

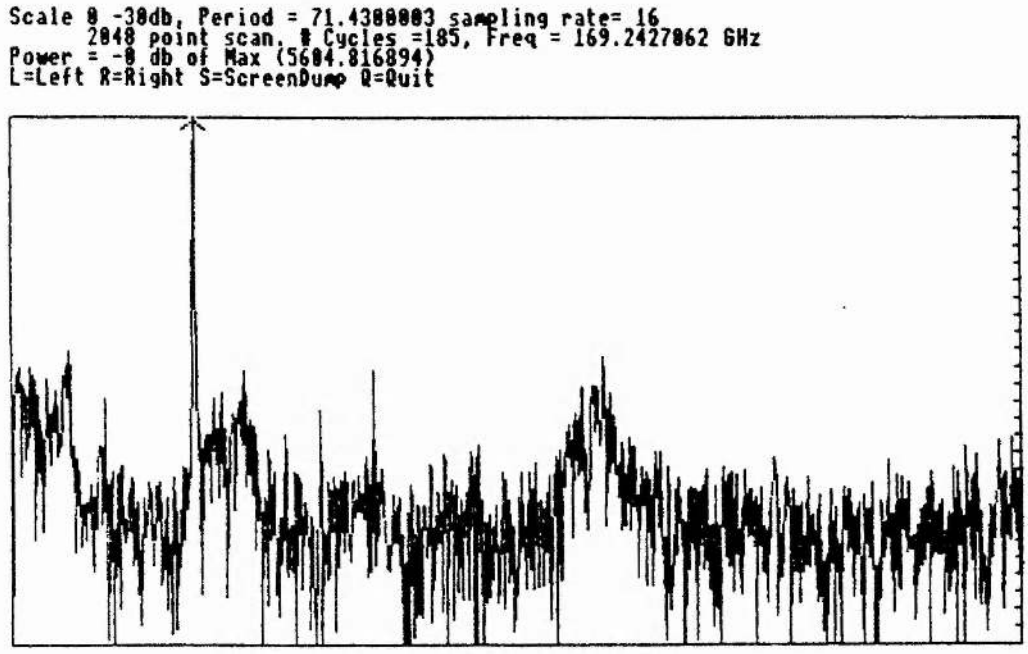

Figure 9.11. 1.0V reverse bias. Second harmonic component. Horiz. scale 0-1000GHz.

The second device to be sucessfully contacted was from the NU367 wafer, a symmetrical version of the NU366 devices which had already been studied as oscillators (Chapter 8). The NU298 and NU367 devices share virtually identical barrier/well structures, but the NU367 devices have additional undoped clouding layers of GaAs either side of the barriers, which may contribute to a greater series resistance compared with NU298. Certainly, the peak current density of the NU298 devices is greater than that of the NU367 devices, although the peak to valley ratio is slightly less.

The NU367 device was pumped with the the same oscillator as before, and after much tuning of the block, tripled output at 255GHz was observed, again at a very low power level (Figure 9.12). Unfortunately, shortly after the first measurement was taken, contact was lost, and in the process of recontacting the device the choke jammed in the coaxial cavity. Consequently the multiplier block was returned to the workshop for rebuilding.

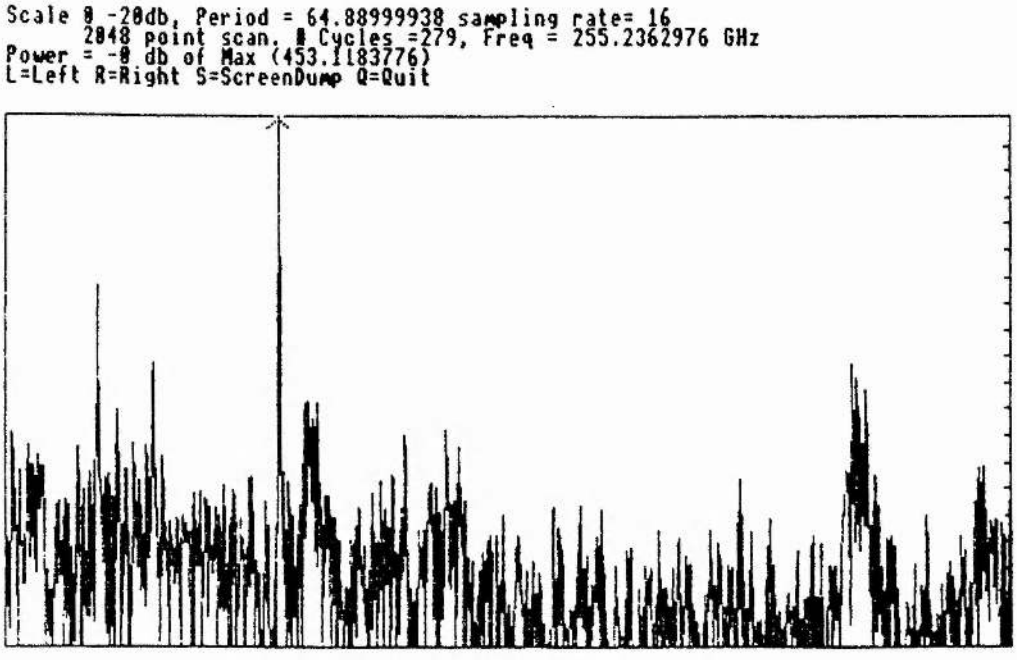

Figure 9.12. Zero-bias tripling from NU367. Horiz. scale 0-1000GHz.

9.5. Conclusion.

Despite the limitations imposed by the multiplier circuit on the efficiency of the tripler, namely the lack of proper isolation between the input and output circuits and the lack of proper impedance matching, it was proved that the Nottingham University QW devices could have some potential as zero-bias triplers. Zero-bias tripling in such devices has the advantage over conventional (e.g. varactor) diodes in that no bias circuit is required, and no provision need be made for the termination of idlers. It may also be possible that QW devices could operate as multipliers at frequencies higher than their maximum oscillation frequency, since the requirement that the device negative resistance be greater than the series resistance is no longer applicable.

Chapter 9 References.

[1] P.D.Batelaan and M.A.Frerking, "Quantum Well Multipliers", *Conference Digest, 12th Int. Conf. Infrared and Millimeter Waves,* ed. R.J.Temkin, IEEE, New York, 1987.

[2] A.Rydberg and H.Grönqvist, "Quantum-well high-efficiency millimeter-wave frequency tripler", *Elect. Lett.*, vol.25, no.5, p.348, 1989.

[3] T.C.L.G.Sollner, E.R.Brown, W.D.Goodhue, and C.A.Correa, "Harmonic multiplication using resonant tunneling", *J. Appl. Phys.*, 64(8), p.4248, 1988.

10. Self-Oscillating Mixing and Chaotic Oscillations in Quantum Well Double Barrier Diodes.

10.1. Introduction

Double-barrier resonant tunneling diodes have been shown to work as high frequency oscillators, detectors, multipliers and mixers by virtue of their non-linear IV and CV characteristics [1-4]. Since the IV curve is non-linear, especially in the negative differential resistance (NDR) region, the same device can act both as an oscillator and as a mixer at the same time. This effect has already been demonstrated at low frequency (10GHz, [5]). Such a device would ideally have a stable, low noise single-frequency output and good conversion efficiency, two characteristics which perhaps place conflicting requirements on the circuit design. This section describes a very simple waveguide circuit into which was mounted a honeycomb array chip of QW double-barrier diodes. The device had a "free-running" oscillation frequency of around 86GHz, and acted as a self oscillating mixer when pumped with a Gunn oscillator. The QW device could be injection locked to the RF signal, and the intermediate frequency (IF) exhibited both upper and sub harmonics. The conversion gain of the device was measured, and under certain conditions the IF could show wideband oscillations extending to about 2GHz [6].

10.2. Device Layer Structure

The QW diode was designed at Nottingham University by Paul Steenson and grown by Mohammed Henini. Designated NU366, the layer structure is shown in Figure 10.1. Once grown, the wafer was etched down to 5μm diameter mesas and diced into chips. This particular layer structure has symmetrical AlAs barriers but has different doping levels either side of the barriers, which gives rise to an asymmetric IV characteristic (Figure 10.2)

4000Å GaAs 2.10^{18} cm^{-3}
17Å GaAs undoped
17Å AlAs undoped
42Å GaAs undoped
17Å AlAs undoped
17Å GaAs undoped
1500Å GaAs 5.10^{16} cm^{-3}
20000Å GaAs 2.10^{18} cm^{-3}
n^+ substrate

Figure 10.1. NU366 Layer Structure

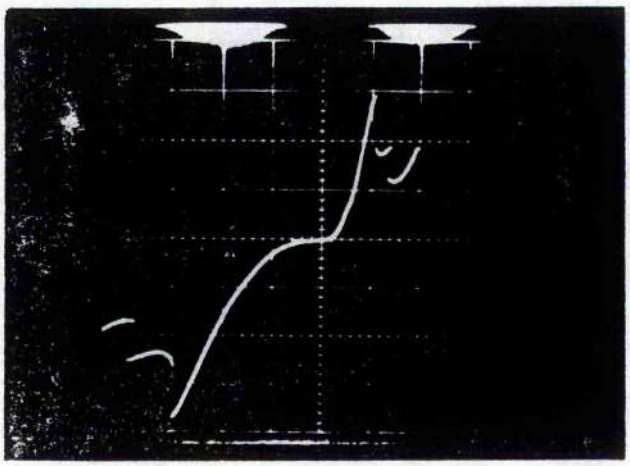

Figure 10.2. DC IV characteristic, NU366.
Scale: Horizontal, 1V/div; Vertical, 1mA/div.

10.3. Diode Circuit.

The diode was mounted in a short (4mm) section of full height WG27 waveguide, which is a modified version of the millimetric crystal detector mount made by Flann Microwave of Bodmin, Cornwall. The modification was carried out at Nottingham University. The diode chip was bonded onto the end of a 1.0mm diameter brass pin, and contact was acheived with a 25μm diameter, 700μm long phosphor bronze wire bent into an S (or question-mark) shape and etched to a point, the precise radius of which is not known. The whisker pin was at the potential of the centre conductor of the nanohex coaxial connector, and the device pin was at the potential of the body of the waveguide (Figure 10.3).

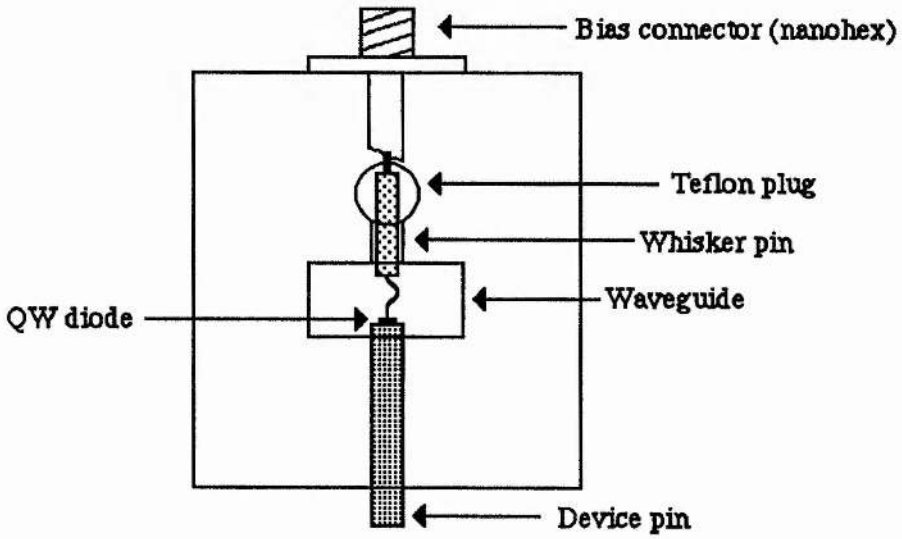

Figure 10.3. Detail of waveguide circuit.

This particular circuit enables many different devices to be investigated with relative ease, as the device pin can be removed and replaced very simply. The major drawback of this configuration is that the point of the whisker can be easily damaged after only a few attempts at contacting the chip, resulting either in no contact at all, or a contact with high capacitance, high series resistance, or an intermittent contact. As one normally expects to use up more whiskers than devices, a more practical design would enable the whiskers to be replaced more easily.

10.4. Test Circuit.

To determine the frequency of oscillation of the QW device, the section of waveguide containing the contacted chip was mounted between a WG27 94GHz corrugated feedhorn and a 2.5mm diameter contacting backshort. When biased to about +1.2V (on the whisker), which corresponds to the "platform" feature seen in the positive, or right-hand half of the IV curve, the device oscillated at about 86GHz, measured on a Martin-Puplett Interferometer. No oscillations could be detected if the device was biased either to the peak or to the valley of the negative resistance region.

Substituting the feedhorn for a Boonton 4220 power meter gave a maximum power measurement from the QW device of 2.14μW at 1.182V bias. In order to pump the device with a signal that was comparable both in frequency and power to that produced by the QW, a Gunn oscillator was first tuned to 86GHz and then its power reduced by a factor of approximately 100 by two 10dB couplers (Figure 10.4).

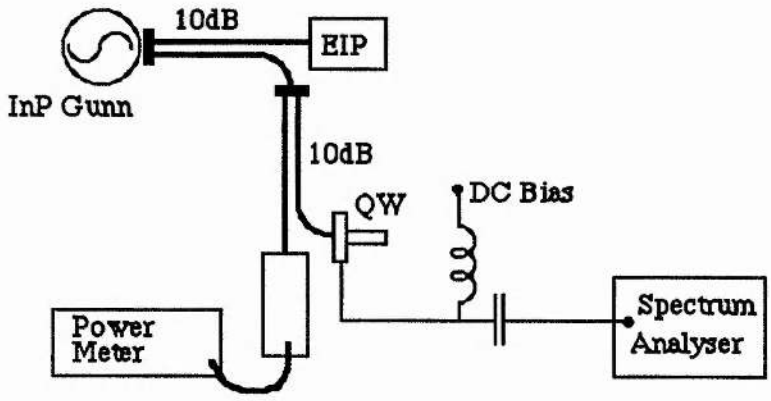

Figure 10.4. Test Circuit

The RF signal level reaching the QW diode would therefore range from a few microwatts to a few tens of microwatts, and the power meter on the straight-through arm of the second 10dB coupler enabled the signal power to be monitored with an accuracy of ±0.5dB. The Gunn oscillator was connected as shown to the external mixer of an EIP 578 microwave counter to provide both a measure of the frequency and phase lock to the Gunn, via the Gunn bias supply. The DC bias and the IF from

the QW were separated using a bias tee with a bandwidth of 10kHz - 10GHz and the IF was observed on a HP8590A spectrum analyser.

10.5. Self-Oscillating Mixing.

With the QW biased into the NDR region, the Gunn oscillator was tuned first to just above 86GHz and then to just below 86GHz until an IF could be observed in both cases. By tuning the Gunn oscillator closer in frequency to the QW, the IF could be reduced; conversely, tuning the Gunn further away from the QW increased the IF, confirming that self-oscillating mixing was taking place.

10.6. Injection Locking.

When the signal power of the phase-locked Gunn was increased, the IF was observed to reduce. This effect was the same irrespective of whether the Gunn was tuned above or below the QW in frequency, which suggested that the oscillation frequency of the QW was being pulled towards the RF signal. Eventually, as the RF signal power was increased beyond a certain point, the IF would disappear completely from the spectrum analyser, either because the QW was now locked to the Gunn, or because the QW oscillations had been quenched. Reducing the RF power at this point resulted in the reappearance of the IF. Figure 10.5 shows the effect of the signal power on the IF with the Gunn oscillator phase-locked to 86.27GHz and the QW bias set to about 1.2V. By reducing the signal power and retuning the Gunn closer to the QW, lower IF's could be achieved.

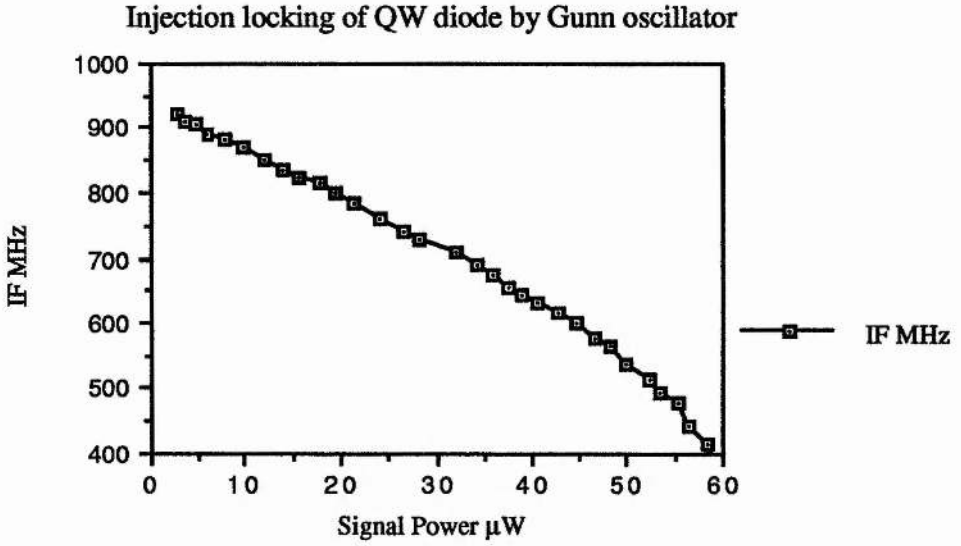

Figure 10.5. Evidence of injection locking of the QW by the RF signal. The Gunn oscillator was tuned above the QW in this case.

The IF level observed at the bias tee is shown in Figure 10.6. As the signal power is increased, the IF level increases and then decreases. It is not certain whether this is a saturation effect of the QW as a mixer, or, as a consequence of pumping the QW hard, the QW oscillation power is being reduced.

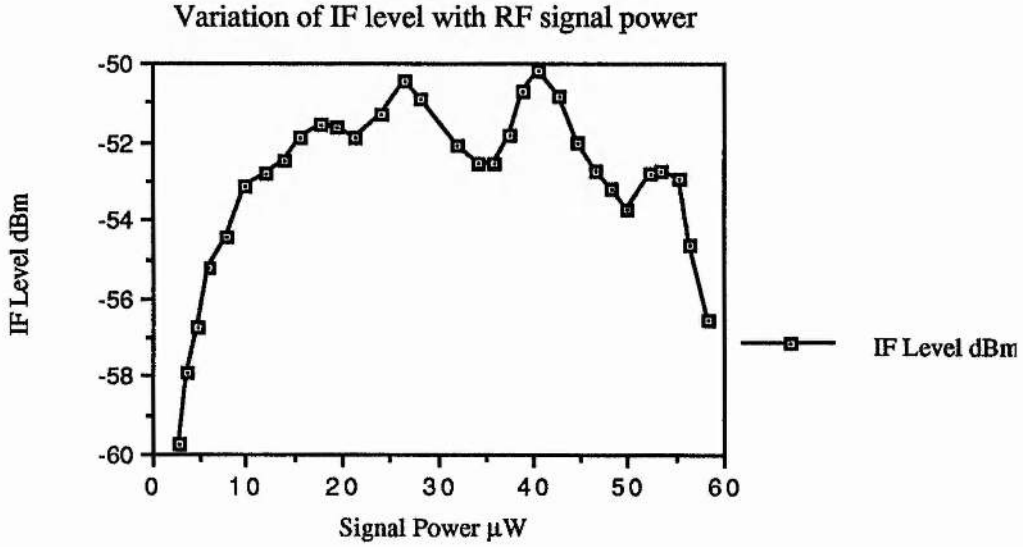

Figure 10.6. IF level v. signal power.

10.7. Conversion Loss.

The data shown in Figure 10.6 is rearranged in Figure 10.7 which shows the mixer conversion loss as a function of the signal power, and appears to confirm that as one pumps the QW diode harder, the conversion loss becomes greater. However, it must be stressed that with a simple circuit such as this it is not possible to optimise separately the oscillation power of the device *and* its mixer performance. It is therefore difficult to draw definite conclusions about the behaviour of the self-oscillating mixer from data such as the conversion losses shown in Figure 10.7. It must be borne in mind that when a certain adjustment is made, such as signal power, QW bias or backshort position, one is altering not a single parameter but a set of parameters which are related in a complex way. Systematic measurements are therefore difficult to make. In addition, it appears that recreating a particular set of parameters may not always give the same result as before. Therefore, it could be argued that *in this particular case*, as the signal power was increased and thus the QW oscillation frequency was changed (increased), the backshort behind the QW was no longer in the correct position to optimise the LO power, and the LO power was reduced, so the IF level dropped. It could equally well be argued, however, that we are seeing a saturation effect in the QW as a mixer as the signal power increases.

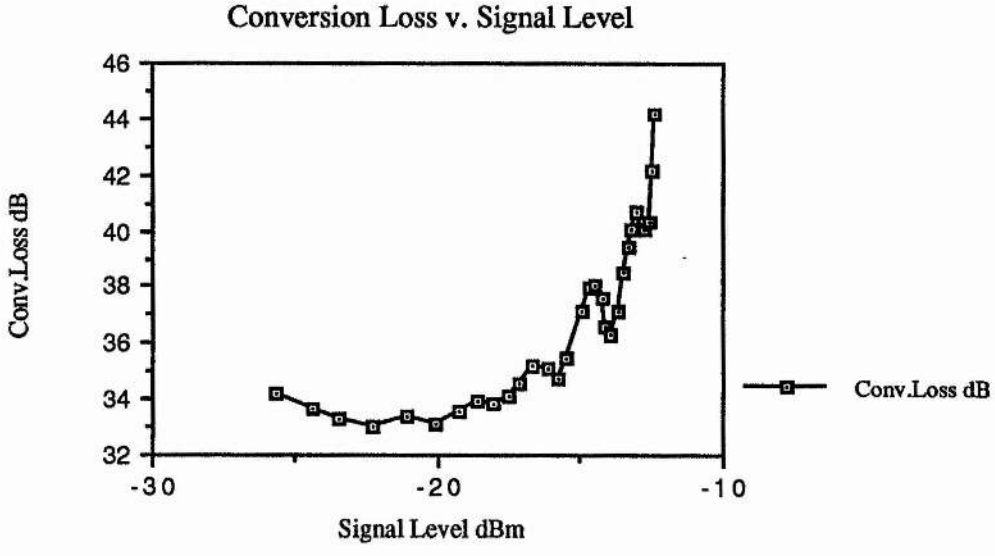

Figure 10.7. Mixer conversion loss v. RF signal level.

The conversion losses could be reduced by careful adjustment of the system, and the best (i.e. smallest) conversion loss achieved was 18.79dB using an RF signal of -26.46dBm (2.26μW) at 85GHz, giving an IF level of -45.25dBm at 1129MHz (Figure 10.8).

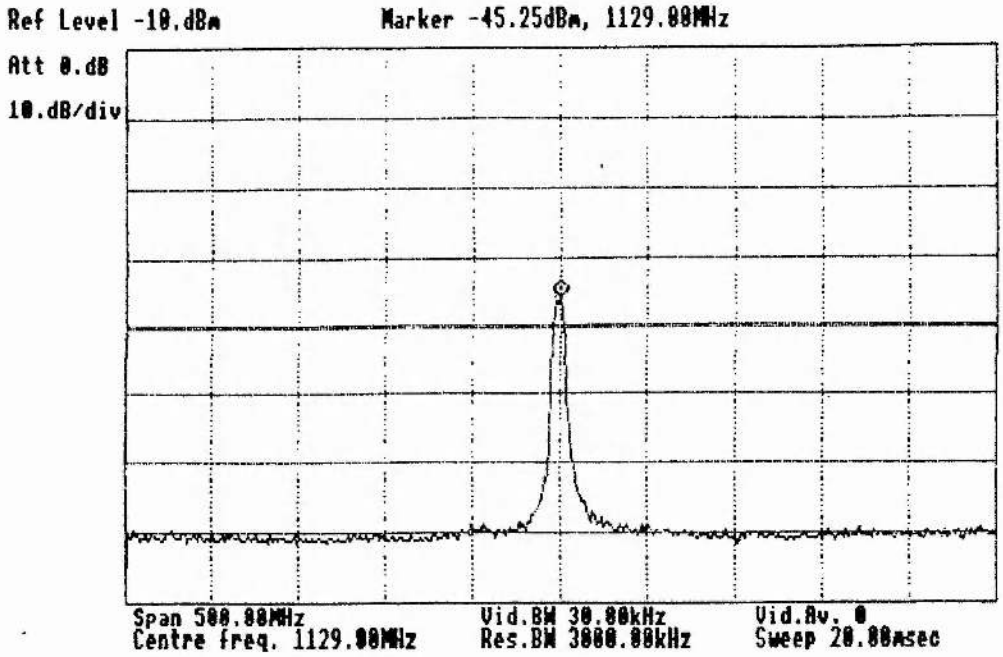

Figure 10.8. IF with 18.79dB conversion loss.

10.8. IF Stability.

One can identify two main effects which cause frequency instability in the IF: long term thermal drift, and short term frequency hopping. Only the Gunn oscillator exhibited thermal drift, with the frequency stabilising about 40 minutes after switch-on. From then on, the free-running frequency could be defined by phase-locking the Gunn oscillator to the EIP counter via the bias. In contrast, the QW oscillator showed no appreciable overall drift in frequency after it was turned on. The principal instability effect, however, was frequency hopping in the IF, over a range typically of a few MHz to a few tens of MHz. There are several possible mechanisms by which this sort of effect can occur:

1. Random fluctuations (noise) on the bias lines originating from the bias supply. The QW bias supply used in these measurements ran off a 10V bench power supply, and was a simple design using only one transistor. No voltage regulators were used in an attempt to avoid problems with oscillation, the design philosophy being the simpler the circuit, the less chance of unwanted noise. However, noise and ripple from the bench supply are likely to be poorly rejected, resulting in AM to FM conversion in the QW diode. A possible solution here is to use a battery supply.

2. Random fluctuations in the conductivity of the whisker/diode contact. Oxidation in and around the contact area can result in fluctuations in both the series resistance and the series capacitance of the contact. As both the inherent resistance and capacitance of the device are non-linear, variations in the bias current caused by degradation of the contact could lead to frequency variations.

3. Inherent frequency hopping arising from the wideband non-linearity of the QW. It is known that QW diodes can exhibit non-linear IV and CV characteristics over a wide bandwidth, and it is therefore possible that at both the LO and the IF the device is able to oscillate at more than one frequency.

10.9. Upper and Sub-Harmonics and Quasi-Chaotic Behaviour.

When the RF signal power was high compared to the power level generated by the QW oscillator, or when the QW backshort was adjusted to couple more power into the diode, the IF could exhibit both upper and sub-harmonics and wideband noise. Figure 10.9 shows the main IF spike marked at 581MHz with one sub-harmonic and three upper harmonics each separated by about 280MHz. The Gunn oscillator was locked to 86.2GHz and the RF signal power was 34μW. The presence of these harmonics is thought to be due to the wideband non-linearity of the QW diode.

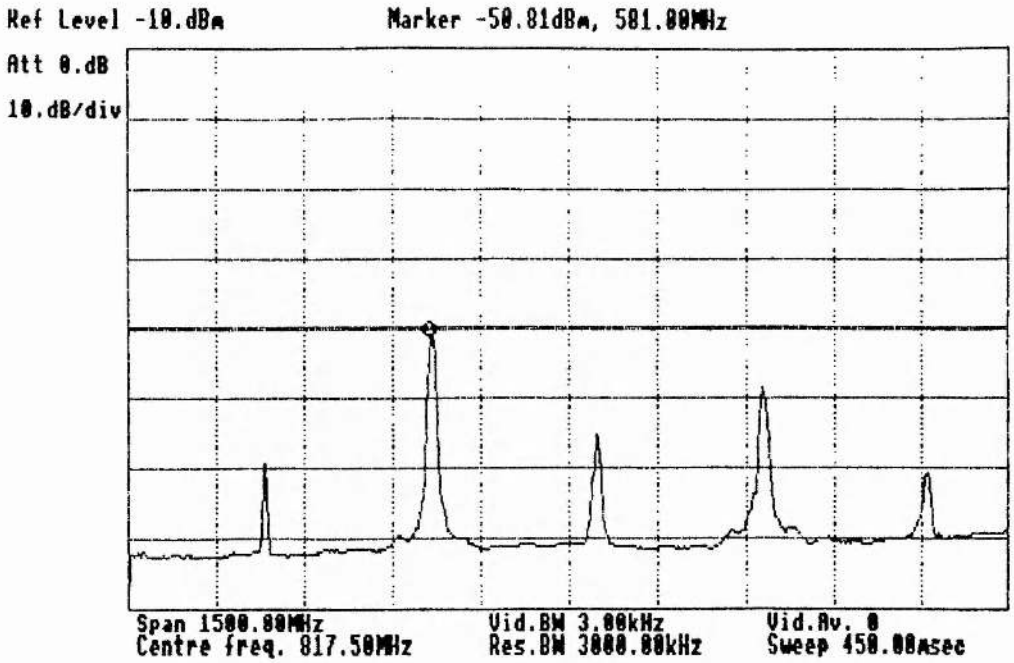

Figure 10.9. Typical set of harmonics on the IF when the QW device is pumped hard.

The other effect most often observed was the wideband noise, or quasi-chaotic oscillations which appeared on the IF. Normally, the transition from a single spike on the spectrum analyser to a noisy trace could be achieved simply by altering one parameter of the system, i.e. the QW bias, the QW backshort position, or the RF signal level. Figures 10.10 to 10.16 show the spectrum analyser trace as the signal power was increased from 18.9μW to 43.0μW. The Gunn oscillator was locked to 86.3GHz, and the QW bias was 1.072V. No other parameter other than the signal power was varied, and all spectrum analyser settings were identical. In Figure 10.10, the "initial conditions", the IF is already showing some wideband structure - it is the large spike on the right of the trace. It should be noted that in this series of traces, the trace was never static. In other words the structure of the IF spike, or wedge, varied between successive sweeps of the spectrum analyser, and so the "trace hold" function was used to grab a frame and put a marker on the IF as a reference point.

As the signal power is increased, the main IF spike moves to the left (as expected from observations of injection locking), and starts to broaden out (Figures 10.11 to

10.14). A further increase in signal power of only 0.3μW causes the IF to spread out suddenly into wideband oscillations (Figure 10.15), with no discrete IF spike being visible. As before, the detail of the structure varies with each successive sweep of the spectrum analyser.

Increasing the power further to 43.0μW changes the shape of the envelope of the oscillations (Figure 10.16). This was the highest signal power used to pump the QW oscillator before the trace disappeared from the spectrum analyser.

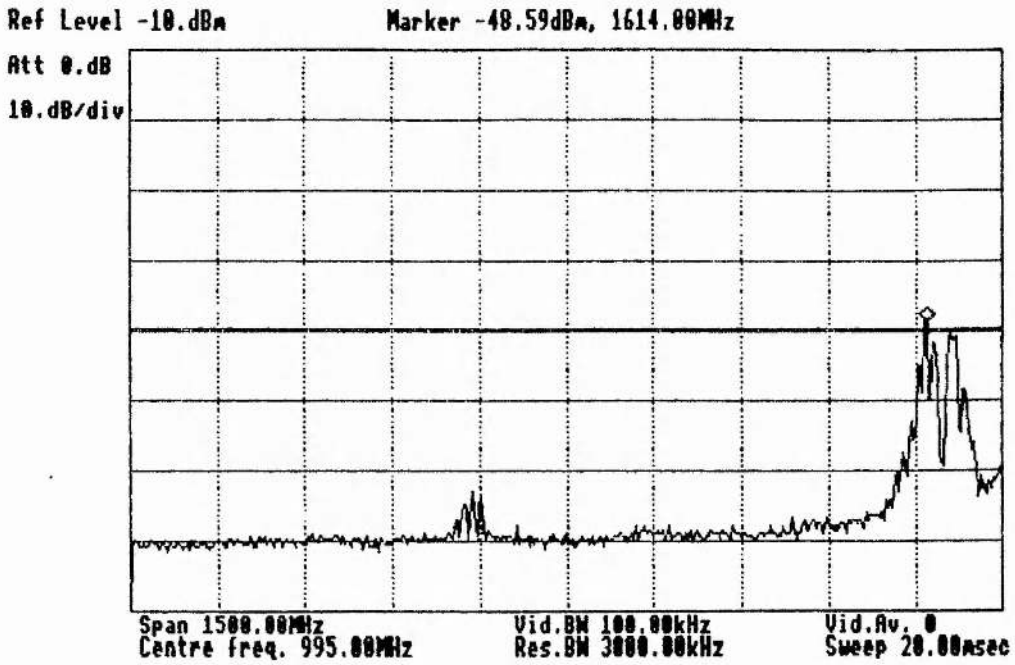

Figure 10.10. IF showing some wideband structure. QW bias 1.072V. Signal level 18.9μW at 86.3GHz

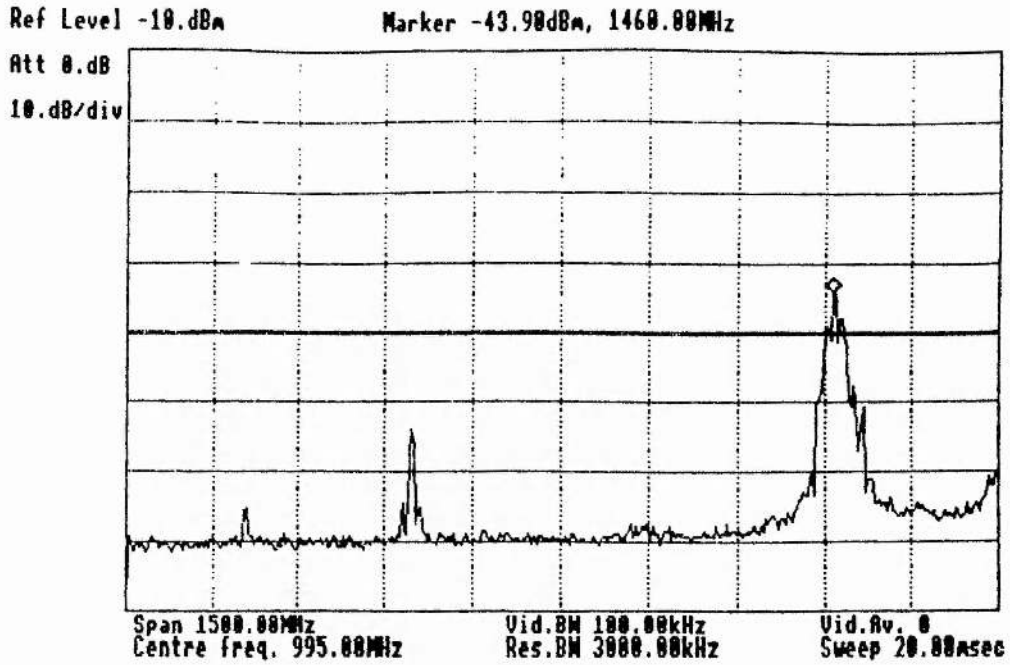

Figure 10.11. Signal level 24.8μW

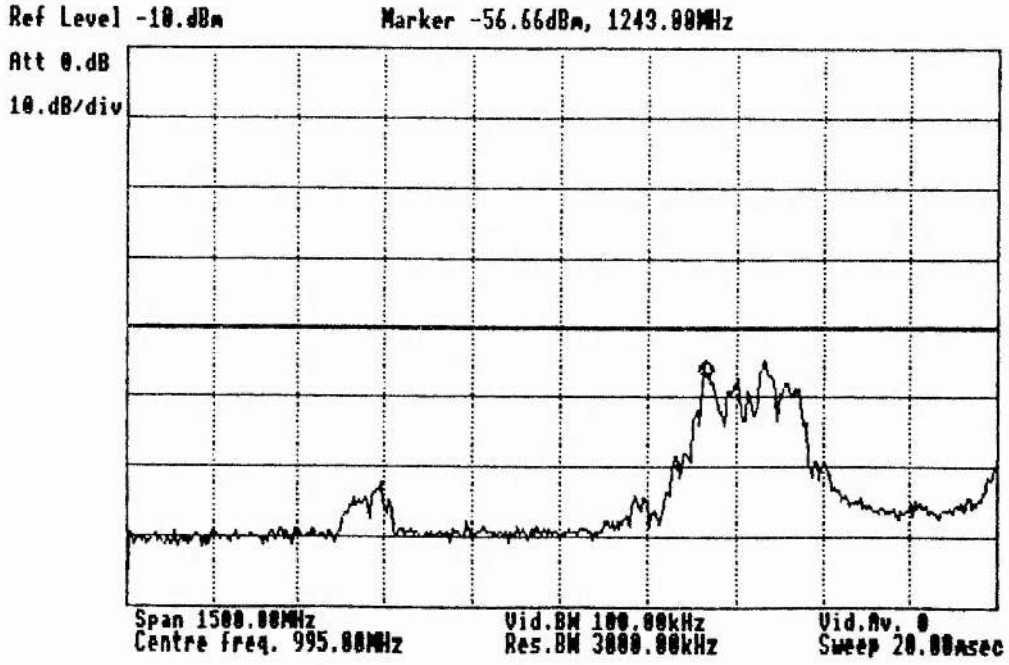

Figure 10.12. Signal level 28.1μW

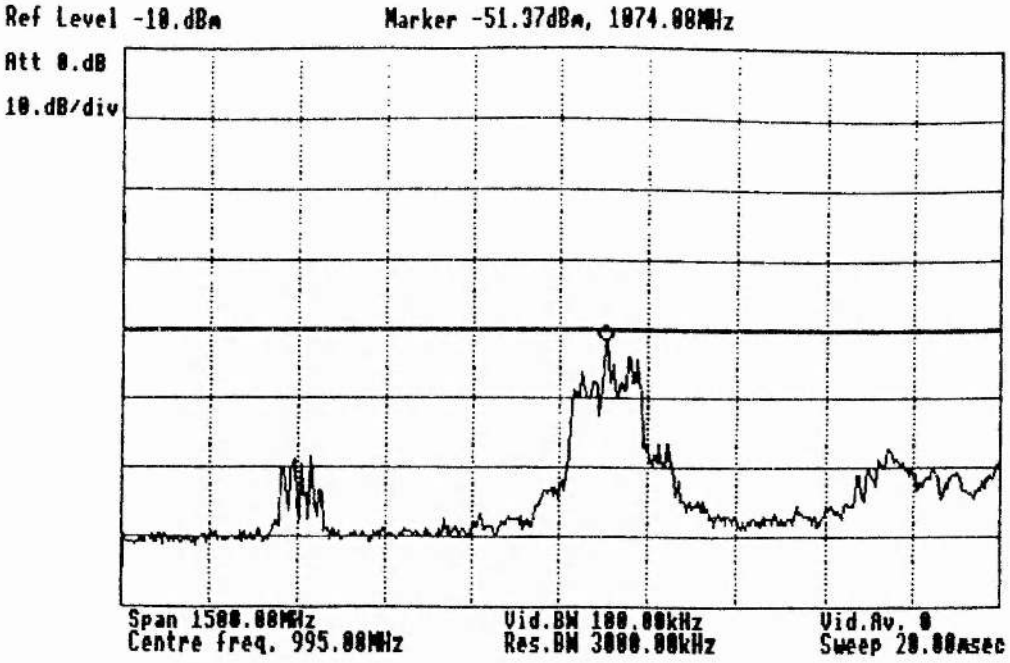

Figure 10.13. Signal level 32.0μW

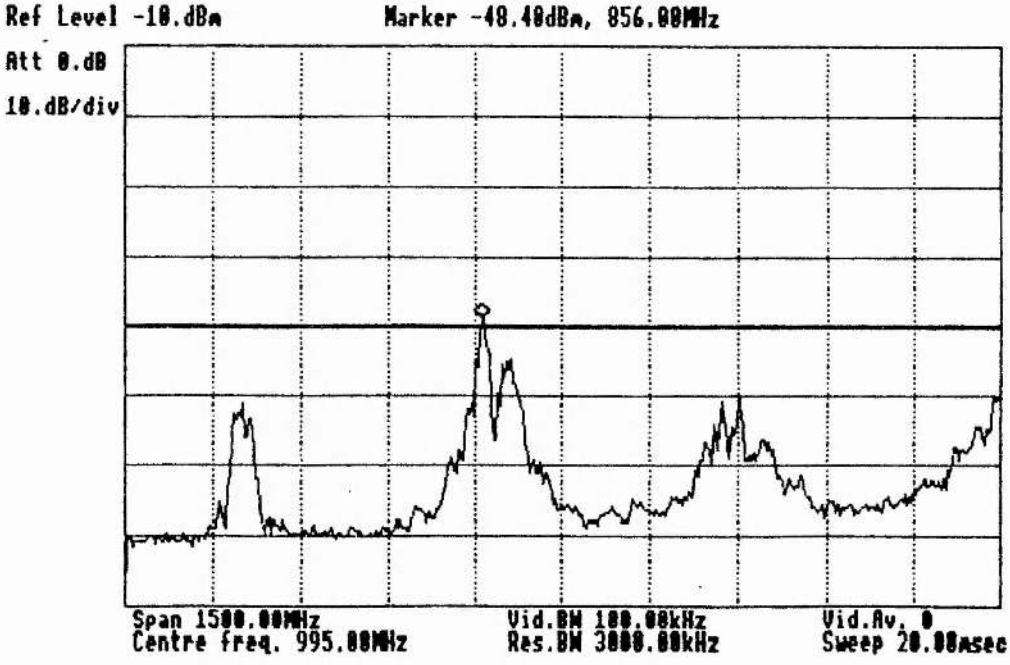

Figure 10.14. Signal level 35.6μW

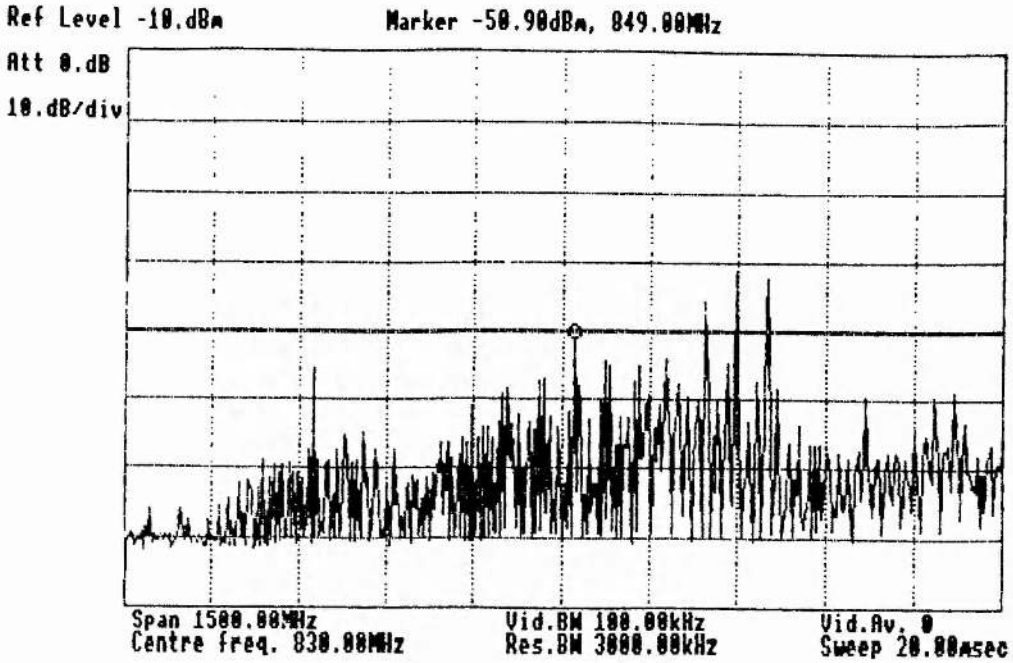

Figure 10.15. Signal level 35.9μW

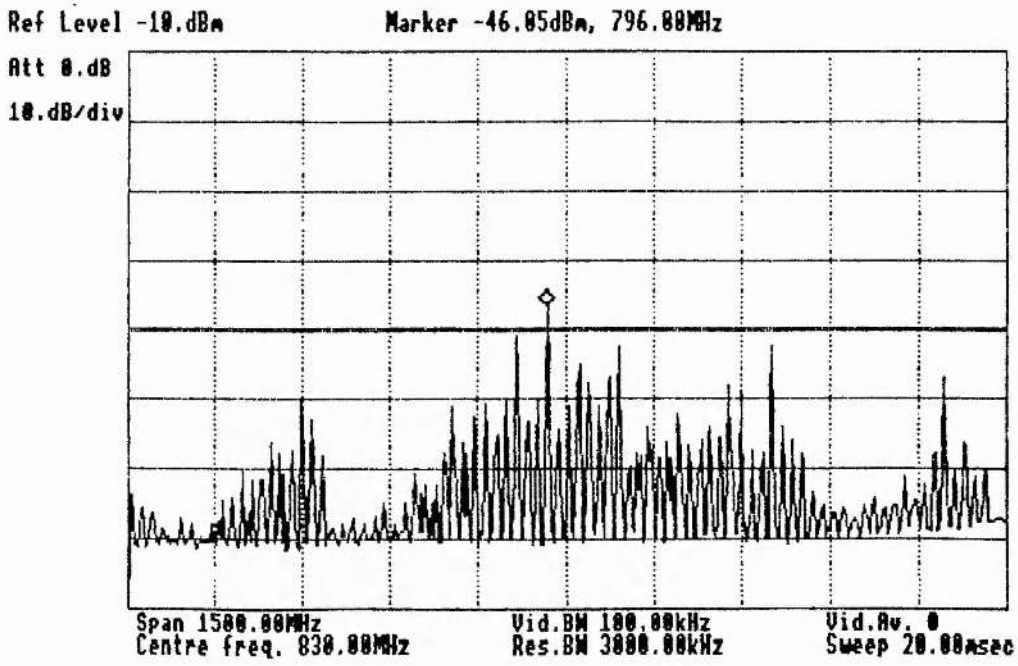

Figure 10.16. Signal level 43.0μW

The following set of traces were obtained by varying the QW bias only, increasing from 1.062V (Figure 10.17) to 1.086V (Figure 10.27). The signal level was 24.3μW at 86.3GHz at all times. The traces show a similarity to the previous set, with the IF initially showing some broadband structure and finally spreading out into wideband oscillations. The IF disappeared completely when the bias was increased to 1.089V. As before, the spectrum analyser traces were not static but varied slightly between successive sweeps of the analyser.

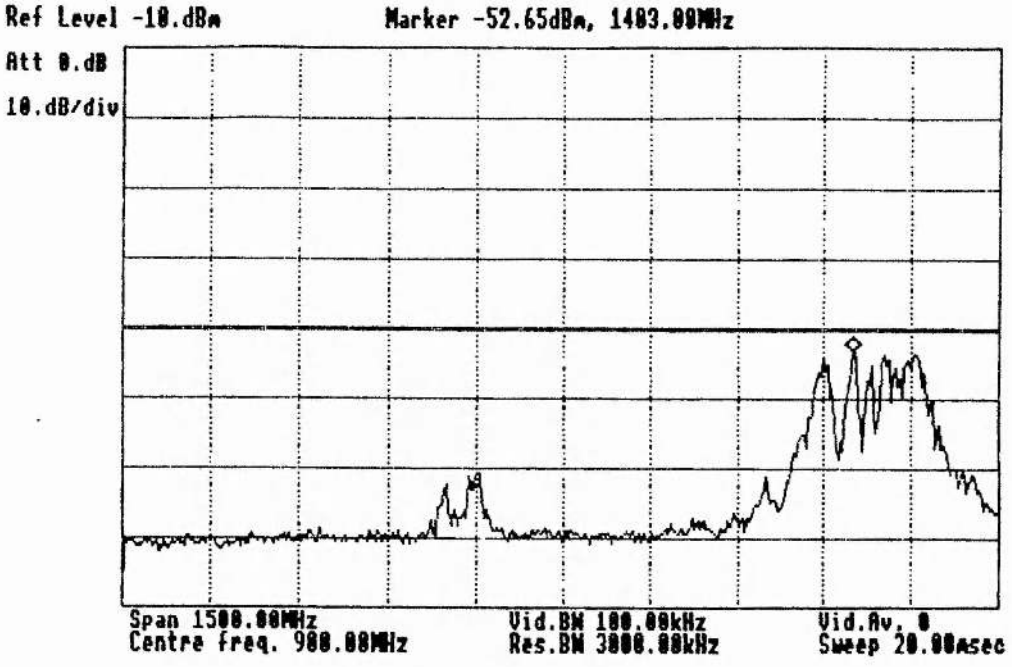

Figure 10.17. Signal level 24.3μW at 86.3 GHz.
QW bias 1.062V

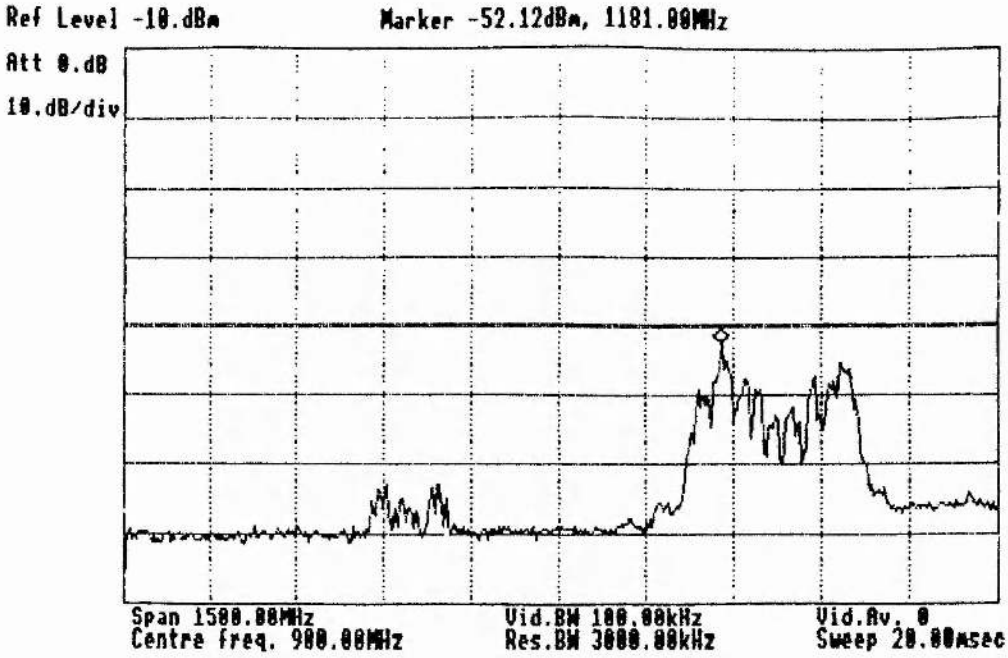

Figure 10.18. QW bias 1.066V

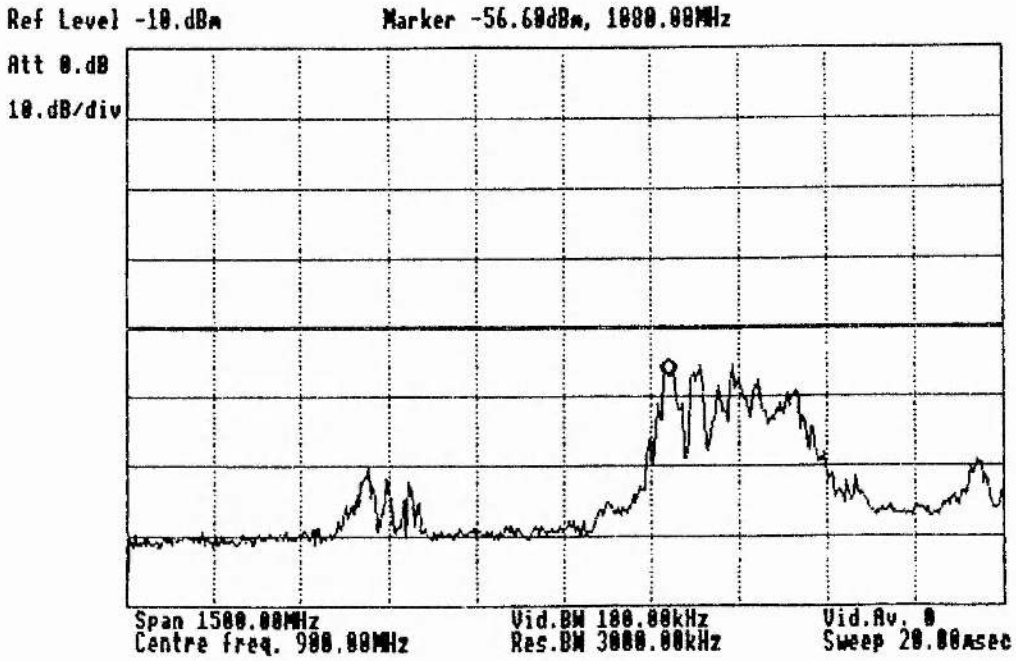

Figure 10.19. QW bias 1.068V

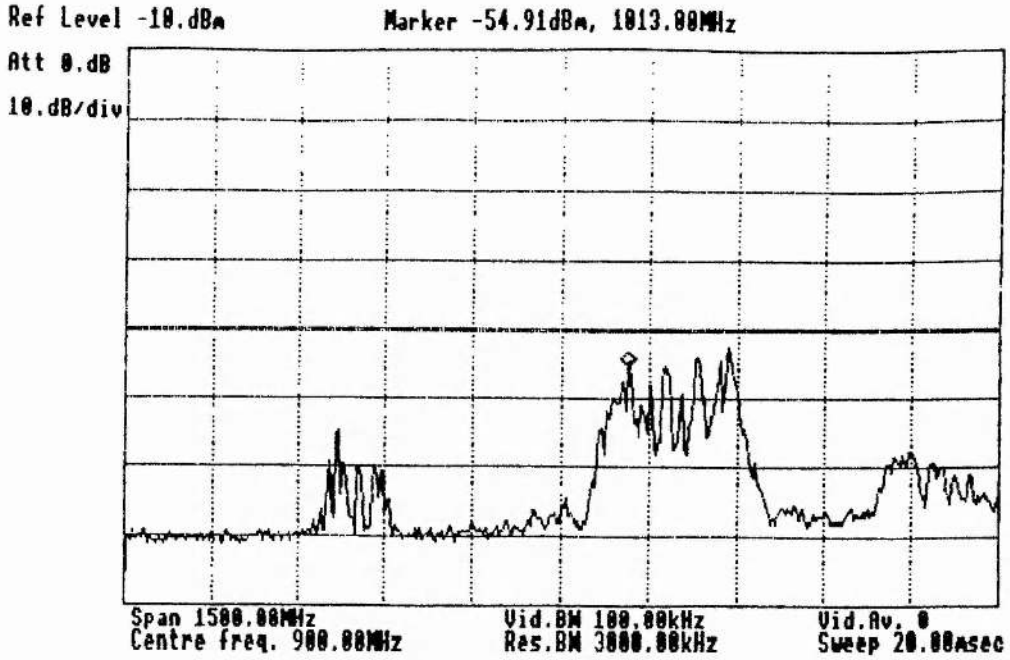

Figure 10.20. QW bias 1.070V

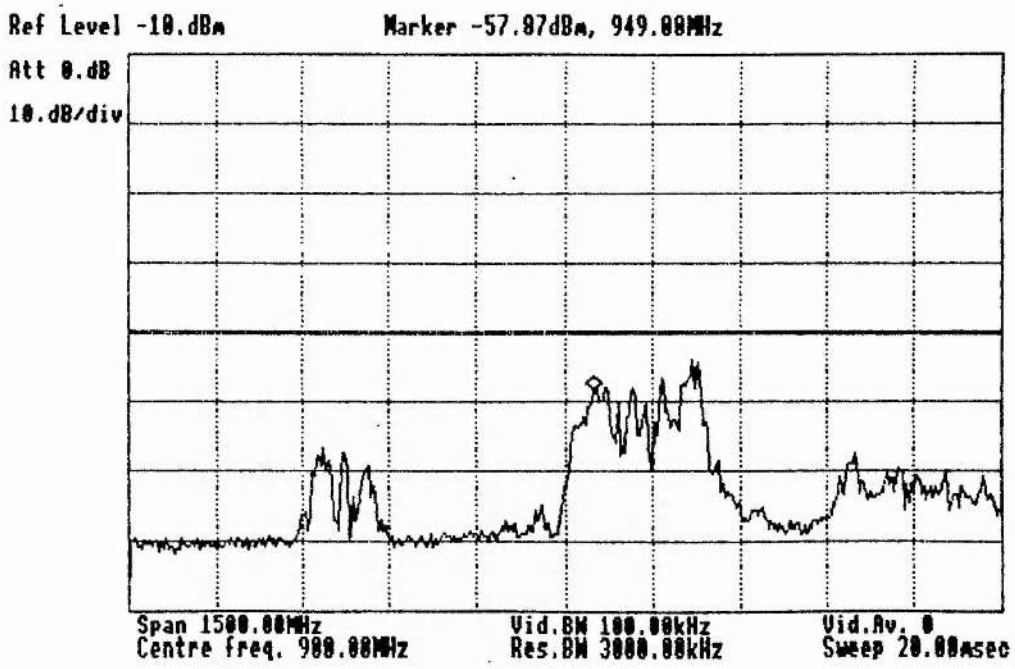

Figure 10.21. QW bias 1.072V

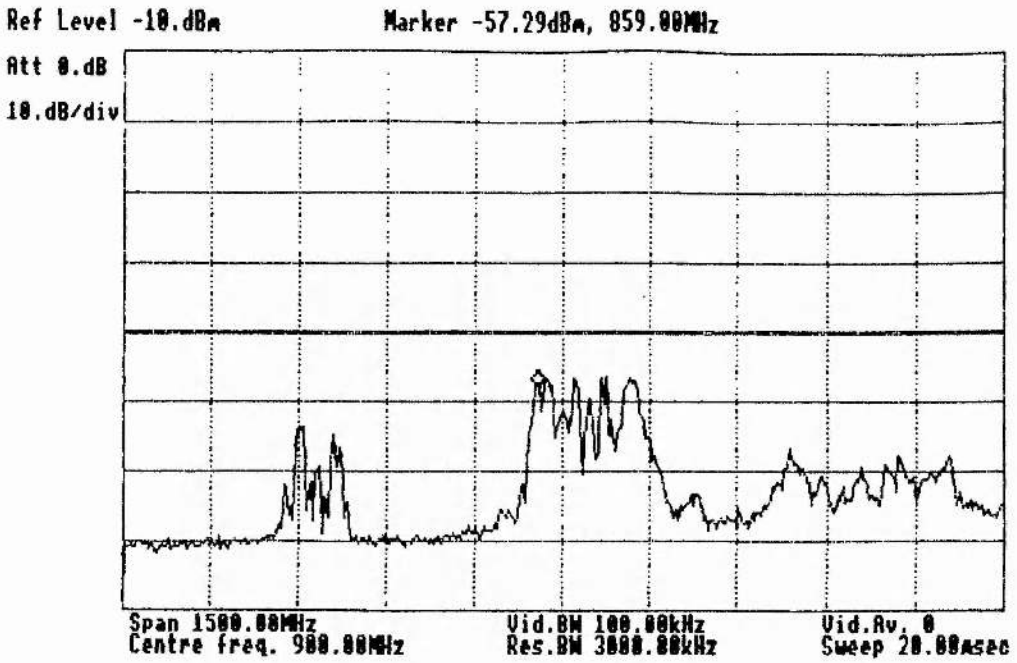

Figure 10.22. QW bias 1.074V

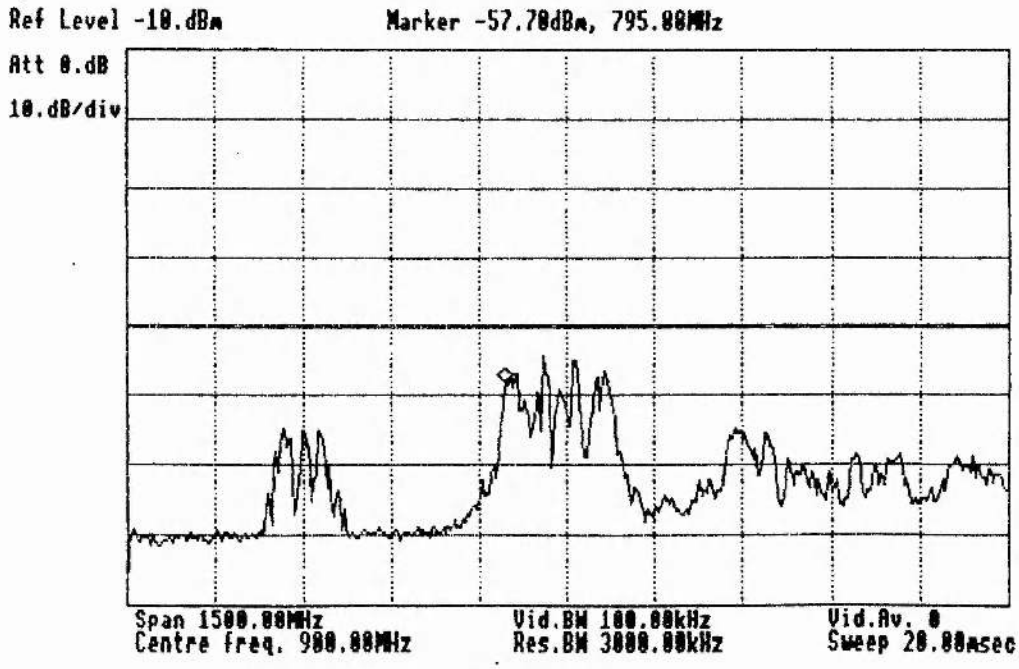

Figure 10.23. QW bias 1.076V

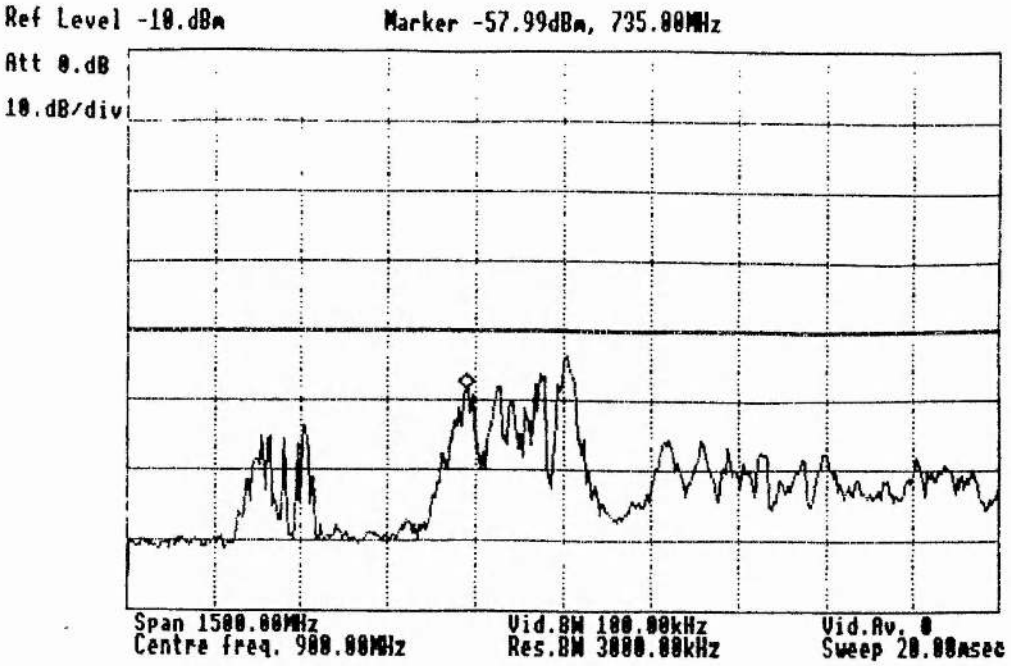

Figure 10.24. QW bias 1.078V

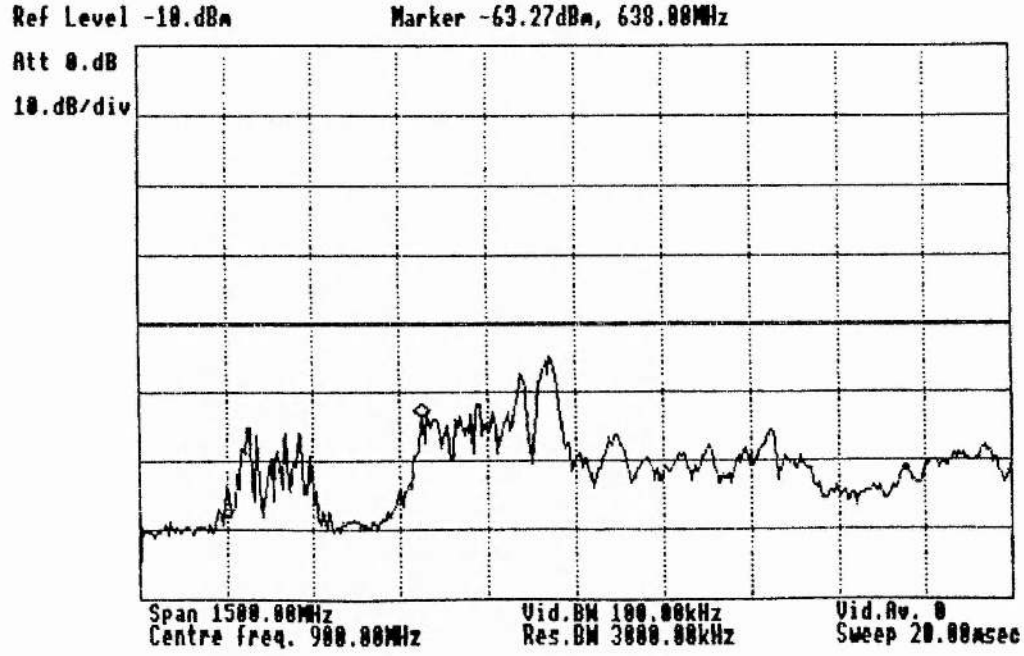

Figure 10.25. QW bias 1.080V

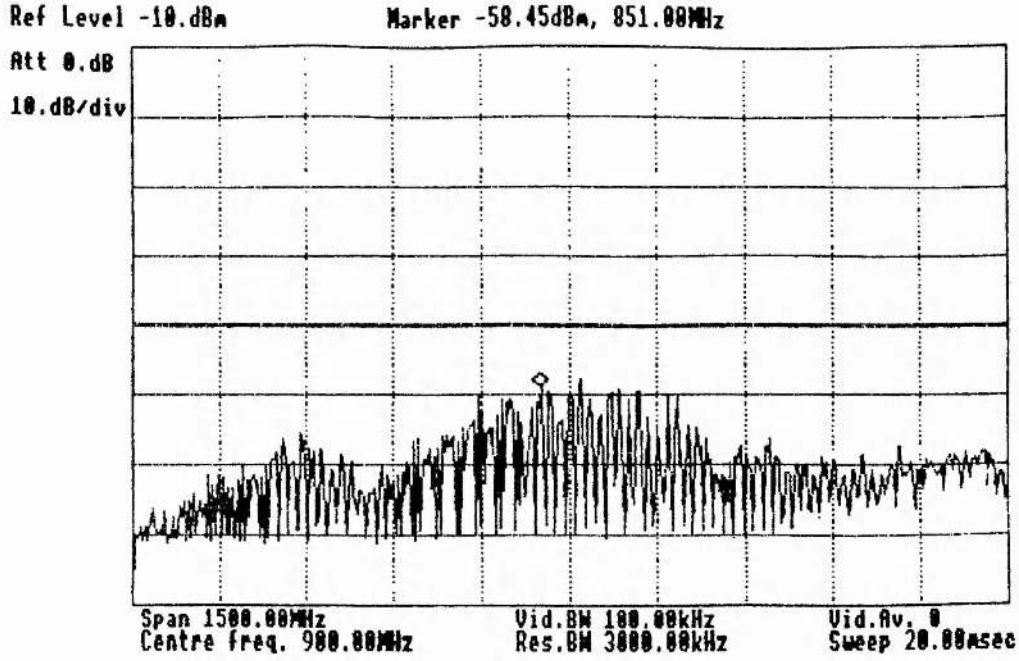

Figure 10.26. QW bias 1.082V

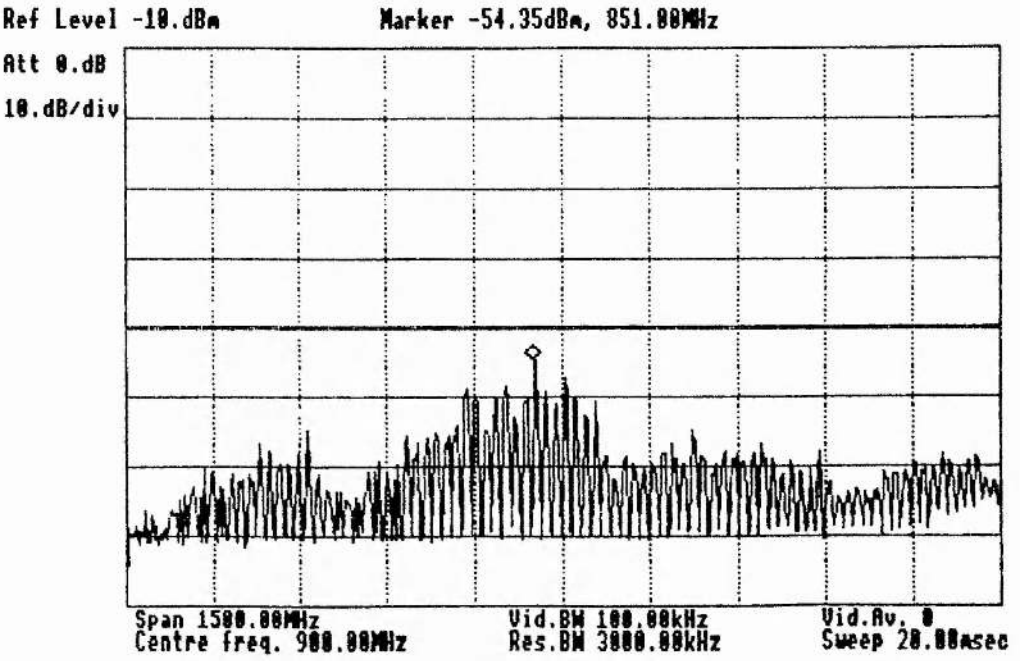

Figure 10.27. QW bias 1.086V

10.10. Conclusion.

The notion of a self-oscillating mixer is an attractive one, with the possibility of combining both the local oscillator and the mixer in a single device. The quantum well resonant tunneling diode has now been demonstrated as being a possible candidate for the development of a self-oscillating mixer at high frequencies. However, the performance of such a device suffers from several conflicting requirements, most notably that the device should have a stable oscillation frequency with reasonable power, and good mixer performance. The particular layer structure investigated in this chapter was not designed specifically as a self-oscillating mixer; but it is not clear how this particular problem could be approached.

The discovery of wideband "chaotic-like" oscillations opens up the possibility of developing QW devices as high frequency noise sources with bandwidths of several GHz. While the wideband noise exhibited by this particular diode cannot be said to be truly chaotic, or simply very complex without extensive further analysis, the fact that such complex behaviour has been observed is encouraging. Since it is relatively straightforward to grow wafers with (within limits) what might be termed "designer" IV's and CV's, the path is now open to generate a theoretical device by computer, analyse its behaviour numerically, and grow an actual device which reproduces in real time the type of spectrum one requires.

Chapter 10 References.

[1] E.R.Brown, T.C.L.G.Sollner, C.D.Parker, W.D.Goodhue and C.L.Chen, "Oscillations up to 420GHz in GaAs/AlAs resonant tunneling diodes", *Appl. Phys. Lett.*, vol.55, no.17,p.1777, 1989.

[2] T.C.L.G.Sollner, W.D.Goodhue, P.E.Tannenwald, C.D.Parker and D.D.Peck, "Resonant tunneling through quantum wells at frequencies up to 2.5THz", *Appl. Phys. Lett.*, vol., no.6,p.588, 1983.

[3] A.Rydberg and H.Grönqvist, "Quantum-well high efficiency millimetre-wave tripler", *Electronics Letters*, vol.25, no.5,p.348, 1989.

[4] T.C.L.G.Sollner, E.R.Brown and W.D.Goodhue, "Microwave and millimetre-wave resonant tunneling diodes", International Workshop on Future Electron Devices - Superlattice Devices, Tokyo, 1987.

[5] G.Millington, R.E.Miles, R.D.Pollard, D.P.Steenson, and J.M.Chamberlain, "A resonant tunneling diode self-oscillating mixer with conversion gain", *IEEE Microwave and Guided Wave Lett.*, vol.1, no.11,p.320, 1991.

[6] M.R.Robertson and J.C.G.Lesurf, "Self-oscillating mixing in a QW double barrier diode at W-band", *Int. J. Infrared and Millimeter Waves,* vol.12, no.12,p.1379, 1991.

11. Chaotic Systems and Noise Sources.

11.1. Introduction.

The contents of this chapter form part of a feasibility study undertaken from August 1991 to January 1992 for the National Physical Laboratory at RSRE, Malvern [1]. The main purpose of the study was to assess the feasibility of exploiting chaotic and semi-chaotic processes in non-linear systems to provide novel forms of noise sources for standards measurements. The study may be summarised here in three sections:

1. A general introduction to chaos, and an explanation of chaotic and semi-chaotic processes.
2. Consideration of the possible applications of chaotic and semi-chaotic processes.
3. Assessment of Gunn diodes and Double-Barrier diodes as chaotic or semi-chaotic noise sources.

11.2. Chaotic and Semi-Chaotic Processes.

The study of chaos theory and its applicability to virtually any discipline has grown rapidly in the last few years [2-5]. One of the most astonishing aspects of chaotic systems is that a system need not be complex in order behave in an extremely complex manner; in fact, it can be extremely simple. Take, for example, the non-linear mapping x^2-1. Repeated iteration of this mapping results in a simple cycling between two values, 0 and -1. If one then tries the mapping $2x^2$-1, the result is chaotic: no value is visited more than once. Furthermore, if the starting value of x is changed by only a tiny amount, then after a few iterations the waveform one gets bears no resemblance to the previous set of iterations. Generalising the mapping to kx^2-1, and choosing different values of k allows one to observe very complex behaviour. The pattern may appear to be regular at first, and then become chaotic; or it may start off by appearing chaotic and eventually settle down into a regular pattern, perhaps cycling through a set of values.

The above example illustrates two aspects which are common to all chaotic systems; they function in a deterministic framework, and they are extremely sensitive to initial conditions. Tiny discrepancies are quickly amplified through feedback mechanisms, resulting in rapid divergence of the state of the system. Chaotic systems in nature are everywhere, with the weather and population dynamics being two of the best known examples.

We can make a distinction between processes which are truly chaotic, and processes which may be called *semi-chaotic*. Both are deterministic, but while the truly chaotic process is essentially unpredictable and non-periodic, the semi-chaotic signal is ultimately predictable and periodic over long intervals. The distinction between chaotic and semi-chaotic processes, although important, is not always obvious.

Take, for example, a non-linear system being driven by a periodic signal such as a sine wave. Such a system could be a voltage-dependent capacitor (varactor) at the end of a simple linear T-network [1]. For given component values of the network, a given capacitance curve of the varactor and a given driving frequency, we can observe the output waveform of the circuit and compare it with the input waveform. By varying only one input parameter, in this case the dc component of the driving signal, we can observe a range of effects which are typical of chaotic systems. If we plot a graph where the vertical axis represents the value of the output waveform at a given phase of the driving sine wave, and step the value of the dc bias along the horizontal axis, then we observe the phenomenon known as bifurcation, or period doubling (Figure 11.1). A single line represents just one period in the output waveform. At a certain threshold value of the dc bias, however, the period of the output signal suddenly doubles. This process may repeat itself over and over again, until, in some cases, the number of periods becomes infinite, and we have chaos.

The bifurcation diagram is really only a two-dimensional section through a many-dimensional surface, each point on which describes the state of the system at a particular instant in time. Such surfaces are known as *attractors*, and are common to all dynamical systems.

In the example shown, the system passes through a region in which there are a great many frequency components, but not an *infinite* number. This region is shown in more detail in Figure 11.2. We can say that the output of the system is semi-chaotic

Under certain circumstances it may become virtually impossible to distinguish between truly chaotic and semi-chaotic signals. Firstly, although a semi-chaotic signal does have a finite period, if it is measured over a period of time which is less than the period of the semi-chaotic signal, then the signal will appear to be truly chaotic. Secondly, random noise, which is external to the set of differential equations which define the state of the system at any point in time, will tend to randomise the semi-chaotic signal. Thirdly, the elements of the system may themselves change their properties over a period of time, such as thermal ageing in semiconductors.

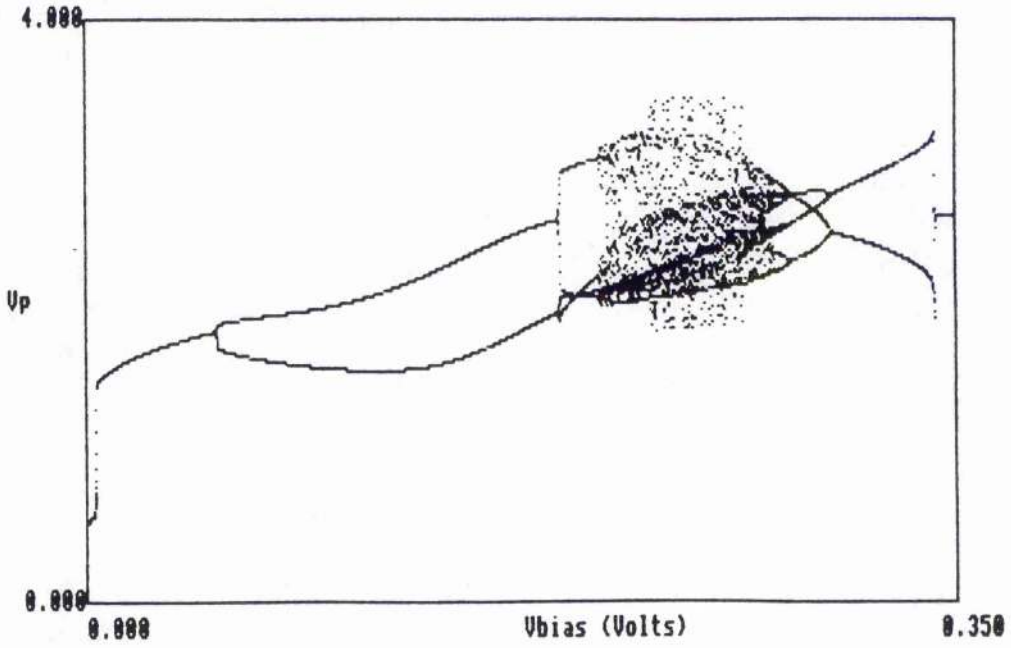

Figure 11.1. Bifurcation diagram of varactor system model.

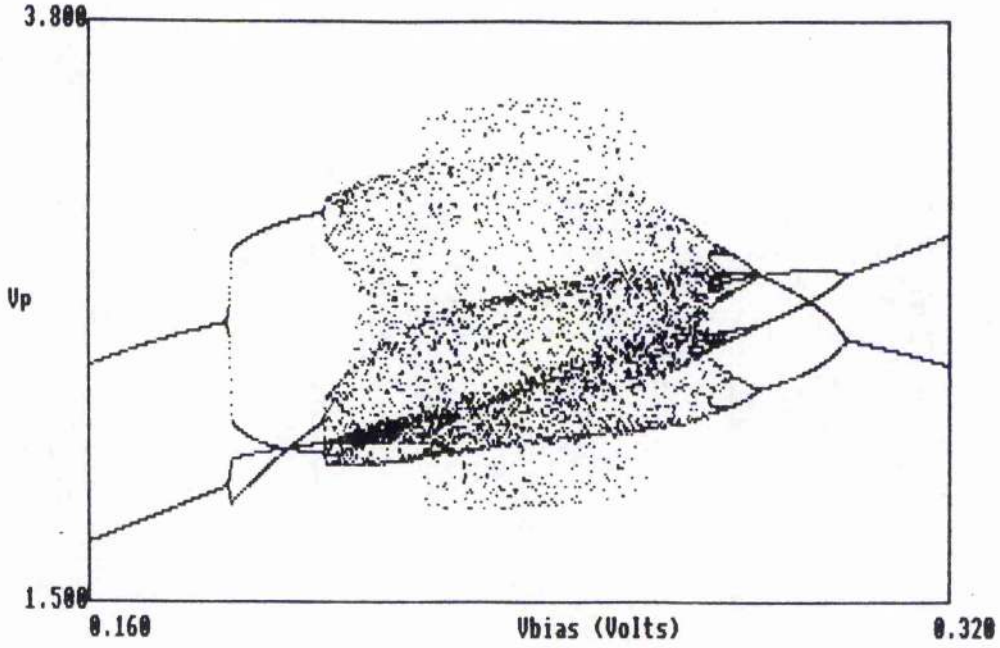

Figure 11.2. Close-up of the semi-chaotic region of Figure 11.1.

11.3. Possible Applications.

For the purposes considered in the feasibility report, semi-chaotic signals were of more interest than truly chaotic ones. Semi-chaotic signals are more controllable, predictable and repetitive, and can appear to be random within a limited time interval.

Such signals can provide wideband incoherent or partially-coherent waveforms for the following millimetre-wave applications:

1. Spread-spectrum signals for radar applications;
2. Broadband signals for communications;
3. Noise sources for calibration or standards measurements.

11.3.1. Radar Applications

The use of semi-chaotic radar signals has advantages in that they are much more difficult to recognise over background noise than coherent sources, unless the general semi-chaotic signature of the transmitted signal is known. Spread-spectrum radar probes can also be useful in scientific applications such as plasma diagnostics on fusion tori. With such machines, which are contained within a shielded hall, millimeter-wave signals are passed down long, overmoded waveguide runs to the torus itself. These long waveguide runs produce severe instrumental signature which can alter when the plasma is fired and the torus and runs distort. Semi-chaotic signal techniques could provide an alternative to the CW-FM and pulse techniques which are currently employed to tackle the problem.

11.3.2. Communications.

In communications, the use of semi-chaotic modulation could have applications in the encryption of signals over wide bandwidths at high data rates. Semi-chaotic modulation may also be useful in spread-spectrum broadcasting techniques, which give more efficient coverage than conventional VHF/FM transmitters, which generally suffer from multipath reflections.

11.3.3. Noise Sources.

Noise sources are used in calibration and standards measurements to provide broad-band signals of a well-defined power level. Broadly speaking, conventional noise sources fall into two categories: thermal (black body) sources; and sources

which employ a process which is not in thermal equilibrium, e.g. avalanche processes. The noise temperature of a thermal source may be defined by making an accurate measurement of its physical temperature, which for practical thermal sources is limited to a few hundred degrees Kelvin. Non-thermal noise sources such as discharge tubes and avalanche diodes have higher effective noise temperatures, of the order of 10,000K. However, these noise temperatures produce powers that are too low to be detected by room temperature detection systems, and must therefore be measured using either a heterodyne radiometer system or a cooled bolometer system. In practice, the heterodyne radiometer system is the most widely used.

Since most of those who use noise sources do so to calibrate sensitive heterodyne receivers, we can identify a 'circular' calibration problem: namely that the noise source which is being used to calibrate the receiver of interest must first itself be calibrated by a heterodyne receiver! Clearly, it is desirable to find some other way of determining accurately the noise temperature of the source.

The use of noise sources based on semi-chaotic processes in non-linear solid-state devices would eliminate circular calibration problems in two ways. Firstly, a semi-chaotic signal produced by a deterministic system described by a few simple equations lends itself well to computational modelling. By comparison, avalanche processes must be treated statistically. Secondly, semi-chaotic noise sources should provide power levels many orders of magnitude greater than conventional noise sources. This will prove valuable in that the noise power may be measured directly and continuously using room temperature power measurement systems.

11.4. Modelling Non-Linear Processes.

Two approaches were employed in parallel in order to determine suitable devices and circuits for semi-chaotic systems. The first was to develop mathematical models, the states of which were calculated by computer. In this way any particular system parameter, such as a voltage or a current, could be observed to evolve with time, and graphical techniques such as bifurcation plots could be employed. The second approach was to build equivalent analog models of the circuits, and observe their behaviour over a period of time.

The computational method has two basic problems, which arise from the way in which computers store numbers, and from the way in which the differential equations are calculated. Since a computer can only store numbers in a finite number of bits, any model will be confined to a *finite* number of states. Thus a digital computer can never completely represent true chaos. In addition, the effect of rounding errors can influence the maximum number of available states of the model. The differential equations are represented in the computer programs by *difference* equations, and new values of the system parameters are calulated with finite precision for each time step 'dt'. We can force the model to behave as if the time differential was smooth by reducing the time step dt, but reducing the value of dt too much can result in the computer failing to record changes of state as the value of dt reaches the limit of resolution of the computer. In effect, the system appears to 'freeze'.

In order to avoid the quantisation and truncation effects associated with digital computers, analog models were also built. Despite being relatively inflexible when compared with the computer models, they offered some useful features. Instead of being clocked along in finite time steps, the system parameters obey the actual differential equations; and the models can run much faster than on a digital computer (a few kHz compared with 10Hz). The validity of the combined digital/analog modelling approach was confirmed when visibly identical results to that shown in Figure 11.1 was obtained from an analog system.

11.5. Gunn Diodes as Noise Sources.

Gunn diodes are two-terminal devices which exhibit negative differential resistance (NDR) which may be regarded as a form of gain mechanism. As part of the feasibility study, a simple mathematical model of a Gunn diode, intended to mimic its IV characteristic, was examined. The model showed regions of chaotic behaviour as the input dc bias was varied. An equivalent analog model showed very similar behaviour.

To those familiar with real Gunn oscillators, complex behaviour is nothing new. However, incoherent or partially coherent output, normally observed when the diode is 'underbiased', are usually dismissed as bias oscillations. Much effort is spent in

trying to suppress these oscillations. It is possible that when the output of an underbiased Gunn oscillator is examined in detail, the hallmarks of chaos will be there. This leads us to the concept of an inherently chaotic Gunn diode.

Normally, Gunn diodes are developed to have well-behaved characteristics - low noise, a stable oscillation frequency, and restricted bias tuning. However, discussions with N.Couch of GEC indicate that it should be possible to design Gunn diodes with modified IV/CV characteristics, whose behaviour would be of interest in generating chaotic or semi-chaotic signals.

An alternative approach to developing a Gunn-based noise source is to apply a deterministic semi-chaotic signal to the bias line of the device to produce related FM modulation of the oscillator output. Computer programs, controlling digital to analog convertors, would generate any desired semi-chaotic waveform. Modification of the source power spectrum, such as pre-whitening, would also be possible, and higher modulation bandwidths may be achieved if the computer generated signals were replaced with dedicated hard-wired digital systems.

It is likely that chaotic modulation of Gunn oscillators will lead to the development of useful noise sources in a reasonably short period of time, as the required devices and techniques already exist. In practice, a chaotic-FM source would be indistiguishable from a true noise source if the bandwidth of the detector equalled or exceeded the output bandwidth of the source. One advantage a chaotic-FM source has over the true noise source is that the power level does not vary in a random manner. As the output power of the source is known, the noise need not be averaged over more than a few cycles of the modulating signal. In addition, a semi-chaotic FM source can repeatedly generate nominally identical signals which would enable comparitive measurements to be made, without resorting to statistical calculations.

It was mentioned in section 11.3.3. that semi-chaotic noise sources should provide noise temperatures well in excess of those available from conventional noise sources. If we take the example of a chaotic-FM Gunn source, producing a nominal power level of 1mW over a 10GHz bandwidth, then from P=kTB we get a noise temperature of around 7.2×10^9K. This sort of power output is far in excess of that required for most calibration purposes, and thus enables a large fraction of the power to be used for continuous monitoring of the noise level.

11.6. Double-Barrier Diodes as Noise Sources.

Resonant tunneling double-barrier diodes, or quantum well (QW) devices, are also two-terminal devices which exhibit NDR. From results obtained at St.Andrews ([6], see chapter 10), we have demonstrated that they may prove to be suitable as chaotic noise sources. QW devices and related multibarrier structures have several features which are relevant to the development of noise sources. Firstly, their inherent response time is very fast, implying operation at high frequencies and wide bandwidths. Secondly, their IV and CV characteristics may be chosen with quite a high degree of flexibility, which is a significant advantage in the design of improved noise sources.

A simple mathemetical model of a QW device was run on a computer, and chaotic behaviour was observed. It must be stressed, however, that the capacitance-voltage characteristics of QW devices are not yet well understood. In fact, most models of QW devices assume that the capacitance is constant. Clearly, an accurate description of the various capacitances of these devices is essential when attempting to model their behaviour [7].

11.7. Conclusion.

The study of chaotic systems holds a certain fascination for many people, not only because of the often stunning visual effects which chaos can generate, but also because of the way in which hitherto unexplained or unwanted effects can now be put into context. This chapter has set out to expain how chaos can be deliberately exploited to produce a new class of millimetre-wave devices: noise sources whose complex output obeys a simple set of deterministic equations. Within this class appear two distinct types of noise source: those which are modulated with a complex signal, and those which exhibit inherent complexity. Both types warrant further development.

Chapter 11 References.

[1] M.R.Roberston and J.C.G.Lesurf, "Report on the Feasibility of 'Chaotic' MM-Wave Noise Sources", NPL Agreement no. NPL 82/A/0536, January 1992

[2] "The New Scientist Guide to Chaos", ed. Nina Hall, Penguin Books, London 1991.

[3] G.L.Baker and J.P.Gollub, "Chaotic Dynamics - an introduction", Cambridge University Press 1990.

[4] J.Gleick, "Chaos", Cardinal, London, 1988.

[5] I.Stewart, "Does God Play Dice? The Mathematics of Chaos", Basil Blackwell, Oxford, 1989.

[6] M.R.Robertson and J.C.G.Lesurf, "Self-oscillating mixing in a QW double barrier diode at W-band", *Int. J. Infrared and Millimeter Waves,* vol.12, no.12,p.1379, 1991.

[7] J.Genoe, C.Van Hoof, W.Van Roy, J.H.Smet, K.Fobelets, R.P.Mertens, and G.Borghs, "Capacitances in Double-Barrier Tunneling Structures", *IEEE Trans. Electron Dev.*, vol.38, no.9,p.2006, 1991.

Conclusions

The purpose of this work has been to identify ways in which solid-state sources could cover a greater part of the millimetre and submillimetre wave band than at present. Gunn oscillators remain a very important means of generating low to medium power at frequencies below 200GHz, not simply as low-noise sources in themselves, but also as a means of pumping frequency multipliers with a clean signal. The potential for extending the frequency of Gunn oscillators themselves is limited by the response time of the bulk material of the diode, so one must look elsewhere for high frequency sources.

The development potential of devices based on resonant-tunneling double-barrier diodes, or quantum-well devices, is enormous. Despite the fact that the QW devices measured at St.Andrews were essentially first-generation devices, it was clearly demonstrated that they would detect, mix, multiply and oscillate, in simple waveguide circuits. Work carried out elsewhere on the InAs/AlSb material system has yielded the highest oscillations to date from a solid-state oscillator, at 712GHz. Furthermore, the power density available from this device material is 50 times greater than the more usual GaAs/AlAs system. The significance of this is that QW devices may now be capable of delivering useful power to detectors and mixers up to the terahertz region.

The discovery of so-called chaotic oscillations in resonant-tunneling diodes has opened the door for the exploitation of chaos theory to produce broadband noise sources. Chaos theory may also be applied to the modulation of Gunn diodes to produce sources suitable for noise standards work, spread spectrum radar and communications. Ultimately, however, the much greater flexibility offered by resonant-tunneling diodes in terms of materials and electrical characteristics will prove irresistible.